Index

Abstract

Alterations in cellular metabolism are among the most consistent hallmarks of cancer. The non-oxidative part of the Pentose Phosphate Pathway is controlled by transketolase enzymes, among which, the TKTL1 isoform is specifically upregulated in malignancies and predicts poor patients prognosis.

TKTL1-suppressed HCT116 cell clones using shRNA technology were established to investigate the role of TKTL1 in tumor maintenance. As expected, TKTL1-suppressed cells have lower D-Glucose consumption and L-lactic acid production rate. In parallel, these clones grow slower, suggesting TKTL1 plays a role in cell growth and proliferation in cancer cells. In addition, we found the mitochondria respiration of TKTL1-suppressed cells is enhanced. These cells exhibit higher oxygen consumption and enhanced glucose degradation switch to aerobic respiration, which may increase the side production of electrons transport chain: reactive oxygen species (ROS). Also some anti-ROS defensive enzymes of these TKTL1-suppressed cells decreased, leading to enhanced sensitivity towards oxidative stress-induced apoptosis. The induction of growth-suppressive genes, i.e., p21, as well as the increased intracellular ROS in TKTL1-suppressed cells, may contribute to increased cellular senescence.

Hypoxia-inducible factor 1α (HIF-1α) activates transcription of genes that are involved in crucial aspects of cancer biology, including angiogenesis, cell survival, glucose metabolism and invasion. TKTL1-suppressed HCT116 cells have reduced HIF-1α expression and stability, and display also attenuated invasiveness, migration and transformation features in vitro, indicating that TKTL1 is involved in the maintenance of tumor malignancy.

In a murine tumor xenograft model, TKTL1-suppressed cells showed slower tumor growth and less tumor occurring rate, which may be the consequence of reduction in initiating cell marker. Mice bearing TKTL1-suppressed tumors also displayed less severe cachexia phenotypes. The tumors formed by TKTL1 suppressed cells have less vascularization and less necrosis area, indicating these tumors are less malignant than the corresponding controls. These data provide new clues on the importance of TKTL1 in tumors as has been recently suggested by clinical studies. Since the sustained TKTL1 activation might benefit tumor growth and metastasis, it could be considered as a good target for anti-cancer therapy.

Abbreviations

8-oxo-dG	8-oxo-2'-deoxyguanosine
8-oxo-G	8-oxo-2'-guanine
ADP	adenosine diphosphate
AIF	apoptosis inducing factor
ATP	adenosine 5'-triphosphate
bp	base pair
cDNA	complementary DNA
CIC	cancer-initiating cells
CMXRos	Chloromethyl-X-rosamine
c-myc	proto-oncogene myc
CO_2	carbon dioxide
CSC	cancer stem cells
CuZnSOD (SOD1)	Copper/Zinc superoxide dismutase
DCFH	2',7'-dichlorofluorescin
DHE	dihydroethidine
DMSO	dimethyl sulfoxide
DNA	deoxyribonucleic acid
DNAse	recombinant human deoxyribonuclease
EDTA	ethylenediaminetetraacetic acid
eGFP	enhanced green fluorescence protein
ETC	electron transport chain
FAD	flavin adenine dinucleotide
$FADH_2$	flavin adenine dinucleotide reduced form
FACS	fluorescence-activated cell sorting
FBS	fetal bovine serum
G418	Geneticin
G6P	glucose-6-phosphate
GAPDH	glyceraldehyde 3-phosphate dehydrogenase

GPx	glutathione peroxidase
GR	glutathione reductase
Grx	glutaredoxin
GSH	glutathione (L-gamma-glutamyl-L-cysteinylglycine)
GSSG	glutathione oxidized form
GST	glutathione-S-transferase
H_2DCFDA	2',7'-dichlorofluorescin diacetate
H_2O_2	hydrogen peroxide
HIF	hypoxia-inducible factor
HMP shunt	Hexose Monophosphate Shunt
HPLC	high performance liquid chromatography
mL	mililiter
mM	miliMolar
MnSOD (SOD2)	manganese-containing superoxide dismutase
mRNA	message RNA
mtDNA	mitochondria DNA
NAD^+	nicotinamide adenine dinucleotide (oxidised form)
NADase	NAD+ glycohydrolase
NADH	nicotinamide adenine dinucleotide (reduced form)
$NADP^+$	Nicotinamide adenine dinucleotide phosphate (oxidised form)
NADPH	Nicotinamide adenine dinucleotide phosphate (reduced form)
NeoR	Neomycin resistance
O_2-•	superoxide anion
OH•	hydroxyl radical
OXPHOS	oxidative phosphorilation
p53	tumor suppressor TP53
PBS	phosphate buffered saline
PCR	polymerase chain reaction
PDH	pyruvate dehydrogenase
PDK	pyruvate dehydrogenase kinase

PET	positron-emission tomography
Pi	inorganic phosphate
PI	propidiumiodide
PPP	pentose phosphate pathway
Prx3	peroxiredoxin3
Prx5	peroxiredoxin5
PT pore	permeability transition pore
qRT-PCR	quantitative RT-PCR
R5P	ribose-5-phosphate
RNA	ribonucleic acid
RNAse	recombinant human ribonuclease
ROS	reactive oxygen species
RT-PCR	reverse transcriptase PCR
SC	subcutaneous
SDS-PAGE	sodium dodecyl sulfate polyacrylamide gel electrophoresis
-SH	thiol
shRNA	short hairpin RNA
siRNA	small interfering RNA
SOD	Superoxide dismutases PCR
TK	thymidine kinase
TKT	Transketolase
TKTL1	Transketolase like protein 1
TKTL2	Transketolase like protein 2
Trx2	thioredoxin 2
TrxR2	thioredoxin reductase 2
UCPs	The uncoupling proteins
μL	microliter
μM	microMolar

1. Introduction

Over 80 years ago, Warburg performed experiments on the metabolic aspects of tumor and normal tissues and proposed the model for the pathogenesis of cancer (Warburg, 1956b). He reported that tumor tissues consume more glucose than their normal counterparts, they convert glucose to lactate, via the reduction of pyruvate, even in the presence of oxygen, whereas normal tissues use pyruvate, derived from glycolysis, plus oxygen to produce ATP via mitochondrial respiration. These changes in glucose metabolism in cancer cells are known as the phenomenon of aerobic glycolysis. Cancer cells are supposed to produce ATP from aerobic glycolysis, compared to normal cells, which produce ATP mainly from oxygen-dependent respiration via mitochondrial respiration. The efficiency of producing energy from degradation of glucose is much lower in the first case. According to Warburg, cancer is a disease derive from an impairment of cellular respiration (Warburg, 1956a). Although cancer is now viewed as a disease resulting from cancer-causing genes that deregulate cellular proliferation, differentiation, and death, the relationship between these genes and the deregulation of energy production is only partially understood. Despite the controversy on the relation between aerobic glycolysis and cancer cell biology (Garber, 2004; Gatenby and Gillies, 2004), the widespread clinical use of positron-emission tomography (PET) in the assessment of viable tumors and recent findings make scientists revisit Warburg's theory. For example, during tumorigenesis, cells depend more and more on aerobic glycolysis and become least dependent on the mitochondrial machinery for ATP synthesis (Ramanathan et al., 2005).

Although the biochemical and molecular mechanisms leading to increased aerobic glycolysis in cancer cells are rather complicated, many factors could contribute to the changes of metabolic aspects of tumors, such as mitochondrial dysfunction, hypoxia and oncogenic signals, with similar metabolic consequences: the malignant cells become addited to aerobic glycolysis for ATP production. Because ATP generation via glycolysis is far less efficient (two ATP per glucose) than through oxidative phosphorlation (36 ATP per glucose), cancer cells have to consume far more

glucose to maintain sufficient ATP supply. The enhanced glucose uptake in cancer cells is also the basis for PET imaging. Due to the hyper-active metabolism and proliferation behavior in cancer cells, maintaining a high level of glycolytic activity is essential to fulfill the requisition of growth and survival. This metabolic feature has led to the hypothesis that glycolysis inhibition may severely interfere with ATP generation in cancer cells and thus may preferentially kill the malignant cells (Munoz-Pinedo et al., 2003; Xu et al., 2005).

One of the most important considerations in cancer chemotherapy is to kill cancer cells preferentially, without obvious toxicity to normal cells. Understanding the biological differences between normal and cancer cells is essential for the applicability and efficacy of any anticancer drugs. Since metabolic alterations are common in cancer cells of various tissue origins, targeting the glycolytic pathway may preferentially kill the malignant cells without harming normal cells since they do not rely that much on glycolysis for energy supply. It is likely that targeting aberrant metabolic pathway(s) in cancer cells could have broad therapeutic applications.

1.1. Glucose metabolism and cancer

Two main biochemical pathways of glucose metabolism have been identified. The Embden-Meyerhof pathway or glycolysis pathway is the best known pathway to degrade glucose into pyruvate. In addition, glucose is also degraded via the pentose phosphate pathway (PPP).

1.1.1. The glycolysis pathway

Within this pathway, one molecule of glucose is oxidized to 2 molecules of pyruvate. The following equation shows the overall glycolytic reaction:

Glucose + 2 ADP + 2 NAD^+ + 2 Pi --> 2 Pyruvate + 2 ATP + 2 NADH + 2 H^+

The glycolysis pathway can be seen as consisting of two separate phases. The first is regarded as preparatory phase since the chemical priming requires energy (ATP). The second is the pay-off phase since energy is yielded in the form of ATP. In

the first phase, two molecules of ATP are used to convert one molecule glucose to fructose 1,6-bisphosphate (F1,6BP). In the second phase one molecules F1,6BP is degraded to pyruvate, with the production of 4 molecules of ATP and two molecules of NADH (Figure 1).

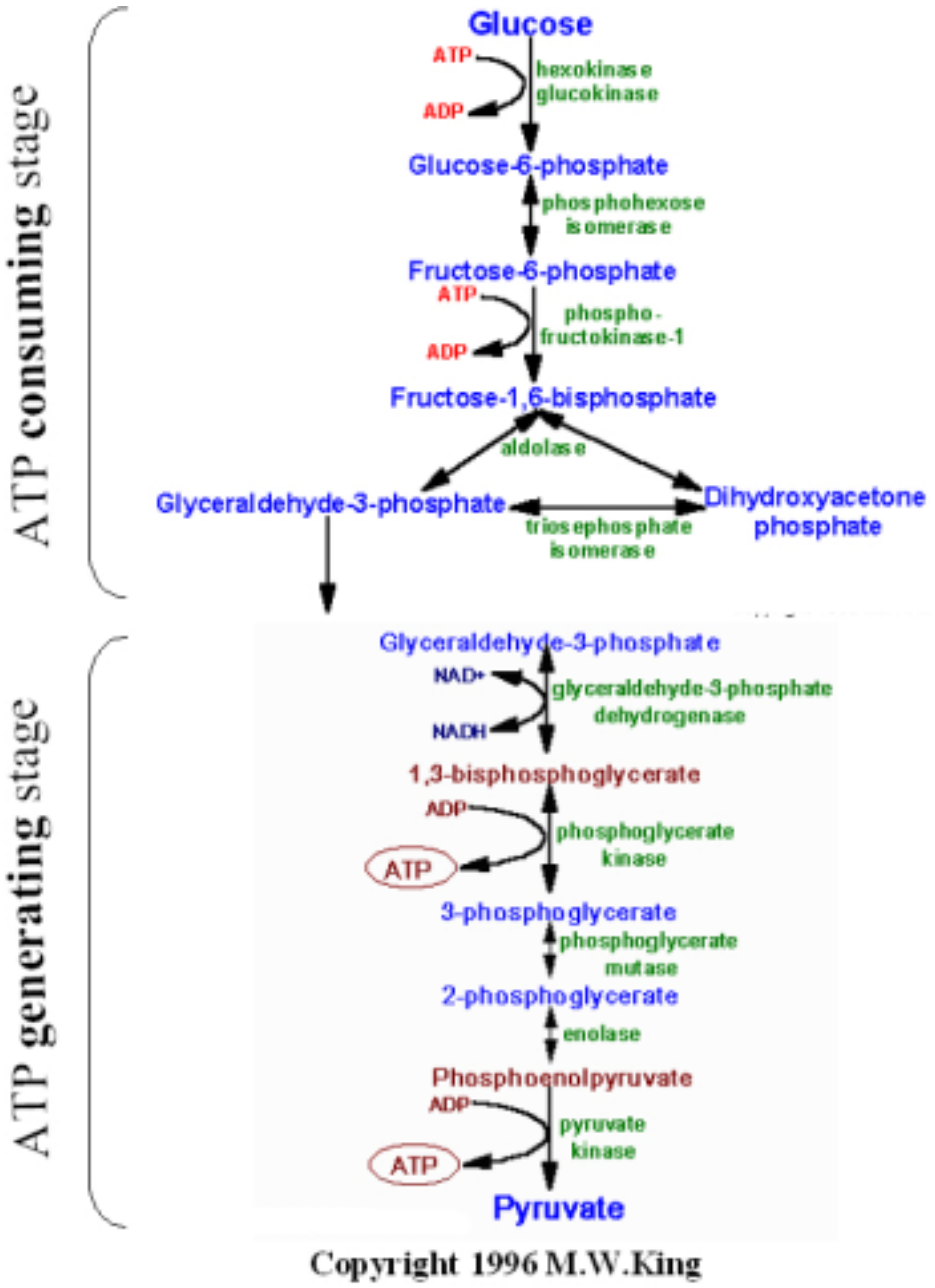

Figure 1 Diagram showing the pathway of glycolysis from glucose to pyruvate. Substrates and products are in blue, enzymes are in green. The two high energy intermediates whose oxidations are coupled to ATP synthesis are shown in red (1,3-bisphosphoglycerate and phosphoenolpyruvate).

Under aerobic conditions, the dominant product in most tissues is pyruvate and

the pathway is known as aerobic glycolysis. The end product pyruvate could also be converted to acetyl-CoA by pyruvate dehydrogenase (PDH) or oxaloacetate by pyruvate carboxylase. When oxygen is lacking, pyruvate is mainly converted to L-lactate by lactate dehydrogenase (LDH), known as anaerobic glycolysis.

1.1.2. The pentose phosphate pathway (PPP)

The pentose phosphate pathway (also called Phosphogluconate Pathway, or Hexose Monophosphate Shunt [HMP shunt]) is a process that serves to generate NADPH and the synthesis of pentose (5-carbon) sugars. The pentose phosphate pathway consists of an oxidative and a non-oxidative phase. The oxidation steps, utilizing glucose-6-phosphate (G6P) as the substrate, occur at the beginning of the pathway and are the reactions that generate NADPH. The reactions catalyzed by glucose-6-phosphate dehydrogenase and 6-phosphogluconate dehydrogenase generate one molecule of NADPH each for every molecule of glucose-6-phosphate (G6P) that enters the PPP (Figure 2A). The non-oxidative reactions of the PPP are primarily designed to generate R5P. Equally important reactions of the PPP are the conversion of dietary 5 carbon sugars into both 6 (fructose-6-phosphate) and 3 (glyceraldehyde-3-phosphate) carbon sugars, which can then be utilized by the pathways of glycolysis (Figure 2B). The non-oxidative pathway is controlled by transketolase enzyme reactions (Gibbs and Horecker, 1954; Horecker et al., 1954).

The primary functions of this pathway are:

1. It serves as an alternative pathway to degrade glucose.

2. It provides the cell with ribose-5-phosphate (R5P) needed for the synthesis of the nucleotides and nucleic acids.

3. It generates reducing equivalents, in the form of NADPH, for reductive biosynthesis reactions and redox regulation in cells.

Interestingly, inhibition of transketolase by oxythiamine seems to have anticancer activity (Rais et al., 1999), suggesting an important role of the pentose pathway in cancer.

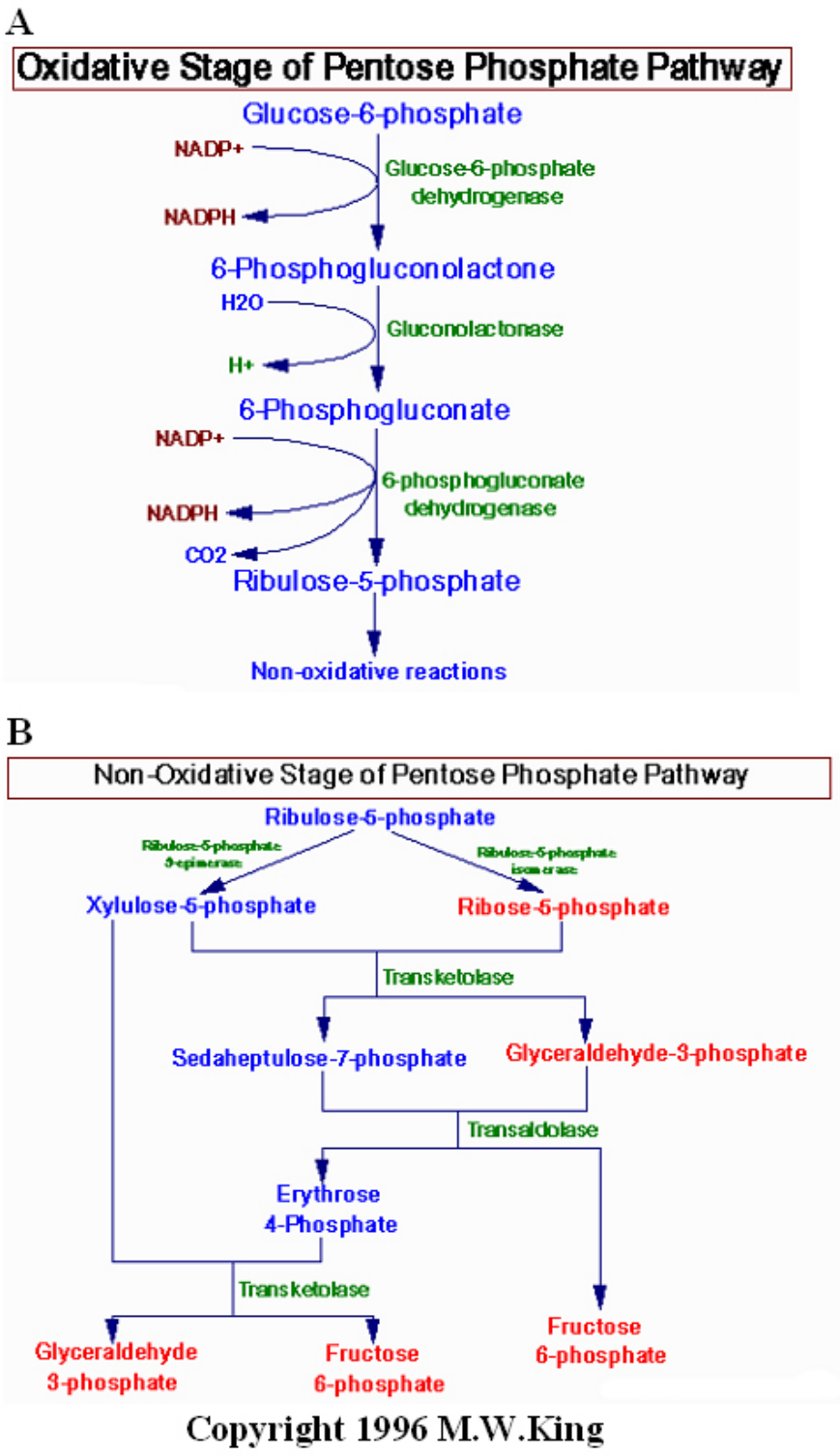

Figure 2 Diagram of the pentose phosphate pathway. (A) The oxidative stage of the PPP. In this stage, one mole of Ribulose-5-phosphate and two moles of NADPH are generated by oxidization of one mole of glucose-6-phosphate. (B) Ribulose-5-phosphate is further converted into 1. Ribose-5-phosphate for nucleic acids synthesis; 2. Glyceraldehyde-3-phophate; and 3. Fluctose-6-phosphate, both to enter glycolysis for degradation of pyruvate. Enzymes are in green, substrats or intermidiate products are shown in blue, end products are shown in red.

1.1.3. The Transketolase like protein 1 (TKTL1)

Transketolase is a thiamine-dependent diphosphate enzyme, which catalyzes a reversible reaction by transfer a two-carbon fragment, a glycolaldehyde residue, from a ketose (donor substrate) to an aldose (acceptor substrate). In the PPP, xylulose-5-phosphate, fructose-6-phosphate, sedoheptulose-7-phosphate, erythrulose, etc. serve as the donor substrates; ribose-5-phosphate, erythrose-4-phosphate, glyceraldehydes-3-phosphate, glycolaldehyde, etc. are used as the acceptor substrates (Kovina and Kochetov, 1998).

The TKTL1 gene represents one of three highly similar transketolase (-like) genes in the human genome (TKT, TKTL1, TKTL2). The TKT and TKTL1 share a similar gene structure, whereas the TKTL2 gene is an intronless pseudo-gene (Coy et al., 2005; Langbein et al., 2006). These three genes have more than 60% nucleic acid and amino acid sequence identity. Orthologues of TKT, TKTL1, TKTL2 were also identified in mice and rats. All transketolases including TKTL1 are highly conserved among species (Table 1).

Organism	**Gene**	**Locus**	**Description**	**Human Identity [%]**	**NCBI accessions**
dog (*Canis familiaris*)	TKTL1	X	transketolase-like 1	82.72*(n)* 79.53*(a)*	XP_538204.2
chimpanzee (*Pan troglodytes*)	TKTL1	X	transketolase-like 1	97.6*(n)* 94.8*(a)*	XP_001140116.1
rat (*Rattus norvegicus*)	TKTL1	Xq37	similar to transketolase-like 1	78.13*(n)* 69.46*(a)*	XP_001065706.1

mouse (*Mus musculus*)	TKTL1	X A7.3	transketolase-like 1	78.34*(n)* 70.03*(a)*	AF285571
fruit fly (*Drosophila melanogaster*)	CG8036	3R	transketolase	54*(a)*	NM_169232

Table 1 Comparison of TKTL1 orthologs among 5 spieces with human. *(a)* amino acids; *(n)* nucleic acid

The TKTL1 gene was originally considered as a pseudo-gene since the third putative coding exon harbours a stop codon. It turned out later that the authentic TKTL1 transcripts miss the stop codon-harboring exon (amino acids homologous to yeast transketolase amino acid residues 68-107) (Coy et al., 2005). TKTL1 is located in X28, one of few X chromosomal regions, in which a number of gene related to malignancy and cell cycle are mapped (Glinsky et al., 2003a; Glinsky et al., 2003b). The TKT and TKTL2 gene are not located in such cancer-related genomic regions. Notably, it was recently observed that TKTL1, but not transketolase (TKT) or transketolase-like protein 2 (TKTL2), is highly expressed in a variety of human cancer tissues (Coy et al., 2005; Langbein et al., 2006).

In yeast, an active-site H103 in transketolase is a possible enzymic group that binds the C1 hydroxyl group of the donor substrate and stabilizing the reaction intermediate (Wikner et al., 1995). Compared to the yeast transketolase, the human TKTL1 gene has the above-mentioned deletion of the stop codon-harboring exon including a His residue homologous to yeast H103. This leads to an altered substrate specificity and enzymatic activity concomtant with an increased Km values for the coenzyme thiamine. TKTL1 is enzymatically active performing a one-substrate reaction with xylulose-5-phosphate as sole substrate (Coy et al., 2005). The products of this one-substrate reaction are glyceraldehyde 3-phosphate and erythrulose (Bykova et al., 2001). The production of glyceraldehyde 3-phosphate can channel the PPP to the energy-yielding phase of the glycolysis pathway to generate ATP and

lactate. Glyceraldehyde 3-phosphate occurs as a reactant in the biosynthesis pathway of thiamine (Vitamin B_1), an essential substance that cannot be produced by the human body. Thiamine itself serves as a co-enzyme for transketolase (Langbein et al., 2006). This one-substrate reaction would also favor the production of pentose-5-phospate and NADPH needed for tumor growth, and to generate lactate through the metabolic intermediate glyceraldehyde 3-phosphate. This may provide a biochmecal clues suggest that TKTL1 protein may play an important role in altered glucose metabolism of tumors.

1.2. Mitochondria, metabolism and cancer

Mitochondria are dynamic intracellular organelles that generate most of the cell's supply of ATP via oxidative respiration, in addition, mitochondria also play an important role in generating apoptotic signals. Genetic and/or metabolic alterations in this organelle lead to a variety of human diseases including cancer. These alterations could be either causative or contributing factors.

1.2.1. Mitochondrial structure

A mitochondrion contains inner and outer membranes composed of phospholipid bilayers and proteins (Alberts, 2002). The two membranes, however, have different properties due to different protein mosaics. This double-membraned organization forms five distinct compartments within the mitochondrion. There is the outer mitochondrial membrane, the intermembrane space (the space between the outer and inner membranes), the inner mitochondrial membrane, the cristae space (formed by infoldings of the inner membrane), and the matrix (space within the inner membrane).

Outer membrane The outer mitochondrial membrane, which encloses the entire organelle, has a protein-to-phospholipid ratio similar to that of the eukaryotic plasma membrane. It contains numerous integral proteins called *porins*. Porins form large aqueous channels that permit the bidirectional passage of molecules of up to 5,000 Daltons in molecular weight (Alberts, 2002).

Inter membrane space The inter membrane space is the space between the outer

membrane and the inner membrane. Because the outer membrane is freely permeable for small molecules, the inter membrane space is chemically equivalent to the cytosol with respect to small molecules. Because proteins must have a special amino acid sequence to cross the outer membrane, the protein composition of this space is different than the protein composition of the cytosol. Of note, cytochrome c is resident within the inner membrane space (Chipuk et al., 2006).

Inner membrane The inner mitochondrial membrane contains proteins with four types of functions: Those that perform the oxidation reactions of the respiratory chain; the ATP synthase, which generates ATP in the matrix; specific transport proteins that regulate metabolite passage into and out of the matrix and protein import machinery.

Cristae The inner mitochondrial membrane forms numerous cristae, which expand the surface area of the inner mitochondrial membrane, enhancing its ability to produce ATP. Cristae are not simple random folds but rather invaginations of the inner membrane, which can affect overall chem-iosmotic functions (Mannella, 2006).

Matrix The matrix is the space enclosed by the inner membrane. It contains about 2/3 of the total proteins of a mitochondrion. The matrix is important for the production of ATP with the aid of the ATP-synthase contained in the inner membrane. The matrix contains a highly-concentrated mixture of hundreds of enzymes, in addition to the special mitochondrial ribosomes, tRNA, and several copies of the mitochondrial DNA genome. Of the enzymes, the major functions include oxidation of pyruvate and fatty acids, and the citric acid cycle (Alberts, 2002).

Mitochondria have their own genetic material, and part of the machinery to manufacture their own RNAs and proteins. The human mitochondrial DNA sequence consists of 16,569 base pairs encoding 37 total genes, 24 tRNA and rRNA genes and 13 peptide genes (Anderson et al., 1981). The 13 mitochondrial peptides in humans are integrated into the inner mitochondrial membrane, along with proteins encoded by genes that reside in the host cell's nucleus.

1.2.2. Mitochondrial functions

Energy production

The main function of the mitochondrion is the production of energy, in the form of adenosine triphosphate (ATP). Cells use acetyl-CoA mainly from glucose breakdown to generate ATP via the tricarboxylic acid cycle (TCA cycle) in mitochondria. The energy is used to perform the specific reactions necessary for cell survival and function.

The highest ATP production is achieved via oxidative phosphorylation (OXPHOS), which is carried out by mitochondrial respiratory chain or electron transport chain (ETC). A series of 5 enzyme complexes are embedded in the innner mitochondrial membrane (Hatefi, 1985; Saraste, 1999). The 5 enzyme complexes of the respiratory chain consist of ~90 subunits, 13 of which are encoded by the mitochondrial genome.

Table 2 Mitochondria Enzyme Information

		kDa	Polypeptides
Complex I	NADH dehydrogenase (or) NADH-coenzyme Q reductase	800	25
Complex II	Succinate dehydrogenase (or) Succinate-coenzyme Q reductase	140	4
Complex III	Cytochrome c -coenzyme Q oxidoreductase	250	9-10
Complex IV	Cytochrome c oxidase	170	13
Complex V	ATP synthase	380	12-14

The mitochondrial electron transport chain removes electrons from an electron donor (NADH or $FADH_2$) and passes them to a terminal electron acceptor (O_2) via a series of redox reactions. A proton gradient across the mitochondrial inner membrane is established coupled with this reaction. Complex I, III, and IV function as proton pumps in this case. The transmembrane proton gradient generated is used to generate ATP via ATP synthase.

Besides glucose breakdown, acetyl-CoA could have also been generated from oxidation of fatty acids. Fatty acids are one of the most important energy sources for cells. The breakdown of fatty acids is carried out either in peroxisomes or mitochondria. Only the oxidation of fatty acids in mitochondria produces energy products (Alberts, 2002). Fatty acids were degraded via β-oxidation, during which acetyl-CoA molecules are produced. **M**edium **C**hain **A**cetyl-CoA **D**ehydrogenase (MCAD) plays a major role in breakdown of fatty acids.

Mitochondria and programmed cell death

Mitochondria also play an important role in the regulation of cell death. Many pro-apoptotic proteins such as apoptosis inducing factor (AIF), Smac/DIABLO and cytochrome c are stored in mitochondria. When cells receive pro-apoptotic signals, such as cell stress, free radical damage or growth factor deprivation, proteins of bcl-2 family may activate the formation of permeability transition pores (PT pores) in the mitochondrial membrane, leading to the release of these pro-apoptotic proteins from the mitochondria through PT pores (Green and Reed, 1998).

1.2.3. Mitochondrial dysfunction and cancer

Mitochondria are involved either directly or indirectly in many aspects of altered metabolism in cancer cells (Peluso et al., 2000). There are distinct differences between the mitochondria of normal versus transformed cells (Pedersen, 1978; Weinhouse, 1955). For instance, cancer cells are normally addicted to aerobic glycolysis for energy supply since their mitochondrial functions are impared (Warburg, 1956a). This is reflected by the fact that various tumor cell lines exhibit differences in the number, size and shape of mitochondria relative to normal controls. In cancer cells mitochondria numbers are reduced, they are smaller in size and have fewer cristae, which all leads toimpaired activities (Carew and Huang, 2002; Pedersen, 1978; Pelicano et al., 2006). Mitochondrial DNA mutations are also commonly found in oncocytic tumors (Brandon et al., 2006; Copeland et al., 2002).

In addition to the fact that there are striking changes occuring in glucose metabolism, studies in human cancer patients also suggest that free fatty acid

metabolism is also increased (Hyltander et al., 1991). The changes include fatty acids synthesis, turnover, oxidation and clearance. Many lipid-mobilizing factors, such as fatty acids synthase and all the oxidation enzymes are enhanced during the process (Russell and Tisdale, 2002).

1.3. Reactive oxygen species (ROS) and cancer

1.3.1. The definition of ROS

Reactive oxygen species (ROS) is the phrase used to describe a variety of molecules and free radicals (chemical species with one unpaired electron) derived from molecular oxygen (Turrens, 2003). ROS are generally very highly mobile molecules and are highly reactive due to the presence of unpaired valence shell electrons. The formation of ROS in cells is via sequential reduction of O_2 due to leakages in the electron transport chain (ETC). Three main forms of ROS are listed below.

· superoxide anion ($O_2\bullet^-$)

· peroxide (hydrogen peroxide, H_2O_2)

· hydroxyl radical

The structure of these radicals is shown below, along with the name on the bottom (H_2O_2 appear as $O_2\bullet^{2-}$), blue dots represent paired electrons while red dots represent unpaired electrons. The most common ROS found in cells are O2•- and H_2O_2.

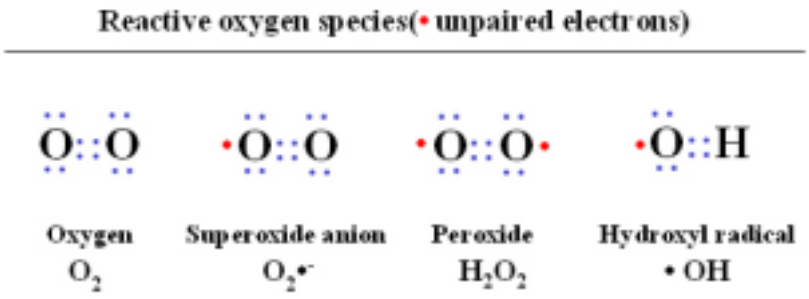

1.3.2. The formation of ROS

In normal aerobic life, oxygen-derived radicals are constantly generated. They are

formed in mitochondria ETC where oxygen is reduced. ROS are also formed in a variety of enzyme reactions, during which, ROS are produced as necessary intermediates and ROS are even functioning as signaling molecules.

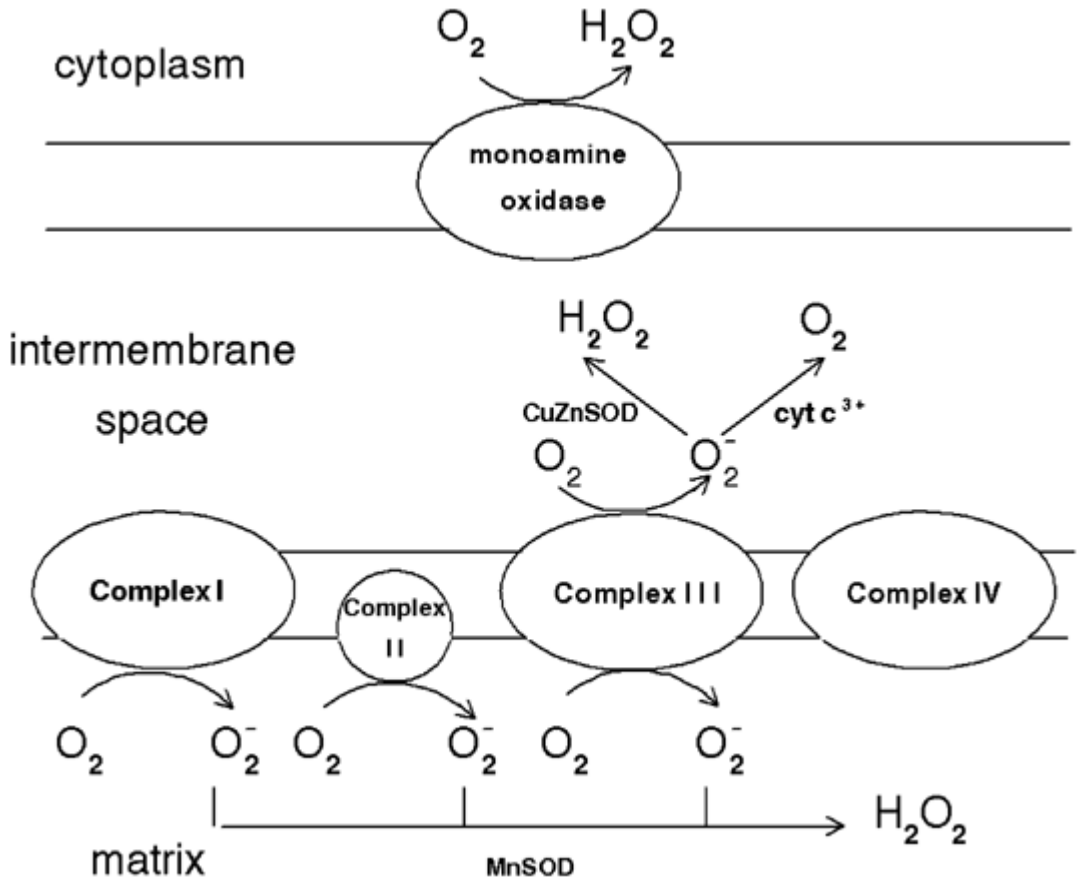

Figure 3 Sites of ROS formation in the respiratory chain (Turrens, 2003).

Since mitochondra are the place where most of the oxygen is consumed in cells, the majority of ROS are produced in this organelle via oxidative respiration. During normal physiological respiration, not all of the O_2 is fully reduced to H_2O, approximately 1%–2% of the O_2 consumed is converted into superoxide radicals (Turrens, 2003). The superoxide anion ($O_2^{\bullet -}$) is a relatively stable intermediate produced by one-electron reduction of O_2, $O_2^{\bullet -}$ can be regarded as the precursor of most ROS. Electron leakage occurring in various respiratory complexes leads primarily to $O_2^{\bullet -}$, which is mainly produced in several complexes, and subsequently, dismutated into hydrogen peroxide (H_2O_2) and oxygen spontaneously or via

superoxide dismutases (SOD). The production of superoxide anion is closely related to mitochondria coupling efficiency: uncoupled ETC could dramatically increases superoxide anion production (Andreyev et al., 2005; Turrens, 2003; Turrens et al., 1985).

1.3.3. The targets of ROS

ROS generated by mitochondria, or elsewhere in the cell, can cause damage to cellular macromolecules, including nucleic acids, phospholipids, and proteins.

Lipid modification Polyunsaturated fatty acid residues in phospholipids are extremely sensitive to oxidation (Esterbauer et al., 1991). The hydroxyl radical (OH•, generated via the Fenton reaction) is one of the most potent inducers of lipid peroxidation, although its reactivity limits its targets to macromolecules in the immediate vicinity of its site of formation..

DNA damage Oxidative damage to DNA causes modification of the purine and pyrimidine bases, the deoxyribose backbone, single and double strand–breaks, as well as cross-links to other molecules. Many of these DNA modifications are mutagenic, contributing to cancer, aging, and neurodegenerative diseases (Bohr, 2002; Croteau and Bohr, 1997).

Damage to protein Although protein oxidation is less well characterized, several types of damage have been demonstrated, including oxidation of sulfhydryl groups, oxidative adducts on amino acid residues close to metal-binding sites, reactions with aldehydes, protein-protein cross-linking, and protein fragmentation (Stadtman and Oliver, 1991; Starke-Reed and Oliver, 1989). The direct oxidation of amino acids, in particular lysine, arginine, proline, and threonine residues, promotes the formation of protein carbonyls (Beckman and Ames, 1998; Sohal, 2002). Formation of a protein carbonyl can dramatically alter the tertiary structure of a protein, resulting in its partial or complete unfolding. The unfolding increases protein hydrophobicity, which confers a strong propensity for the protein to form potentially deleterious protein-protein interactions. Hence, oxidation of proteins leads to loss of their normal functions, e.g., enzymatic activity, channel forming properties, etc., and to enhanced

susceptibility to proteolytic degradation.

1.3.4. Mitochondrial antioxidant defences

Mammalian mitochondria possess a multi-leveled ROS defense network of enzymes and non-enzymatic antioxidants. The non-enzymatic defenses are compounds that reduce oxidizing agents, for example the lipid soluble vitamin E and ubiquinone, or the water-soluble vitamin C and glutathione (Orrenius et al., 2007).

The first layer of ROS defenses is formed by the systems protecting membrane lipids from peroxidation. These are phospholipid hydroperoxide glutathione peroxidase (where present) (Lass et al., 1999; Packer et al., 2001).

The second layer of ROS defense is formed by enzymes which could remove ROS generated in mitochondria.

Superoxide dismutases (SOD) are enzymes that catalyze the conversion of two superoxides into hydrogen peroxide and oxygen. The benefit here is that hydrogen peroxide is substantially less toxic that superoxide. SOD accelerates this detoxifying reaction roughly 10,000-fold over the non-catalyzed reaction.

$$O_2^{-\bullet} + O_2^{-\bullet} \xrightarrow{SOD} O_2 + H_2O_2$$

SODs are metal-containing enzymes that depend on a bound manganese, copper or zinc for their antioxidant activity. In mammals, the manganese-containing enzyme is most abundant in mitochondria, while the zinc or copper forms predominant in cytoplasm (McCord et al., 1971).

Catalase. Superoxide dismutation leads to formation of H_2O_2 that *per se* can be quite toxic and has to be detoxified by other enzymes. One such enzyme is catalase, which converts H_2O_2 into O_2 and H_2O (Deisseroth and Dounce, 1970).

Glutathione. Glutathione (GSH, L-*gamma*-glutamyl-L-cysteinylglycine) is a tripeptide featuring the thiol (-SH) of cysteine as its active group. Various aspects of GSH metabolism, biochemistry, functions, and analysis have recently been extensively reviewed (Pastore et al., 2003). Mitochondria contain ~10-12% of total GSH amount in a cell, but due to their relatively small matrix volume the GSH

concentration in the mitochondrial matrix is clearly higher than that in the cytoplasm (Wahllander et al., 1979). Mitochondria lack enzymes needed for GSH biosynthesis; the intramitochondrial pool of GSH is replenished by rapid net uptake of GSH from the cytoplasm (Griffith and Meister, 1985; Martensson et al., 1990). The concentration of glutathione within mitochondria is in the range from 2 to 14 mM (Griffith and Meister, 1985; Wahllander et al., 1979); about ~90% of glutathione is in its reduced form, GSH (Wahllander et al., 1979).

Glutathione peroxidase. Classical glutathione peroxidase is probably the best studied mitochondrial enzyme that utilizes GSH for the reduction of H_2O_2 to H_2O. This enzyme is ubiquitously expressed in mammalian tissues (Lenzen et al., 1996) and can be detected in various cellular compartments including the mitochondrial matrix (Panfili et al., 1991; Utsunomiya et al., 1991) and intermembrane space (Panfili et al., 1991).

Glutathione reductase. Reduced glutathione can either scavenge superoxide and hydroxyl radicals non-enzymatically or by serving as an electron-donating substrate to several enzymes involved in ROS-detoxification (Dringen, 2000). In either case, GSH is oxidized to GSSG that cannot be exported to the cytosol (Olafsdottir and Reed, 1988) and has to be reduced back to GSH in the mitochondrial matrix. The reduction is catalyzed by a specific enzyme, glutathione reductase (GR, GSSG reductase, GSR, EC 1.8.1.7, formerly EC 1.6.4.2), which is present in the matrix of mitochondria (Panfili et al., 1991). This enzyme utilizes intramitochondrial NADPH as a source of reducing equivalents.

Peroxiredoxins. Peroxiredoxins, or thioredoxin-dependent peroxide reductases, are recently discovered peroxidases that reduce H_2O_2 and lipid hydroperoxides (Fujii and Ikeda, 2002).

Two isoforms of peroxiredoxins (Prx3 and Prx5) are found in mammalian mitochondria. Prx3 and Prx5 are ubiquitously present in various tissuesand function as antioxidants in mitochondria, protecting them against oxidative damage (Banmeyer et al., 2004; Fujii and Ikeda, 2002).

Both Prx3 and Prx5 are regenerated into their active form by disulfide

oxidoreductase thioredoxin (Trx2), a part of the mitochondrial thioredoxin system. Trx2 is reduced by thioredoxin reductase (TrxR2) that utilizes intramitochondrial NADPH as the source of reducing equivalents. Therefore, the efficient operation of Prx3 and Prx5 are dependent on efficient mitochondrial bioenergetics, similar to the GSH-linked systems described above.

Hypothetical antioxidant function of NAD(P)H. Some authors hypothesize that NAD(P)H *per se* can serve as a directly operating non-enzymatic antioxidant (Kirsch and De Groot, 2001). Mammalian mitochondria contain high concentrations of NADH and NADPH (~3-5 mM each), which can react with and scavenge oxygen-centered radicals such as trioxocarbonate and nitrogen dioxide, thereby preventing damage to mitochondrial proteins and DNA (Tischler et al., 1977).

1.3.5. ROS stress in cancer cells

The biological functions of ROS and their potential roles in cancer development and disease progression have been investigated for several decades. Cancer cells are known to be metabolically active and under increased oxidative stress, presumably associated with uncontrolled cell proliferation and dysfunction of metabolic regulation. Some key findings relevant to ROS-mediated stress in cancer, the potential underlying mechanisms, and biological consequences were summarized (Pelicano et al., 2004).

Growing evidence suggests that cancer cells in general are under increased oxidative stress compared to normal cells. Such evidence includes (a) enhanced ROS generation in cancer cells, (b) increased accumulation of ROS-mediated reaction products in cancer cells and their detection in the plasma and urine, (c) over-expression of antioxidant enzymes in response to oxidative stress in cancer cells (Konstantinov et al., 1987).

The expression of antioxidant enzymes, such as superoxide dismutases (SOD), catalase, and glutathione-*S*-transferase, is regulated by complex mechanisms, oxidative stress being a major factor that induces the adaptive expression of these enzymes (Storey, 1996). The activities of SOD, glutathione peroxidase (GPx), and

glutathione-*S*-transferase (GST) are increased significantly in the mitochondria of colorectal cancer tissues compared to adjacent normal tissues of the same subjects (Kanbagli et al., 2000). Increased SOD levels were also observed in breast cancer tissue from 23 patients (Punnonen et al., 1994). In summary, these findings suggest that malignant cells of different cancer types exhibit heterogeneity in levels of oxidative stress, associated with various expression levels of SOD and other antioxidant, detoxifying enzymes.

1.3.6. Mechanisms of increased ROS stress in cancer cells

Despite the prevalent ROS stress observed in a wide spectrum of human cancers, the precise mechanisms responsible for such stress remain to be defined. The degree of oxidative stress in a cell is dependent on the dynamic balance between ROS generating and eliminating processes. Several potential mechanisms are thought to contribute to the increased ROS in cancer cells. First, oncogenic signals have been shown to cause increased ROS generation. The oncogene *c-myc*, for example, increases ROS generation, induces DNA damage, and mitigates p53 function. This is thought to be a mechanism for oncogene-induced genetic instability (Behrend et al., 2003; Vafa et al., 2002). Another possible mechanism by which cancer cells generate increased amounts of ROS may involve malfunction of the mitochondrial respiratory chain. The fact that cancer cells exhibit an increased dependency on glycolysis to meet their ATP need (the Warburg effect) may reflect an inefficient ATP generation in mitochondria, or “respiration injury” (Warburg, 1956a, b). Because the mitochondrial respiratory chain is the major site of ROS generation due to electron bifurcation, malfunction of the mitochondrial respiratory chain associated with mtDNA mutations is likely to result in more free radical production due to increased “leakage” of electrons from the respiratory complex. In fact, there seems to be a correlation between mtDNA mutations and increased ROS contents in primary leukemia cells isolated from patients (Carew and Huang, 2002). Cancer cells in general are metabolically active and require a high level of ATP supply to maintain their active biochemical functions associated with uncontrolled cell growth and proliferation. This

energy demand places a further stress on the mitochondrial respiration chain, and is likely to contribute to increased ROS generation. Since the intracellular level of ROS depends on the balance between ROS generation and elimination, a decrease in the expression or the activity of antioxidant enzymes may also cause ROS accumulation.

Increase in ROS stress can induce various biological responses, ranging from a transient growth arrest and adaptation, increase in cellular proliferation, DNA damage and genetic instability, cellular injury and cell death and alterations in drug sensitivity (Davies, 1999; Pelicano et al., 2004). The actual outcomes are likely to be dependent on the cellular genetic background, the types of the specific ROS involved, and the levels and duration of the ROS stress.

1.4. Hypoxia, energy metabolism and cancer

As a tumor incrases in size, the existing vasculature supplies nutrient for its growth. When nutrient and oxygen are deprived, the outside of the tumor still grows, but the center will die of necrosis or apoptosis or both (Dang and Semenza, 1999). Tumors acquire the ability to obtain nutrients or oxygen by modifying the surrouding microenvironment to provide adequate supply vessels (angiogenesis), or by disseminating to different areas of the organism where nutrients are more readily available (metastasis) (Harris, 2002). In most cases, tumors must adapt to the hypoxic environment. The transcription factor hypoxia-inducible factor (HIF) directly transcribes genes involved in the regulation of glycolytic metabolism for hypoxic adaptation as well as genes involved in angiogenesis and metastasis. Included among these genes are vascular endothelial growth factor (VEGF), erythropoietin (EPO), glucose transporters (GLUT), and nearly all glycolysis enzymes (Semenza, 2003).

1.4.1. Hypoxia-inducible factor (HIF)

Most, if not all, aerobic species express the highly-conserved transcriptional complex HIF-1, which is a heterodimer composed of two basic helix-loop-helix proteins, HIF-1α and the aryl hydrocarbon nuclear translocator (ARNT or HIF-1β),

both of which are ubiquitously expressed (Wang et al., 1995). The regulation of the HIF-1 complex is mainly dependent on the degradation of the HIF-1α subunit. HIF-α is rapidly destroyed by a mechanism that involves ubiquitylation by the von Hippel-Lindau tumor suppressor (pVHL) E3 ligase complex. This process is suppressed by hypoxia and iron chelation, allowing transcriptional activation. HIF-1α accumulates in the presence of the iron displacing metals like cobalt or under hypoxic conditions. A family of prolyl hydroxylase enzymes (PHD) regulates the binding of pVHL to HIF-1α by hydroxylating key proline residues on the HIF-1α protein (Huang et al., 1998; Jaakkola et al., 2001).

1.4.2. HIF and energy metabolism

HIF-1 activation is highly associated with cancer cell growth and survival, tumor development, tumor angiogenesis, and poor clinical prognosis (Harris, 2002; Kung et al., 2000). The HIF-1 complex binds to hypoxia-resposive elements (HREs) in promoters of target genes. HRE elements are found in the promoters of cell surface glucose transporter GLUT1 and almost all the core enzymes of glycolysis. HIF-1 also directly contributes to the inhibition of OXPHOS. OXPHOS is governed by the availability of its two major substrates: oxygen and pyruvate. Pyruvate is the end product of glycolysis and enters the mitochondria after having been converted to acetyl-CoA by the pyruvate dehydrogenase complex (PDH). This reaction is irreversible and a critical control point of energy metabolism. PDH activity is inhibited through phosphorylation by pyruvate dehydrogenase kinase (PDHK), which is a HIF-1 target gene (Kim et al., 2006; Papandreou et al., 2006). Inhibition of PDH leads to the cytoplasmic accumulation of pyruvate, which is then converted to L-lactate by another HIF-1 target gene lactate dehydrogenase (LDH). The observations led to the idea that the glycolytic switch is through a specific transcriptional program initiated by HIF-1 (Semenza et al., 1994).

A number of experimental studies have shown that besides the end products of glycolysis, pyruvate and lactete, some major metabolites in the TCA cycle stabilize HIF-1α (Lu et al., 2002; Pollard et al., 2005; Selak et al., 2005). Since the

hydroxylation of HIF-1α by prolyl hydroxylases uses 2-oxoglutarate as co-substrate and generates succinate as an end product (Schofield and Ratcliffe, 2004), the increase of succinate in the TCA cycle antagonizes HIF hydroxylation, leading to HIF activation. Fumarate is another metabolite in TCA cycle, which could competitively blocking 2-oxoglutarate binding to prolyl hydroxylases, thereby leading to HIF stabilization (King et al., 2006).

1.4.2. HIF provides tumors with survival advantages

It is conceivable that during rapid progression, most of tumor cells are under hypoxic conditions. The adaptation to an anaerobic state provides tumors with survival advantages. On the other hand, stabilization of HIF-1 under hypoxic conditions mediates neovascularization, which provides nutrient supply needed for tumor survival and growth. In addition, HIF-1 plays a major role in enhancing glycolysis, which rapidly generates ATP in the cytosol. The breakdown of glucose provides necessary precursors for the synthesis of nucleotides (via the Pentose Phosphate Pathway), and amino and fatty acids (from glycolytic and TCA cycle intermediates, mainly acetyl-CoA) (Coy et al., 2005).

1.4. Objectives

Oncogenes and metabolism are required for full malignant tumors, TKTL1 is overexpressed in many tumor types, especially in advanced malignant tumors or metastatic areas of tumors. The aim of this study is to investigate the role TKTL1 plays in cancer cell growth, viability and malignancy.

In order to analyze the functions of TKTL1, we generated TKTL1-suppressed HCT116 cells (human colon carcinoma cell line). Since TKTL1 is an enzyme involved in the Pentose Phosphate Pathway (PPP), which is an alternative glucose degradation pathway, changes in the metabolic features of HCT116 with suppressed TKTL1 will be determined. As aerobic glycolysis is the major manner for glucose oxidation, the contribution of TKTL1 to the addiction to the unefficient ATP

producing pathway will be studied. The PPP also provides cells with ribose-5-P, precursors for nucleic acids, we would like to know whether suppression of TKTL1 leads to shortages of nucleic acids needed for cell growth and replication. The PPP is also an important pathway to produce NADPH, an antioxidant agent to protect cells from oxidative stress, so we are interested in whether TKTL1 suppression leads to changes in NADPH production, thus affect the anti-ROS defences of cells.

HIF-1α is a putative link between metabolism and cancer (Esteban and Maxwell, 2005), we want to address the question whether metabolic changes mediated via TKTL1 suppression influence HIF-1α functions. Lactic acids produced by aerobic glycolysis are closely related to tumor malignancy (Walenta et al., 2000), therefore, we will use several in vitro assays to assess invasiveness, migration and transformation of HCT116 cells upon TKTL1 suppression.

Finally, we want to study the tumor formation and growth ability of TKTL1-suppressed HCT116 cells in nude mice xenograft model to get first hand data whether by suppression of TKTL1 could lead to retarded tumor growth, which may be very useful for anti-cancer treatment strategies.

2. Materials and Methods

2.1 Materials

2.1.1. siRNA oligos

The siRNA oligos used in this study are listed below.

siRNA Oligos	offset	Target sequences (from 5'end to 3' end)
TKTL1-1	1406	ACC AGA AAC TAT GGT TAT TTA
TKTL1-2	2175	AAG TGT TTC CTT CGT GAA TAA
TKTL1-3	560	CGA GCA CTG CAT AAA CAT CTA
TKT	263	AAT CCG CAC AAT GAC CGC TTT

Table 3. **Human TKTL1 and TKT mRNA sequence as taken from accession number:** NM_012253 and NM_001064 respectively. All siRNA oligos were purchased from Qiagen.

2.1.2. Primer sets

The primer pairs used in this study are listed below.

Gene	Forward primer	Reverse primer	Fragment
RT-PCR primers			
β-actin	ACAATGAGCTGCGTGTGGCT	TCTCCTTAATGTCACGCACGA	375bp
TKTL1	GCTGAACAAAACATGGTGAGC	ACATCCCCTTGGCATTGGCT	148bp
qRT-PCR primers			
β-actin	ACTCTTCCAGCCTTCCTTC	ATCTCCTTCTGCATCCTGTC	171bp
TKTL1	AAGCCTTTGGGTGGAACACTTA	CTGAGAAGCCTGCCAGAATACC	80bp
TKTL2	AAACTAGGCTTATTTCTAAAAAGTCAAG	GGCTTTGCTTTAAAAGAAACAG	140bp
TKT	TGTGTCCAGTGCAGTAGTGG	ACACTTCATACCCGCCCTAG	176bp
CD133	GCGTGATTTCCCAGAAGATA	CCCCAGGACACAGCATAGAA	144bp
HIF1α	GAATGCTCAGAGAAAGCG	AGATTTGCATCCTTTTACACG	139bp
GAPDH	ATGACATCAAGAAGGTGGT	CATACCAGGAAATGAGCTTG	177bp
MnSOD	ACTGCAAGGAACAACAGGCCT	CTCCCACACATCAATCCCCA	52bp

hMCAD	TGCCCTGGAAAGGAAAACTTT	GTTCAACTTTCATTGCCATTTCAG	89bp
Prx3	TTGCAGGGAGATGGCTCAGCG	GTCCACACCACTGTGCGTGG	285bp
Catalase	GAATCGCATTCTTAGGCTTCTC	GACAATCAGGGTGGTGCTCC	343bp
Prx5	CCAATCAAGGTGGGAGATGCC	GCAGGTGTGTCTTGGAACATC	154bp
PGC1α	GGCAGTAGATCCTCTTCAAGATC	TCACACGGCGCTCTTCAATTG	262bp
PDK2	AGGACACCTACGGCGATGA	TGCCGATGTGTTTGGGATGG	162bp
Sirt4	ACTTCGTAGGCTGGCCTCAATTCT	ACATCTGGTTTCAGATGGCCTCCA	367bp
Sirt6	AGAGCTCCACGGGAACATGTTTGT	ATGTACCCATCGTGATGGACAGGT	257bp
Cloning PCR primers			
TKTL1-HA	GGGAAGCTTGCCACCATGGCGGATGCTGAGGCGA	GGGTCTAGATTAAGCGTAATCTGGAACATCGTATGGATAGTTCAGCAACATGCAT	
TKTL2-HA	GGGAAGCTTGCCACCATGATGGCCAACGACGCCA	GGGTCTAGATAAAGCGTAATCTGGAACATCGTATGGATACTTCATTAAAGTAAGTGT	
TKT-HA	GGGAAGCTTGCCACCATGGAGAGCTACCACAAG	GGGCTCGAGTAAAGCGTAATCTGGAACATCGTATGGATAGGCCTTGGTGATGAGG	
mTKTL1	GGGGAATTCAATGTCGGAAGCTGAGGC	GGGAGATCTCCGGTCATTAAGATGCATTTC	
mTKTL2	GGGGAATTCAATGGCCTTGGCCAGAGAT	GGGAGATCTCCTTTCATTACGGTATCTTTCAC	
mTKT	GGGGAATTCAATGGAAGGTTACCATAAG	GAAAGATCTCCGCCCTTGGTGACAAGG	
eGFP	GAAAAGCTTGCCACCATGGTGAGCAAGGGCGAGGA	GAATCTAGATTACTTGTACAGCTCGTCCA	
TKTL1	GGGGAATTCAATGGCGGATGCTGAGGCGA	GGGTCTAGATTAGTTCAGCAACATGCAT	
eGFP-	GAAAAGCTTGCCACCATGGTGAGCA	GAAGAATTCCCCTTGTACAGCTC	

TKTL1	AGGGCGAGGA	GTCCA	
shRNA construction primers			
shRNA #1	GATCCCCCAGAAACTATGGTTATTTAT TCAAGAGATAAATAACCATAGTTTCT GTTTTTGGAAA	AGCTTTTCCAAAAACAGAAACTA TGGTTATTTATCTCTTGAATAAATA ACCATAGTTTCTGGGG	
shRNA #2	GATCCCCGTGTTTCCTTCGTGAATAAT TCAAGAGATTATTCACGAAGGAAAC ACTTTTTGGAAA	AGCTTTTCCAAAAAGTGTTTCCTT CGTGAATAATCTCTTGAATTATTC ACGAAGGAAACACGGG	

Table 4. Primer sets from 5' end to 3' end. All primers were purchased from Invitrogen or in-house primer services.

2.1.3. Cell lines and culture media

Cell lines	description	Culture media
HCT116	Human colon carcinoma cell line which has a mutation in codon 13 of the ras proto-oncogene (information from ATCC database, cells from lab stock).	RPMI 1640, 10% FBS, 100U Penicillin + 100mg/ml Streptomycin, 2 mM L-GlutaMax™
HCT116 TR5	HCT116 cells clones which contains tet repressor constructs pcDNA6/TR (from Dr. H. Clevers, Utrecht The Netherlands).	RPMI 1640, 10% FBS (tetracycline free), 100U Penicillin + 100mg/ml Streptomycin, 2 mM L-GlutaMax™, 5µg/ml Blasticidin
NIH 3T3	Mouse fibroblast with high contact-inhibition (lab stock).	DMEM, 10% FBS, 100U Penicillin + 100mg/ml Streptomycin, 2 mM L-GlutaMax™
293T	Human embryonic kidney cells	DMEM, 10% FBS, 100U

	containing SV-40 large T antigen(lab stock).	Penicillin + 100mg/ml Streptomycin, 2 mM L-GlutaMax™

2.1.4. Plasmids

Name	Source
pcDNA3.1	Invitrogen
pSUPER•neo•GFP	From Dr. W. Walcack (DKFZ)
pSUPERior•puro	From Dr. I. Hoffman (DKFZ)
pcDNA™/TO	Invitrogen
pcDNA6/TR	From Dr. W. Feng (DKFZ)
Full Length cDNA Clone for human TKTL1	RZPD IRATp970A0125D
Full Length cDNA Clone for human TKTL2	RZPD DKFZp434L1717Q
Full Length cDNA Clone for human TKT	RZPD IRAUp969E1160D
Full Length cDNA Clone for murine TKTL1	RZPD PX00926B10
Full Length cDNA Clone for murine TKTL2	RZPD PX00623E18
Full Length cDNA Clone for murine TKT	RZPD IRAVp968A12128D

2.1.5. Buffers

1 × Phosphate-buffered saline (PBS)

4.3 mM $Na_2HPO_4 \cdot 7\ H_2O$ 1.4 mM KH_2PO_4

137 mM NaCl 2.7 mM KCl

pH 7.4

1× PBST

1× PBS 0.1% Tween® 20

1 × TE Buffer

10 mM Tris-HCl 1.0 mM EDTA

pH 7.5

MiR05 medium

0.5 mM EGTA 3.0 mM $MgCl_2$

K-lactobionate 60mM 20 mM Taurine

10 mM KH_2PO_4 20 mM HEPES

10 mM Sucrose 1.0 g/L BSA faction V

adjust pH to 7.1 with 5.0 M KOH

10 × Fixative Solution for cell senescence staining

20% formaldehyde, 2% glutaraldehyde in 10 × PBS

Staining Solution for cell senescence staining

40 mM citric acid/sodium phosphate 150 mM NaCl

2.0 mM $MgCl_2$ 5.0 mM potassium ferrocyanide

5.0 mM potassium ferricyanide 1.0 mg/ml X-gal

adjust to pH 6.0 with 1.0 M HCl

Cryopreservation medium

10% DMSO 50% FBS

40% defined cell culture medium

LB medium

1% NaCl 0.5% yeast extract

1% tryptone pH 7.0

autoclave before use

SOC medium

0.05% NaCl 0.5% yeast extract

2% tryptone 2.5 mM KCl

10 mM $MgCl_2$ 20 mM glucose

pH 7.0 autoclave before use

1× TAE

40 mM Tris-acetate 1.0 mM EDTA

pH 8.0

shRNA primers annealing buffer

100 mM potassium acetate, 30 mM HEPES-KOH

2mM Magnesium acetate pH7.4

DEPC treated ddH_2O

0.1% (w/v) DEPC was added in miliQ deionized H_2O and incubated overnight, then was autoclaved.

5 × protein Loading Buffer

0.313 M Tris-HCl (pH 6.8 at 25°C) 10% SDS

0.05% bromophenol blue 50% glycerol

20 × Reducing Agent

2.0 M DTT

1 × Blotting buffer for Western blot

20 mM Tris-base 150 mM glycine

20% methanol 0.1% SDS

pH 8.3

GSH-stock solution

125 mM Na_2HPO_4 6.3 mM EDTA

pH 7.5

Blocking buffer for immuno-blot

1 × PBS 500 ml

Milk powder (blotting grade) 15 g

Tween® 20 0.5 ml

4% paraformadehyde

4.0 g paraformadehyde in 100 ml PBS, several drops of 1.0 M NaOH added at 60 ^oC for complete dissolution, prepared freshly

1,000 × DAPI Stock Solution (10 μg/ml in ddH_2O)

100 μg DAPI 10 ml ddH_2O

aliquoted and stored in dark at –20 ^oC

2.1.6. Reagents and chemicals

30% H_2O_2 (H1009, Sigma-Aldrich)

10 × PCR reaction buffer (Perkin Elmer)

4′,6-diamidino-2-phenylindole, dihydrochloride (DAPI) (D1306, Invitrogen)

5 × protein Loading Buffer (R0891, Fermentas)

5,5′-Dithiobis(2-nitrobenzoic acid) (DTNB) (D8230, Sigma)

6 × Orange DNA Loading Dye (R0631, Fermentas)

0.05 % Trypsin, 0.53 mM EDTA•4Na (25300-054, Invitrogen)

Agarose (15510-027, Gibco)

Alexa Fluor® 488 goat anti-mouse IgG (H+L) (A11001, Invitrogen)

Alexa Fluor® 594 goat anti-mouse IgG (H+L) (A11005, Invitrogen)

Amersham HyperfilmTM ECL (28906837, GE Health)

Ammonium peroxodisulfate (APS) (1201.0500, Merck)

Anti AKT (9297, Cell Signaling)

Anti β-actin monoclonal antibody (A5316, Sigma)

Anti Cytochrome c (556433, BD Pharmingen)

Anti GFP (G6795, Sigma)

Anti HA monoclonal antibody (H3663, Sigma)

Anti HIF1α (ab1-250, Abcam)

Anti mouse IgG-HRP secondary antibody (A9044, Sigma)

Anti p21 (550833, BD Pharmingen™)

Anti phospho-AKT (4058, Cell Signaling)

Anti rabbit IgG-HRP secondary antibody (22927704, Promega)

Benzonase® Nuclease (E1014, Sigma)

Blasticidin S HCl (R210-01, Invitrogen)

Blotting grade milk powder (T145.2, ROTH)

β-Mercaptoethanol (1.15433, Merck)

Bovine serum albumine (BSA) (K41-001, PAA biotech)

Calf Intestine Alkaline Phosphatase (CIAP) (EF0341, Fermentas)

Cobalte (II) chloride hexahydrate ($CoCl_2$•$6H_2O$) (C8661, Sigma)

D-glucose measurement kit (10716251035, r-biopharm)

Diethyl pyrocarbonate (DEPC) (40718, Aldrich)

Dihydroethidium (D1186, Molecular Probes)

Dimethyl Sulfoxide (D2650, Sigma)

DL-Dithiothreitol (DTT) (D913, Sigma)

D-MEM (61965-026, Invitrogen)

DNase I, RNase free (04716728001, Roche)

dNTP (R0191, Fermentas)

Doxycycline hyclate (D9891, Sigma)

ECL solutions (PRN2106, GE Health)

EDTA•4Na•H_2O (E5391, Sigma)

EDTA-free Protease Inhibitor Cocktail (04693132001, Roche)

EGTA (E4378, Sigma)

Fast High Fidelity PCR kit (03553426001, Roche)

FBS (3302-p273105, PAN biotech)

Fluoprep (75521,bioMérieux)

G418 disulfate (A1720, Sigma)

GelCode® Blue Stain Reagent (24590, Pierce)

glucose-6-phosphate-dehydrogenase (10165875001, Roche)

Glutardialdehyde (4995.1 ROTH)

glutathione-reductase (G3664, Sigma)

Glycerol (7044, JT.Baker)

H_2DCFDA (D399, Molecular Probes)

HEPES (#1009, GERBU)

Hoechst 33342 (B2261, Sigma)

Imaging Plates (Siemens)

KH_2PO_4 (104873, Merck)

K-lactobionate (61312, Fluka)

KOH (P1767, Sigma)

L-gluta^{Max} (25030-024, Invitrogen)

Lipofectamine 2000 (11668-019, Invitrogen)

L-lactic acid measurement kit (11112821035, r-biopharm)

Matrigel (E1270, Sigma-Aldrich)

methylene blue (M9140, Sigma)

MG132 (474791, CalBiochem)

$MgCl_2 \cdot 6H_2O$ (63072, Fluka)

Milk powder (blotting grade) (T145.2, ROTH)

Mitotracker Red 580 (M22425, Molecular probes)

M-PER Mammalian Protein Extraction Reagent (78503, Pierce)

$NADP^+$/NADPH Assay kit (ECNP-100, BioAssay Systems)

NuPAGE® 4-12% Bis-Tris Gel (NP0323BOX, Invitrogen)

NuPAGE® Antioxidant (NP0005, Invitrogen)

NuPAGE® MOPS SDS running buffer (NP0001, Invitrogen)

NuPAGE® Transfer Buffer (NP0006, Invitrogen)

oligo $(dT)_{18}$ primer (SO132, Fermentas)

One Shot® TOP10 Electrocomp™ *E. coli* (C4040-50, Invitrogen)

OptiMEM (51985-026, Invitrogen)

Paraformaldehyde (0335.2, ROTH)

Phenethyl isothiocyanate (PEITC) (77972, Fluka)

Penicillin/streptomycin (10378-016, Invitrogen)

Power SYBR green master mix (4368577, Applied Biosystems)

Propidium iodide (P4170, Sigma)

Puromycin (P9620, Sigma)

QIAquick Gel Extraction Kit (28706,Qiagen, Germany)

QIAprep Spin Miniprep Kit (27106,Qiagen, Germany)

Restriction enzymes and Buffers (Fermentas)

RNase, DNase free (11119915001, Roche)

RNase Block (300151, Stratagene)

Rotiphorese® Gel 30 (3029.1, TOTH)

Roti®-Quant (K015.1, ROTH)

RPMI 1640 (21875-034, Invitrogen)

Senescence β–Galactosidase Staining Kit (#9860, Cell Signaling)

siRNA suspension buffer (Qiagen)

Sodium dodecyl sulfate (SDS) (2326.2, Roth)

Sodium Pyruvate (P5280, Sigma)

Sucrose (4621.1, Roth)

Super Script^{TM}II reverse transcriptase (18064-014, Invitrogen)

Taq polymerase (EP0281, Fermentas,Germany)

Taurine (T0625, Sigma)

TEMED (N,N,N',N'- Tetramethylethylenediamine) (1.10732, Merck)

Tetracycline free FBS (A15-109, PAA)

Tetramethylrhodamine, methyl ester or TMRM (T668, Invitrogen)

Tris-base (648310, Merck)

Trizol (15596-018, Invitrogen)

Tween 20 (2001, GERBU)

Whatman 3 mm paper (3030/347, Whatman GmbH)

Whatman Protran nitrocellulose membrane (10401196, Whatman GmbH)

Zeocin (212026. Invitrogen)

2.1.7. Materials and equipments

Name	Company
Materials	
Cell culture dishes (6cm/10 cm/15cm)	Nunc
Cell culture flasks and plates	Nunc
Cell scrapers	Costar
Cuvettes (0.2 cm gap)	Steinbrenner
Eppendorf tubes (1.5/2.0 ml)	Eppendorf

Falcon-tubes (15/50 ml)	BectonDickinson
Filters 0.2 µm	Shleicher & Schuell
Filters 0.45 µm	Nalgene
UV-cuvettes micro	BRAND
Glasses and coverslips	Neolab
Cell culture inserts (for 24-well plates)	BectonDickinson
96 well real-time PCR plates and covers	Applied Biosystems
PCR tubes (200 µl)	Kisker

Equipments	
Centrifuge for Eppendorf tubes 5417R	Eppendorf
Centrifuge for Falcon tubes 5804	Eppendorf
Electrophoresis chambers	BioRad
Cell culture incubator	Heraeus
Light microscope CK2	Olympus
pH-Meter calimatic 761	Knick
Power supplies EPS500/400 and 600	Pharmacia
PerkinElmer Ultra-View spinning disc confocal microscope	Perkin Elmer
LEITZ DMR workstation	Leica
Leica inverted microscope	Leica
FACSCalibur FACS machine	BectonDickinson
Mastercycler PCR machine	Eppendorf
Electronic balance	Sartorius
7300 Real-time PCR machine	Applied Biosystems
Oxygen measurement apparatus	Hansatech Instruments
Blood glucosemeter and teststrips	OneTouch
Spectro-Photometer	Hitachi
Isopropanol freezing containers	Nulgene

Rotor SLA 1500, SM24	Sorvall
Ultracentrifuge Sorvall Combi Plus	Sorvall
UV-transilluminator N90 LW 254/366 nm	Konrad Benda
XCell II ^{TM} Blot Module	Invitrogen
SpectraMax 340PC^{384}	Molecular Devices
Microtome RM2125	Leica

2.2 Methods

2.2.1. Cell culture and cryopreservation

Early passage HCT116 cells (ATCC CCL 247) were maintained as monolayers in RPMI 1640 supplemented with 10% heat-inactivated fetal bovine serum (FBS), 2mM L-glutaMax and 1% penicillin/streptomycin at 37°C and 5% CO_2 and 95% humidity. The cells were trypsinized and passaged 1-2 times a week. Up to 1×10^7 cells were removed by trypsin-EDTA solution and pelleted by centrifugation at 1200 rpm for 5 minutes. Cells were resuspended in cold Cryopreservation medium at a concentration of 1-4 million cells/ml. Cells were slowly cooled down in an isopropanol isolated container at –80 ^{o}C for at least 24 hours before long-term storage in liquid nitrogen. Frozen cells were thawed by agitating the cyropreservation tubes carefully and continuously at 37 ^{o}C in water bath. The thawed cells were resuspended and distributed in the cell culture flasks or dished with 20 mL pre-warmed fresh medium. The medium was replaced after 24 hours.

2.2.2. Transformation of bacteria

2.2.2.1. Preparing heat shock competent bacteria

Single colonies of wild *E.coli* DH5α or DH10B stains were picked from antibiotics free LB-agar plates (bacteria plates were kindly provided by RZPD). Then every single colony was inoculated into antibiotics free LB medium, incubated with shaking at 300 rpm at 37 ^{o}C. Overnight culture bacteria were diluted by 1:100 in 500 ml fresh LB, and incubated with shaking at 37° C until O.D. (600 nm) 0.5. Bacteria were then harvested by centrifugation at 5,000 rpm for 30 minutes at 4 ^{o}C. Pellets

were resuspended with 100 ml ice cold 100 mM $CaCl_2$ and incubated on ice for 20 minutes. Bacteria were pelleted by centrifugation at 5,000 rpm for 30 minutes at 4 ^oC, and then resuspended in 25 ml ice cold 100 mM $CaCl_2$ and incubated on ice for one hour. Bacteria were then pelleted again by centrifugation 5,000 rpm for 30 minutes at 4 ^oC and resuspended in 25 ml ice cold 100 mM $CaCl_2$ + 15 % glycerol. Mixtures were aliquoted at ~200 µl per tube and frozed in liquid nitrogen, then stored at -80 ^oC.

2.2.2.2. Heat shock transformation of $CaCl_2$ competent bacteria

In order to amplify bacterial plasmids, 1~10 ng plasmid DNAs were incubated for 30 minutes on ice with 50 µl *E.coli* DH5α or DH10B chemically competent cells (prepared as described in 2.2.2.1.) previously thawed on ice. The mixture was then incubated at 42 ^oC in a thermo incubator for 1 minute and cooled on ice immediately followed by dilution in 500 µl LB or SOC medium. The mixture was then incubated for 45 minutes with gentle shaking at 300 rpm at 37 ^oC. 50~100 µl bacteria were then spread on 10 cm LB-agar-plates containing corresponding antibiotics and incubated over night at 37 ^oC.

2.2.2.3. Electroporation (Transformation of electro-competent bacteria)

For each electroporation, 1~10 ng plasmid DNAs were incubated on ice for 30 to 60 seconds with 50 µl electrocompetent cells (One Shot® TOP10 Electrocomp™ *E. coli,* Invitrogen) previously thawed on ice. The DNA/bacteria mixtures were then pipetted into cold electroporation cuvettes (0.2 cm gap), prechilled on ice. The cuvettes were gently tapped, to ensure that the suspension of DNA/bacteria sits at the bottom of the cuvette, dried from outside, and placed into the Biorad electroporation chamber to deliver electrical pulse of 25 µF capacitance, 2.5 kV and 200 Ohm resistance. The electrical discharge was applied to the cells at the settings and then cuvettes were removed as quickly as possible after the pulse. The DNA/bacteria mixtures were then transferred to 1 ml prechilled SOC medium. The bacteria were incubated with gentle shaking (300 rpm) for 45 minutes at 37 ^oC and spread on LB-agar plates containing corresponding antibiotics.

2.2.3. Preparation and analysis of plasmid DNA

2.2.3.1. Plasmid DNA Miniprep

Plasmid DNA prepared with the Qiagen plasmid miniprep kit is suitable for DNA sequencing, restriction endonuclease digestion, and other applications. Single antibiotic-resistant colonies were picked from the LB-agar plate after overnight incubation and inoculated into LB medium containing antibiotics in a 20 ml culture tube. After overnight growth, bacteria were pelleted by centrifugation for 1 minute at 10,000 g in a 1.5 eppendorf tube. Bacteria were resuspended by adding 250 µl Buffer P1 with RNase A, and then lysed by adding 250 µl Buffer P2, mix thoroughly by inverting the tube 4-6 times. After incubating for 2-3 minuts (no longer than 5 minutes), the mixture was neutralized by adding 350 µl Buffer P3, after mixing by inverting 4-6 times, the lysate was centrifuged at 10,000 g for 10 minutes at Room Temperature (RT). The supernatant was loaded onto a fresh QIA prep spin column in a 2ml collection tube and the DNA was bound to the column by centrifugation for 1 minute at 10,000 g at RT allowing the lysate passing through the membrane. 500 µl Buffer PB added to the column was used to remove protein contamination by centrifugation for 1 minute at 10,000 g. 750 µl of wash buffer PE was added to the column to wash the DNA by centrifugation for 1 minute at 10,000 g. To remove ethanol from the column, the collection tube with the column was centrifuged again for 1 minute at 10,000 g to dry to column matrix. The plasmid DNA was eluted by adding 100 µl sterile deionized water or TE buffer directly to the binding matrix of the column and centrifuged for 1 minute. Five mililiters of overnight culture typically yielded 15 to 25 µg plasmid DNA prepared with Qiagen miniprep kit.

2.2.3.2. Plasmid DNA Maxiprep

Large amounts of plasmid DNA for transfections were prepared using the Qiagen Maxiprep kit. Single colonies picked from selective LB-agar plates were inoculated into a starter culture of 5 ml LB medium containing antibiotics and incubated at 37 ^{o}C for about 8 hours with vigorous shaking at 300 rpm. The starter culture was diluted into 300 to 400 ml selective LB medium and grown at 37 ^{o}C overnight with shaking at

300 rpm. The bacteria were harvested by centrifugation at 6,000 g in a Sorvall SLA 1500 rotor for 15 minutes at 4 ^{o}C. The bacterial pellet was completely resuspended with 10 ml lysis buffer P1. The lysate was incubated at RT for 5 minutes after adding 10 ml buffer P2 and thoroughly mixing. 10 ml prechilled buffer P3 were used to neutralize the solution via mixing immediately and thoroughly. The lysate was transferred into the barrel of the QIAfilter cartridge and incubated at room temperature for 10 minutes. The lysate was then filtered out by inserting the plunger into the QIAfilter Maxi cartridge and applied to a Qiagen-tip 500, pre-equilibrated with 10 ml buffer QBT. The tips were washed twice by 30 ml buffer QC and DNA were eluted with 15 ml buffer QF. Then 10.5 ml isopropanol were added to precipitate the eluted DNAs and then DNA pellets were collected by centrifugation at 15,000 g in a Sorvall MS24 rotor for 30 minutes at 4 ^{o}C. The DNA pellets were washed with 5 ml 70% ethanol with centrifugation at 15,000 g for 10 minutes at 4 ^{o}C and air-dried for 5-10 minutes. The plasmid DNA was redissolved in 300 µl sterile deionized water or TE buffer for later applications.

2.2.3.3. Spectrophotometric determination of DNA concentration

DNA samples were diluted as 1:500 in H_2O and measured at 260 nm in a spectrophotometer (Hitachi). OD260 absorption one corresponds to a concentration of 33 µg/ml for oligonucleotides and 55 µg/ml for double-stranded DNA. The purity of each preparation was determined by measuring the ratio of 260 nm and 280 nm with an optimal value between 1.8 and 1.95.

2.2.3.4. Restriction digestion of plasmid DNA with restriction enzymes

In order to analyze and characterize DNA clones and to clone specific DNA fragments into a plasmid vector, 1 to 10 µg of plasmid DNA were incubated with 5-10 units of the required restriction enzymes at appropriate incubation temperature and buffer as indicated by the supplier in a total reaction volume of 100 µl for 2 hours. To stop a restriction reaction, the mixture was incubated at 65 ^{o}C for 20 minutes which inactivates the majority of restriction enzymes. If the cleavage of plasmid DNA with two restriction enzymes required different buffers, the reactions were performed sequentially. After the first restriction reaction, the DNA was cleared using QIAquick

gel extraction or PCR purification kits (2.2.3.5). Then the second reaction was set up according to the supplier's information. Each restriction digest fragment was analyzed by agarose gel electrophoresis (2.2.3.6).

2.2.3.5. Purification of DNA fragments from enzymatic reactions

QIAquick PCR and gel purification kit was used to purify DNA fragments ranging from 100 bps to 10 kb from enzymatic reactions. In the case of the PCR purification kit, 3 volumes of buffer QG and 1 volume of isopropanol were added to the reaction. The mixture was then applied to a QIAquick spin column, placed in a 2 ml collection tube, and centrifuged at 13,000 rpm for 1 minute. The flow-through was discarded followed by adding 750 µl of washing buffer PE to the column and centrifugation for 1 minute at 13,000 rpm. After discarding the flow-through, the column was centrifuged again at 13,000 rpm for another minute to remove residual washing buffer. To elute the DNA, 50 µl autoclaved deionized water was added directly to the center of the QIAquick membrane. The column was placed into a new 1.5 ml eppendorf tube and was centrifuged at 13,000 rpm for 1 minute after incubation at RT for 1 minute.

2.2.3.6. DNA gel electrophoresis

DNA samples were first mixed with 6 × Orange DNA Loading Dye, 1-2% agarose gels were made in 1 × TAE buffer containing 1 µg/ml ethidium bromide to separate DNA fragments according to their size and to estimate the size and quantity of DNA fragments by comparison with a DNA marker of known length and quantity. 1% agarose gels were used to separate DNA fragments from 250 bps to 12 kb, whereas, for isolating small DNA fragments with size down to 100 bps, 2% agarose gels were used. The DNA samples were mixed with 6 × DNA loading buffer (Fermentas) before loading and electrhophoresis was run at 8-10V/cm for 40 to 90 minutes. The DNA was then visualized under 254 nm UV light and photographed.

2.2.3.7. DNA extraction from agarose gels

To clone a specific DNA fragment into a plasmid vector, the vectors and inserts DNA fragment were extracted and purified from agarose gels with the QIAquick PCR and gel extraction kit before ligation (2.2.3.9). After gel electrophoresis, the isolated

DNA fragments were visualized and excised from the agarose gel with a scalpel under 366 nm UV light. Three volumes of buffer QG were added to one volume of gel and the mixtures were incubated at 55 ^{o}C for 10 minutes with shaking at 300 rpm until the gel slice had completely dissolved. Then one volume of isopropanol was added and mixed by inverting tubes gently. The samples were applied to QIAquick columns and centrifuged for one minute. To wash the DNA in the columns, 0.75 ml of PE buffer were added to the column. The columns were centrifuged for one minute. After discarding the flow-through, the columns were centrifuged for an additional minute to completely remove ethanol from buffer PE. The DNA were eluted by adding 50 µl autoclaved deionized water or TE buffer to the center of the column membrane and centrifuging the column for 1 minute. All centrifugation steps were carried out at 13,000 rpm at RT. The quality of the eluted DNA fragments was determined by comparison with a DNA marker of known concentration on agarose gels.

2.2.3.8. Polymerase chain reaction (PCR)

PCR reaction mixtures were set up in a special hood and disposable tips containing hydrophobic filters were used in order to minimize cross-contamination. A master mix except the template DNA was prepared, and devided into 45 µl aliquots, templates DNA (5 µl) was finally added. The contents of each reaction (50 µl) are shown below:

10 × PCR buffer	5 µl
dNTP mix (2.5mM) thawed on ice	4 µl
forward primer (10 nmol/ml)	1 µl
reverse primer (10 nmol/ml)	1 µl
Taq DNA polymerase	0.5 µl
distilled water	33.5 µl
template DNA (≤ 1µg/reaction)	5 µl
Total	50 µl

A negative control without template DNA was included in every PCR experiment. When high fidelity amplification is needed, we used Faststart High Fidelity PCR System from Roche. Reaction mixture was set up as follows:

10 × PCR buffer (with $MgCl_2$)	5 µl
dNTP mix (10mM)	1 µl
forward primer (10 µM)	2 µl
reverse primer (10 µM)	2 µl
Faststart High Fidelity Enzyme Blend	0.5 µl
template DNA (100pg-10 ng)	1 µl
ddH_2O	38.5 µl
Total	50 µl

The PCR was started by 1 cycle of initial denaturation at 95 ^oC, followed by 25~35 cycles of 3 step cycling: each 30 seconds at 95 ^oC, 55 ~60 ^oC, and 72 ^oC for denaturation, annealing and extension respectively (elongation time depends on products length, ~ 1 minute per kb). One cycle for final extension at 72 ^oC for 7 minutes was performed. The samples were then cooled down to 4 ^oC. When needed, PCR products were purified by gel electrophoresis and QIAquick PCR purification kit (2.2.3.5-7)

2.2.4. Transfection

One day before transfection, cells were plated in appropriate amount of growth medium without antibiotics such that they will reach 80~90% confluency at the time of transfection. For each transfection sample, DNA or RNAi-Lipofectamine 2000 mixtures were prepared as follows. The DNA or RNAi samples were diluted in appropriate amount of OptiMEM medium without serum, and mix gently. Then Lipofectamine 2000 with OptiMEM medium without serum and incubate at RT for 5 minutes. After that, combine these two mixtures and mix gently, incubate for another 20 minutes. Then the solution was added to cultured cells. 4 hours later change to defined fresh medium containing antibiotics.

2.2.5. Transfection of siRNA oligos

In RNase-free enviroment, the lyophilized siRNA was suspended in 1ml siRNA

suspension buffer (Qiagen) to to obtain a 20 μM solution, then the solution was heated to 90 ^{o}C for 1 minute, cooled down in 37 ^{o}C water bath for 60 minute, then it is ready to use and could be stored in -20 ^{o}C. Lipofectamine 2000 (Invitrogen) was used to deliver siRNA into cell lines (2.2.4). In 35mm dish format experiment, 10-50 μL siRNA solutions (20 μM) were used for transfection. HCT116 cells were transfected with a control siRNA (targeting TKT) or 3 siRNA for TKTL1 (Table 3, all the oligos are from Qiagen) using Lipofectamine 2000 (Invitrogen). TKTL1 transcripts were detected by reverse transcriptase PCR using primer sets 5'-GCT GAA CAA AAC ATG GTG AGC -3'and 5'-ACA TCC CCT TGG CAT TGG CT-3', -actin was used as loading control with primer sets 5'-ACA ATG AGC TGC GTG TGG CT-3' and 5'-TCT CCT TAA TGT CAC GCA CGA-3'.

2.2.6. Plasmids construction

Full length of human TKTL1 was amplified with Fast Start High Fidelity PCR kit (Roche) from full length cDNA clone IRATp970A0125D (RZPD) containing HindIII site at the start codon and the antisense primer with HA tag, stop codon and XbaI site at the end, the PCR product and mammalian expression vector pcDNA3.1 (kindly provided by Dr. Sarah Chareza) were both digested with HindIII/XbaI, and the fragmengs were purified as described in 2.2.3.5. To prevent religation of the vector plasmid, the digested vector mixtures (100 μl) were incubated with 3 μl Calf Intestine Alkaline Phosphatase (CIAP) and 11 μl of 10 × buffer at 37 ^{o}C for 1 hour. Then PCR products and linelized vectors were ligated in the 20 μl reaction system as shown below.

10 × Ligation Buffer (Fermentas)	2 μl
T4 ligase (Fermentas)	1 μl
molar ratio 3:1 of PCR products and linelized vectors	12 μl
ddH_2O	5 μl
Total	20 μl

The reaction was carried on at room temperature for about one hour. For heat shock transformation (2.2.2.2.), 5 μl of the reaction mixture were used, for

electroporation (2.2.2.3.), 0.5 µl of the reaction mixture were used. After transformation, *E. coli* were cultured on ampicilin containing LB-agar plates at 37 ^{o}C overnight. Then ampicilin resistant clones were picked and analised by miniprep (2.2.3.1.) and restriction digestion (2.2.3.4.). Obtained clones with correct inserts were sequenced by Dr. Andreas Hunziker (DKFZ), the coding sequences and frames were verified manually according to reference. The other clones were constructed with the same protocol according to different restriction enzyme cutting sites and vectors, respectively.

2.2.7. Construction of shRNA expression vectors

In order to construct shRNA vectors #1 (TKTL1-I), with the same targeting sequence of siRNA #1, each 3 µg of forward primer 5'-GATCCCC CAGAAACTATGGTTATTTATTCAAGAGA**TAAATAACCATAGTTTCTG**TTTT TGGAAA-3' and reverse primer 5'-AGCTTTTCCAAAAACAGAAACTATGGTTA TTTATCTCTTGAA**TAAATAACCATAGTTTCTG**GGG-3' (5'- and 3'- stem sequences underlined and in bold face letters, respetively) were denatured at 95°C for 4 min, annealed at 70 °C for 10 min and then slowly cool down to 4 °C in 50 µl annealing buffer (100 mM potassium acetate, 30 mM HEPES-KOH pH7.4, 2mM Magnesium acetate). shRNA expression vectors pSUPER.neo+GFP (a gift from Dr. Henning Walczak, DKFZ) were digested with BglII/HindIII in 1 × Red buffer (Fermentas) and harvested by gel running and purification (2.2.3.6. and 2.2.3.7.). The double-stranded sequences were then ligated into BglII- and HindIII-digested pSUPER.neo.GFP (a gift from Dr. Henning Walczak, DKFZ), the ligation reaction was described in 2.2.6. After correct ligation, the BglII site was missing, in order to remove self-ligation products, 1µl BglII was added into the reaction mixture and incubated for 30 minutes. Then the reaction mixture were used for transforming bacteria, the positive clones were selected and verified by DNA sequencing. Using the same protocol, shRNA constructs #2 was constructed and sequenced. To generate shRNA constructs based on pSUPERior.puro, just follow the same protocol and replace vector with pSUPERior.puro. The vector maps are shown in Figure 4.

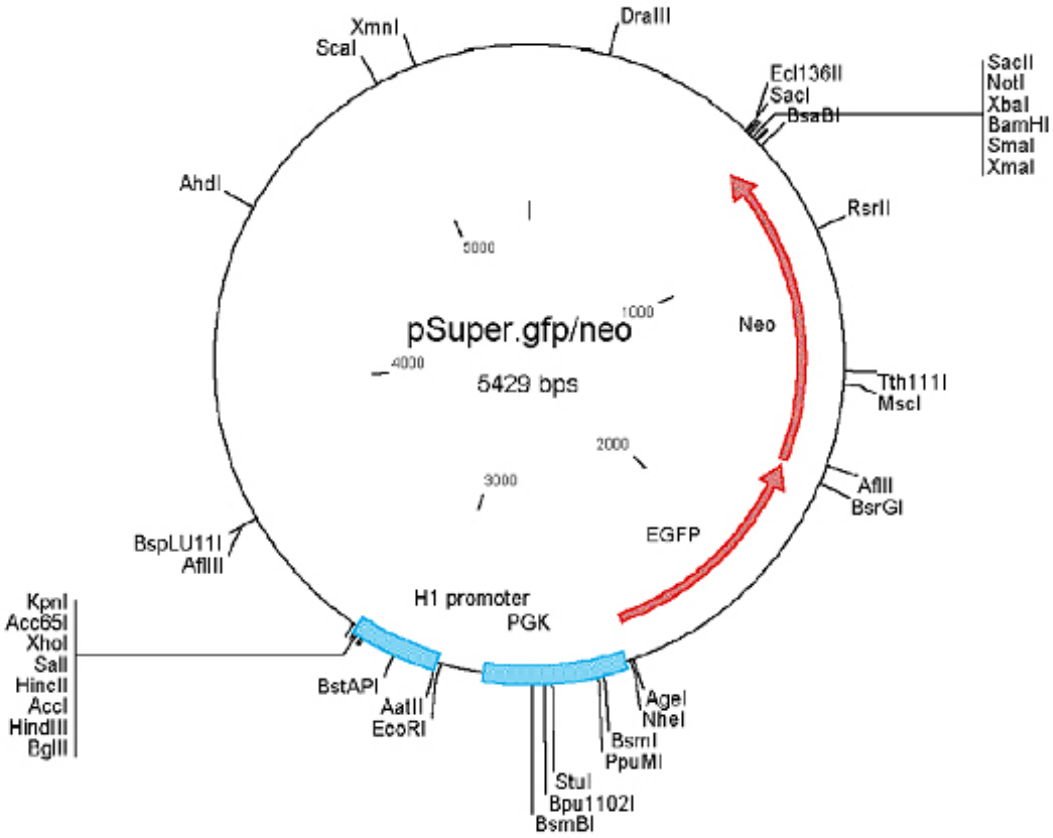
pSuper.gfp/neo
5429 bps
Neo
EGFP
H1 promoter
PGK
DraIII
XmnI
ScaI
Ecl136II
SacI
BsaBI
SacII
NotI
XbaI
BamHI
SmaI
XmaI
RsrII
Tth111I
MscI
AflII
BsrGI
AhdI
BspLU11I
AflIII
KpnI
Acc65I
XhoI
SalI
HincII
AccI
HindIII
BglII
BstAPI
AatII
EcoRI
AgeI
NheI
BsmI
PpuMI
StuI
Bpu1102I
BsmBI

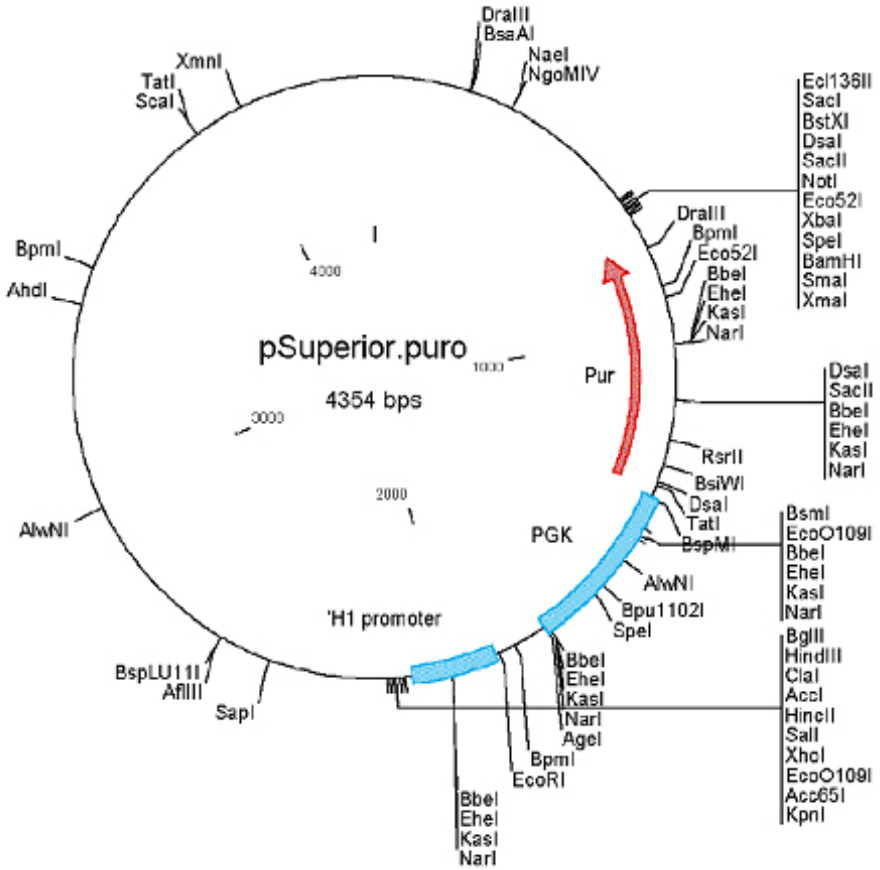
pSuperior.puro
4354 bps
Pur
PGK
'H1 promoter
DraIII
BsaAI
NaeI
NgoMIV
XmnI
TatI
ScaI
Ecl136II
SacI
BstXI
DsaI
SacII
NotI
Eco52I
XbaI
SpeI
BamHI
SmaI
XmaI
BpmI
AhdI
AlwNI
BsiWI
BspMI
Bpu1102I
BsmI
EcoO109I
BbeI
EheI
KasI
NarI
BglII
HindIII
ClaI
AccI
HincII
SalI
XhoI
Acc65I
KpnI
BspLU11I
AflIII
SapI
AgeI
EcoRI

Figure 4 Two shRNA expression vectors. pSUPER.neo+GFP has an H1 promoter to drive shRNA expression and also contains a Neomycin resistantgene, pSUPERior.puro has a Tet-regulated H1 promoter and a Puromycin resistant gene.

2.2.8. Preparation of G418 or puromycin resistant cell clones

About 1.5×10^5 HCT116 cells were seeded in 12-well plate in 500 µl medium without antibiotics. Transfections using 2 µl Lipofectamine2000 and 400 ng plasmid DNA per well was done as recommended by the supplier (2.2.4.). Two days after transfection, cells were transferred into 15cm dishes for about 14 days selection in medium containing 1mg/ml G418 or 1mg/ml puromycin (Sigma). Neo^R or $puro^R$ cell clones were sub-cloned into 6-well plates and maintained in medium with 500 µg/ml G418 or 1mg/ml puromycin.

2.2.9. RNA extraction and quantitative RT-PCR (qRT-PCR)

2.2.9.1. RNA extraction

Total RNA was extracted using Trizol® (Invitrogen) according to the manufacturer's instructions. Cells were plated in 6-well plates and cultured in selection medium till reaching confluency. Then medium were removed and cells were washed once with PBS. After the residual liquid was removed, 1 ml of Trizol was added into each well. Cells were homogenized by pippetting with filter tips. The homogenized samples were transferred to 1.5 ml eppendorf tubes and incubated for 5 minutes at room temperature to permit the complete dissociation of nucleoprotein complexes. Then 0.2 ml of chloroform was added and mix with shaking tubes vigorously by hand for 15 seconds and incubated at room temperature for 2 to 3 minutes. Samples were then centrifuged at 12,000 g for 15 minutes at 4 ^oC. Following centrifugation, the mixture separates into a lower red, phenol-chloroform phase, an interphase and a colorless upper aqueous phase. RNA remains exclusively in the aqueous phase. The aqueous phase were then carefully transffered to another clean eppendorf tube. RNA were precipitated by adding 0.5 ml isopropanol and mix well. The mixtures were then incubated at room temperature for 10 minutes. RNAs were

pelleted by centrifugation at 12,000 g for 10 minutes at 4 ^{o}C. Supernatant was removed and the pellets were washed by vortexed in 1 ml 75% ethanol. RNA were then pelleted again by centrifugation at 7,500 g for 5 mintutes at 4 ^{o}C and briefly air-dried for 5-10 minutes. Afterwards, RNA pellets were dissolved in 50 µl DEPC treated water. RNA concentration was determined by Spectrophotometer (Hitachi) at 260 nm and 280 nm and was calculated using the formular: 1 OD260 Unit = 40 µg/ml for single-stranded RNA. The pure RNA should have the OD260/OD280 ratio between 1.9-2.1.

2.2.9.2. DNase I treatment

When DNase treatment was required, 0.5 µg total RNA was incubated with 2 Units of RNase free-DNase I in DNAse I reaction buffer (Roche) at 37 °C for 30 minutes. The DNase was inactivated by addition of EDTA to a final concentraion of 5.0 mM and subsequent incubation at 75 °C for 10 minutes.

2.2.9.3. First strand cDNA synthesis

First strand cDNA was synthesized using SuperScript II reverse transcriptase kit (Invitrogen). For each reaction, 0.5-1.0 µg of total RNA were mixed with 1 µl of 100 µM $(dT)_{18}$ primers (Fermentas), 1 µl of 10 mM dNTP (Fermentas) and distilled water to 12 µl, denatured at 65 °C for 5 minutes and then chilled on ice. Then 4 µl of 5 First-Strand Buffer, 2 µl of 0.1 M DTT, 1 µl of RNase Block (Stratagene) were added and mixed well. The mixtures were incubated at 42 °C for 2 minutes, then 1 µl of SuperScript II reverse transcriptases were added and mixed by pippetting. Mix contents were incubated at at 42 °C for 50 minutes, then enzymes were inactivated at 70 °C for 15 minutes and the mixtures were cooled down to 4 °C. Synthesized cDNAs were stored at –20 °C.

2.2.9.4. Semi quantitative RT-PCR (semi qRT-PCR)

The cDNA abundance was normalized using the β-actin as an internal control. Concentration of cDNA was adjusted with ddH_2O in order to get comparable β-actin bands by about 25 cycles of amplification. Then the normalized cDNA samples were used to detect targeted gene expression, for example, TKTL1 for about 30-38 cycles of amplification.

2.2.9.5. Quantitative RT-PCR (qRT-PCR)

To determine changes in TKTL1 expression, qRT-PCR was performed using Power SYBR Green MasterMix (Applied Biosystems). Each reaction was prepared as follows: 12.5 µl Power SYBR Green MasterMix, 1 µl of 10 mM primer mix (forward and reverse), 2 µl cDNA, 9.5 µl ddH_2O. The reaction was carried under the following cycling conditions: 10 minutes at 95 °C, then 45 cycles of 95 °C for 15 seconds and 60 °C for 1 minutes in a on the ABI Prism 7300 mashine. The primer pairs are listed in Table 4. The expression of β-actin or GAPDH was determined as endogenous control. Calculations were performed using the δδCt method to determine fold-difference in shRNA transfected HCT116 cells relative to controls.

2.2.10. Protein analysis

2.2.10.1. Eukaryotic cell lysis

Cell lysates were prepared by suspending cell pellets in ice-cold lysis buffer [50 mmol/l Tris–HCl (pH 8.0), 150 mmol/l NaCl, 1% NP40, 0.5% deoxycholate, 0.1% SDS, proteinase inhibitor cocktail (Roche) and 2 mmol/l phenylmethylsulfonyl fluoride (PMSF)], incubated on ice for about 30 minutes. The lysate was centrifuged at 12,000 g for 1 minute at 4 ^oC, the supernatant (cytoplasmic protein fraction) was then collected and could be stored at –20 ^oC. The pellet (nuclear fraction) was re-suspended in ice-cold lysis buffer containing Benzonase® Nuclease (Sigma), incubated at 37 ^oC for 30 minutes and sonified for 1 minute to dissolve the pellet. Protein concentration was measured using the Bradford assay. Each 1 ml Bradford assay reaction contains 0.2 ml Roti-Quant solution (ROTH), 0.8 ml ddH_2O and 2 µl protein samples. Absorbance at 595 nm (OD_{595}) of the mixture was recorded. The concentration of protein is calculated as the following equation.

$c = OD_{595} \times 11$ (µg/µl)

The protein samples were mixed with 5 × Loading buffer (Fermentas) and 20 × reducing agent and then cooked at 70 ^oC for 10 minutes. The samples were then kept either on ice or –20 ^oC or immediately loaded on a SDS-PAGE (sodium dodecyl sulfate polyacrylamide gel electrophoresis). Equal amount of proteins (10–40 µg)

were loaded onto SDS polyacrylamide gels for electrophoresis.

2.2.10.2. Western blot

To separate proteins in the lysates by apparent molecular weight cellular lysate samples were subjected under denaturing condition in to SDS-PAGE. The gels were assembled first by polymerizing the separating gel in the gel chambers followed by the stacking gel which harboured the loading wells. The separating gel concentration used was 12.5% while the stacking gel was always made in a 7% concentration of polyacrylamide. The gels were assembled in self-assembled glass plates. The gel ingredients were as follows:

12.5% Separating Gel

Rotiphorese® Gel 30 (Acrylamide/Bis-acrylamide 30%/0.15%)	8.4 ml
Separating gel Buffer (1.5 M Tris-HCl pH 8.8; 0.4% SDS)	5.0 ml
ddH_2O	6.6 ml
10% APS	0.2 ml
TEMED (N,N,N',N'- Tetramethylethylenediamine)	10 µl

7% Stacking Gel

Rotiphorese® Gel 30 (Acrylamide/Bis-acrylamide 30%/0.15%)	3.5 ml
Separating gel Buffer (1.5 M Tris-HCl pH 8.8; 0.4% SDS)	3.75 ml
ddH_2O	7.75 ml
10% APS	0.12 ml
TEMED (N,N,N',N'- Tetramethylethylenediamine)	6 µl

Samples were loaded onto the stacking gel using either a Hamilton syringe or Gilson pipettes and electrophoresis was performed in a minigel chamber containing 1 × NuPAGE® MOPS Running buffer supplemented with 500 µl NuPAGE® antioxidant in the chamber at 200 V for ~1 hour. The gel was stained overnight with a solution of GelCode® Blue Stain Reagent after being briefly rinsed in tap water and washed with tap water before drying and scanning.

For protein analysis by immuno-blotting the unstained gel was directly subjected to western blotting. The stacking gel was removed and the separating gel,

nitrocellulose membrane, Whatman 3 mm paper, and the blotting sponge pads were separately soaked in 1 × NuPAGE® Transfer buffer (containing 20% mathanol). The transfer apparatus was assembled in the XCell II™ blot module with two pre-soaked blotting sponge pads placed into the cathode (-) core of the blot module followed by one piece of pre-soaked Whatman 3 mm paper and the separating gel. Air-bubbles were carefully and completely removed by glass pipette. The nitrocellulose membrane was then covered by one Whatman 3mm paper followed by two blotting sponge pads and the anode (+) core on top of the pads to tightly hold the gel/membrane sandwich thus ensuring complete contact of all the components. The gel membrane sandwich in the XCell II™ blot module was then placed vertically in XCell Sure Lock™ mini cell and transfer buffer was filled up into the XCell II™ blot module to cover the gel membrane sandwich. The "wet" transfer was done at 30 V for 75 minutes.

For "semi-dry" blotting the separating gel, nitrocellulose membrane, and Whatman 3 mm paper were separately soaked in 1 × blotting buffer for semi dry transfer. The transfer apparatus was assembled with 5 pieces of pre-soaked Whatman 3 mm papers on the anode (+) lower plate followed by the pre-soaked nitrocellulose membrane and onto it the separating gel whilst removing air bubbles with a glass pipette. The gel was then covered by three pieces of pre-soaked Whatman 3mm papers and air bubbles removed by glass pipette. The gel membrane sandwich was then covered with the cathode (-) plate and the "semi-dry" transfer conducted at 1.5 mA/cm^2 for 75 minutes.

2.2.10.3. Immuno-blot

After the transfer, the nitrocellulose membrane was then incubated in blocking buffer for ~1 hour to reduce background and then incubated with primary antibody overnight at 4 ^oC with gentle shaking. The antibodies were diluted in blocking buffer as indicated below. After removal of the primary antibody the membrane was then washed three times for 5 minutes each with 1 × PBST (1 × PBS with 0.1% Tween®20). After the wash the membrane was then incubated with secondary antibody diluted in blocking buffer to concentrations indicated below for ~1 hour with gentle shaking and then washed again twice for 5 minutes with 1 × PBST and once for 5 minutes with 1 ×

PBS. To image the specific proteins detected by the primary antibody, the membrane was rapidly developed using ECL™ Western blotting detection reagents (GE Healthcare), composed of an equal volume of ECL™ Western blotting detection reagent 1 and 2 for ~2 min and the signals were captured on the Amersham Hyperfilm™ ECL (GE Healthcare) for a time ranging from 5s to 3 min. The hyper film was then developed in the AGFA developing machine. The image observed on the film were signals derived from the unequal distribution of peroxidise activity from peroxidise conjugated secondary antibody. The secondary antibody bound unequally to the primary antibody specific for a cell antigen gives the position of the antigen when developed by the ECL solutions.

Anti β-actin	1:10,000
Anti p21	1:1,000
Anti AKT	1:1,000
Anti pAKT	1:1,000
Anti HA	1:1,000
Anti eGFP	1:5,000
Anti cyclin D1	1:1,000
Anti mouse IgG-HRP	1:5,000
Anti rabbit IgG-HRP	1:5,000

2.2.11. D-Glucose consumption and L-Lactic acid production assay

Cells were plated in 12-well plates at the density of 4×10^4 per well. After cells attached (in about 12 hours), 500 µl of medium was changed and 100 µl was collected after certain period of time. All medium collected was then applied for D-Glucose and L-Lactic acid determination using D-Glucose and Lactate acid detection kits (r-biopharm, Darmstadt), the consumed D-Glucose and produced L-Lactic acid were calculated accordingly.

2.2.11.1. D-Glucose concentration assay

D-Glucose concentration was measured via UV-method. D-Glucose is phosphorylated to D-glucose-6-phosphate (G-6-P) in the presence of the enzyme

hexokinase (HK) and adenosine-5'-triphosphate (ATP) with the simultaneous formation of adenosine-5'-diphosphate (ADP) (1).

(1) D-Glucose + ATP ---------> G-6-P + ADP

In the presence of enzyme glucose-6-phosphate dehydrogenase (G6P-DH), G-6-P is oxidized by nicotinamide-adenine dinucleotide phosphate (NADP) to D-gluconate-6-phosphate with the formation of reduced nicotinamide-adenine dinucleotide phosphate (NADPH) (2)

(2) G-6-P + $NADP^+$ ---------> D-gluconate-6-phosphate + NADPH + H^+

The amount of NADPH formed in this reaction is stoichiometric to the amount of D-Glucose. The increase in NADPH is measured by means of its light absorbance at 340 nm.

Two solutions are in D-Glucose kit. Solution 1: approximate 2.5 mg/ml $NADP^+$ and 5.8 mg/ml ATP; solution 2: approximate 290 U/ml hexokinase and 145 U/ml G6P-DH.

Reaction suspension for samples was made by mixed 1.0 ml sulotion 1, 0.1 ml samples (with 1:5 dilution) and 1.9 ml ddH_2O, in blank group, 0.1 ml ddH_2O replaced samples. Part of the suspension (1.0 ml) was transferred to an UV-cuvette with 1.0 cm light path (BRAND), and the absorbance at 340 nm was recorded as (A_1). Then 0.02 ml of solution 2 was added and mixed. About 10-15 minutes later, the absorbance of the suspension was recorded again at 340 nm (A_2) until the absorbance increased constantly. The absorbance differences (A_2-A_1) were determined for both, blank and samples. The absorbance difference of blank was subtracted from the absorbance difference of the samples to make ΔA.

$\Delta A = (A_2\text{-}A_1)_{\text{sample}} - (A_2\text{-}A_1)_{\text{blank}}$

D-Glucose concentration was then calculated according to the general equation:

$c = 0.864 \times \Delta A$ (g /l)

2.2.11.2. D-Glucose concentration assay

L-lactic acid concentration was measured via UV-method. In the presence of L-lactate dehydrogenase (L-LDH), L-Lactic acid (L-lactate) is oxidized to pyruvate by nicotinamide-adenine dinucleotide (NAD) (1).

(1) L-Lactate + NAD^+ <---------> Pyruvate + NADH + H^+

The equilibrium of the reaction lies on the side of lactate. By trapping pyruvate in a subsequent reaction catalyzed by the enzyme glutamate-pyruvate transaminase (GPT) in the presence of L-glutamate, the equilibrium can be displaced in favour of pyruvate and NADH (2).

(2) Pyruvate + L-glutamate <---------> L-alanine + 2-oxoglutarate

The amount of NADH formed in the above reactions is stoichiometric to the amount of L-lactic acid. The increase in NADH is determined by means of its light absorbance at 340 nm.

Four solutions are in L-lactic acid kit. Solution 1: glycylglycine buffer, pH 10.0, 14.7 mg/ml L-gutamic acid; solution 2: 35 mg/ml NAD; solution 3: 1.57 U/µl GPT; solution 4: 5.4 U/µl L-lactate dehydrogenase.

Reaction suspension for samples was made by mixed 1.0 ml sulotion 1, 0.2 ml solution 2, 0.02ml solution 3, 0.1 ml samples (with 1:5 dilution) and 0.9 ml ddH_2O, in blank group, 0.1 ml ddH_2O replaced samples. Part of the suspension (1.0 ml) was transferred to an UV-cuvette with 1.0 cm light path (BRAND), and the absorbance at 340 nm was recorded as (A_1). Then 0.02 ml of solution 4 was added and mixed. About 30 minutes later, the absorbance of the suspension was recorded immediately one after another at 340 nm (A_2). The absorbance differences (A_2-A_1) were determined for both, blank and samples. The absorbance difference of blank was subtracted from the absorbance difference of the samples to make ΔA.

$\Delta A = (A_2\text{-}A_1)_{\text{sample}} - (A_2\text{-}A_1)_{\text{blank}}$

L-lactic acid concentration was then calculated according to the general equation:

$c = 0.323 \times \Delta A$ (g /l)

2.2.12. Oxygen consumption measurement

Oxygen concentration was measured using a instrument which consists of a semiminiature Clark electrode (Hansatech Instruments) fitted to a small (600-µl) airtight chamber. The O_2 electrode was calibrated by immersion in dithionite and MiR05 medium equilibrated with room air. The cell suspension was slowly introduced

through an opening in the bottom of the chamber so as to drive out microbubbles through a corresponding opening in the top. The openings were closed simultaneously once the chamber was filled. The cell suspension was continuously stirred with a magnetic bar. The number of viable cells present in the suspension was determined with a hemocytometer, for each measurement, 3×10^5 cells were used. When as substrates of respiration chain (pyruvate and maleic acid) were used, 1×10^5 cells were used at 30 ^oC. The signal from the O_2 electrode was and stored in a PC-compatible computer and data were analysed with Oxyg32 software (Mamchaoui and Saumon, 2000).

2.2.13. Measurement of Intracellular Reactive Oxygen Species (ROS)

HCT116 cells grown in 12-well plates were incubated at 37°C for 1 h with RPMI1640 containing 10%FBS and 1% penicillin/streptomycin. Intracellular oxidative stress was monitored by measuring changes in oxidation-dependent fluorescence of two intracellular probes used at indicated time points. The probe 2',7'-dichlorofluorescin di-acetate (H_2DCFDA, 5 μM, Molecular Probes) enters cells and the acetate group on H_2DCFDA is cleaved by cellular esterases, trapping the non-fluorescent 2',7'-dichlorofluorescin (DCFH) intracellularly. Subsequent oxidation by ROS, particularly hydrogen peroxide (H_2O_2) and hydroxyl radical (OH•), yields the fluorescent product DCF. Thus, increases in DCF fluorescence are indicative of H_2O_2 or OH• generation. Dihydroethidine (5 μM, Molecular Probes) enters cells and can be oxidized by superoxide ($O2•^-$) and/or HO· to yield fluorescent ethidium (Eth). Eth binds to DNA (Eth–DNA), further amplifying its fluorescence. Thus, increased nuclear Eth–DNA fluorescence indicates the accumulation of ($O2•^-$)/ OH•.

2.2.14. Measurement of GSH and NADPH/NADP ratio

2.2.14.1. GSH content measurement

About 5×10^3 cells per well were plated in a 96-well plate, after overnight culture, medium were removed and cells were washed 2 × with PBS. Cell lysate was prepared

by two repetitive freeze-thaw cycles of –80 °C (20 minutes) and 37 °C. Then cell lysate was resuspended with GSH-stock buffer, mixed well by gently pipetting. For reaction, 40 µl of the lysate was transferred to a 96-well plate, GSH standard samples were prepared for standard curve, the series of concentrations are 0, 0.5, 1, 2, 5, 10, 15, 20 µM. For one 96 wells of samples, reaction solution were prepared as following:

ddH_2O	14.56 ml
0.5 M Tris/HCl pH7.5	770 µl
150 mM glucose-6-phosphate	102.6 µl
50 mM $NADP^+$	9.24 µl
6 mM DTNB	2.5 ml
Enzymes were added shortly before reaction	
glucose-6-phosphate-dehydrogenase	30 U
glutathione-reductase	30 U

Reaction buffer (170 µl) was added into each sample (40 µl), mixed by shaking. The absorbance at 412 nm was measured for 5 minutes (each 15 sec one time point) at 37 °C in a SpectraMax 340PC^{384} machine (Molecular Devices). Protein concentration was measured with Bradford assay (2.2.10.1). A series of BSA samples were used for standard curve. GSH content was calculated as GSH concentration/protein amount.

2.2.14.1. NADPH/$NADP^+$ ratio measurement

The NADPH and $NADP^+$ concentration was measured using a kit from Bioassay. Cells were cultured in a 6-cm dish until reaching confluency and then were washed with PBS and pelleted by pipetting and centrifugation at 1,200 rpm at 4 °C. Cells were resuspended with PBS and divided into two equal parts for either $NADP^+$ or NADPH concentrations. Cell pellets were prepared by centrifugation at 1,200 rpm at 4 °C and then homogenized in a 1.5 mL eppindorf tube with either 100 µl $NADP^+$ extraction buffer for $NADP^+$ determination or 100 µl NADPH extraction buffer for NADPH determination. Extracts were incubated at 60°C for 5 min and then add 20 µl Assay Buffer and 100 µl of the opposite extraction buffer to neutralize the extracts. Samples were briefly vortexed and centrifuged 14,000 rpm for 5 min. The supernatant was used for $NADP^+$/NADPH assays. Calibration curve were made by measuring a series

of $NADP^+$ samples at the concentration of 0, 1, 2, 3, 4, 6, 8, 10 µM. For each well of reaction, working reagent was prepared by mixing 50 µl Assay Buffer, 1 µl Enzyme, 10 µl Glucose, 14 µl PMS and 14 µl MTT. Freshly. Samples (40 µl) and working reagent (80 µl) were transferred into the same well in a 96-well plate. The absorbance at 595 nm was read at time "zero" (OD_0) and 30 minutes after reaction (OD_{30}) at room temperature. The absorbance difference (ΔOD) is determined by subtracting OD_0 from OD_{30} for the standard and sample wells. The $NADP^+$/NADPH concentration of samples was calculated from the standard curve by using the ΔOD values.

2.2.15. Cell cycle, cell senescence and apoptosis analysis

For quantification of cell cycle progression and the amount of sub-G1 apoptotic cells, HCT116 cells were detached by trypsin treatment and collected by centrifugation. After re-suspending in PBS, cells were fixed in 70% ethanol, washed in PBS, stained with 50 µg/ml propidiumiodide (PI) containing 50 µg/ml RNAse A (DNase free), and analysed by flow cytometry (FACS-Calibur, Becton Dickenson). FACS results were analysed with Flowjo software. Cell senescence was measured using Senescence β–Galactosidase Staining Kit (Cell Signaling) according to manual. Blue cells (senescence cells) were detected using Leica bright field microscopy.

2.2.16. Mitochondria membrane potential measurement

Cells were stained with 25 nM TMRM (Invitrogen) or 20 nM CMXRos (Invitrogen) for 30 min at 37 ^oC in the dark, afterwards, cells were harvested by tripsinization, washed 2 times with PBS, and then were resuspended in PBS and applied for FACS analysis. For TMRM, cells were measured the emission in Fl-2 channel; CMXRos stained cells were measured in FL-3 channel.

2.2.17. In vitro invasive assay.

Cell culture plate inserts with 8 µm pore size (BectonDickinson) were coated with 100 µl Matrigel/PBS solution (0.2 mg/ml, Sigma) and dried in the culture hood at room temperature for about 30 minutes. All the cells were preincubated in media.

Three hundred microliters of 0.1% BSA-RPMI 1640 containing a single-cell suspension at 1×10^5 cells per well were added to the upper chamber insert and 300 µl of 5% FCS RPMI 1640 were added into the lower well as a chemoattractant. Then, the different cells were incubated at 37°C in 5% CO_2 humidified conditions. After 24, the insert membranes were fixed for 10 min with 10% formaldehyde and stained with 0.5% toluidine blue in 2% Na_2CO_3 solution. The cells on the upper surface of the membrane were removed with cotton wool and discarded. After washing with double distilled water, membranes were cut from the chambers and mounted in DePex. The number of cells migrated to the lower surface of the membrane was counted using a Leica microscope under x100 magnifications from 3 consecutive fields, representing ~60% total area of the membrane. Data presented are the means and standard deviations of two wells from three experiments.

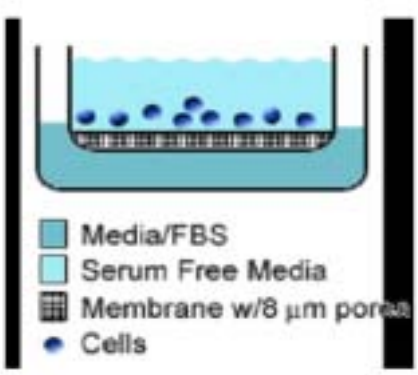

2.2.18. Wound closure assay

HCT116 cells were plated in a tissue culture 6-well plate at an initial density of 1.5×10^5 cells/cm^2. A uniform confluent monolayer was formed in ~2–3 days. All wounding assays were performed in a serum-free medium by first preincubating the cells in the serum-free medium for 30 min before the start of the experiments. A 200µl micropipette was used to create a straight wound in the monolayer by scraping. Debris was twice washed away with PBS. Wound closure was followed for 2 days using an inverted contrast microscope (Leica) and digital images of the wound area were taken every day. Image analysis was done manually.

2.2.19. In vitro transformation assay

For focus formation, different HCT116 cell clones were seeded at a density of 3 $\times 10^5$ per 10-cm plate and grown to confluency in the presence of selection antibiotics. Cultures were maintained for a further 3 weeks after reaching confluency, with the media changed every 4 days. After 3 weeks, the cells were washed twice with PBS and once with ice-cold methanol and then fixed for 10 minutes in methanol before being stained with 0.1% (w/v) methylene blue (Sigma) and photographed.

To measure saturation density, cells were seeded as above, and cultured for several days until cells reached confluency. Cell numbers were determined after trypsinization by counting in a hemocytometer.

2.2.20. Immunofluorescence staining

Cells were grown on chamber slides and incubated in culture medium for 48 hours (when needed, mitochondria were stained with 25 μM TMRM for 40 minutes). Cells were washed twice with PBS and then fixed in 100% methanol solution (-20 ^{o}C) for 10 minutes. The fixed cells were washed three times with PBST and blocked in 3% bovine serum albumin (BSA)/PBST for 30 min. After washing with PBST, cells were incubated with primary antibodies at 4 °C overnight and then washed three times with PBS. They were then incubated with Alexa 594 or Alexa 488-conjugated second antibody (Molecular Probes) in 0.3% BSA/PBST for 45 minutes and washed again with PBST. Cell nuclei were counterstained with DAPI (10 ng/mL). Finally, the chamber slides were mounted with mounting medium Fluoprep (bioMérieux). Images of fluorescence signals were captured by a laser confocal microscopy (PerkinElmer Ultra-View spinning disc confocal microscopy, Nikon Image Center, Heidelberg)

Anti HIF-1α	1:400
Anti cytochrome c	1:200
Alexa 488 conjugated goat anti mouse IgG (H + L)	1:500
Alexa 594 conjugated goat anti mouse IgG (H + L)	1:500

2.2.21. Xenograft animal model

For the establishment of solid tumour in nude mice, tumour cells are treated in a sterile environment under a cell culture hood. Disposable sterile plastic pipettes and dishes are used. Cultures are grown in a BB6220 incubator (Heraeus) at 37 °C and 5% CO_2.

The tumour models used in our laboratory are obtained by subcutaneous (s.c.) injection of the HCT116 cell line in nude mice.

Cells for subcutaneous injection in mice were prepared as follows: From one 150 mm cell culture dish (176 cm^2) with confluent cells, the medium is removed by aspiration. The dish is first washed with 20 ml PBS and then trypsinized with 4.0 ml 0.05%-EDTA trypsine solution (Sigma). The trypsinized cells are transferred into a 15 ml falcon tube and 10 ml medium added. After centrifugation (5 min., 1200 rpm), cells are resuspended in sterile PBS (12 ml) and centrifuged again. The cell pellet is then resuspended in 500-600 µl of PBS and kept in ice, providing material for immdiate subcutaneously injection into 3-4 mice. Cell concentration before injection was determined using a Hemato-cytometer (Sigma). Approximately 2.0×10^6 cells are injected subcutaneously into the right flanks of 6-8 week-old female nude mice. After injection, mice were observed for up to 7 weeks, tumor growth were recorded by measuring maximal diameter (a) and minimal diameter (b) using calipers every week, tumor volume was calculated with the formular $v=0.5 \times a \times b^2$ (Carlsson et al., 1983). During this period, mice body weight, water and food uptake were recorded weekly. Before sacrifice, images of mice carrying tumors were taken using digital camera. Blood glucose concentration was measured by Blood glucosemeter (OneTouch). After sacrifice, the tumors were carefully taken off from the mouse bodies. Half of the tumors were stored in liquid nitrogen and the other half were fixed with ~40% formalin in PBS and applied for immunohistochemistry analysis. Afterwards, the weight of left side of tibialis anterior (TA) muscles, livers, and both sides of pararenal fat tissues were measured to assess a potential cachexia phenotype.

2.2.22. Histological analysis of tumors

After being carefully isolated, tumors were cut into less than 2 × 2 cm pieces and fixed with ~40% formalin overnight, then were embedded in paraffin by the following protocol: tumors were dehydrated by washed in the following solution

1. distilled water
2. 45 minutes 70% Ethanol
3. 45 minutes 80% Ethanol
4. 45 minutes 95% Ethanol
5. 45 minutes 100% Ethanol #1
6. 60 minutes 100% Ethanol #2
7. 60 minutes 100% Ethanol #3
8. 60 minutes Xylene #1
9. 60 minutes Xylene #2
10. 60 minutes Xylene #3
11. 60 minutes Paraffin #1 (55 ^{o}C)
12. 60 minutes Paraffin #2 (55 ^{o}C)
13. 60 minutes Paraffin #2 (55 ^{o}C)

Then tumors were embedded in paraffin blocks, and sectioned at desired thickness (4~5 μm) on a microtome (Leica) float on a 40 °C water bath containing distilled water. The sections were transferred onto a glass slide. Allow the slides to dry overnight and store slides at room temperature until ready for use.

Before staining, tissue slides were deparaffinized and re-hydrated:

Slides were placed in a 55 °C oven for ten minutes to melt the paraffin. Slides were deparaffinized in 2 changes of xylene for 5 minutes each and transferred to 100% Ethanol with 2 changes for 3 minutes each and then once through 95% Ethanol for 3 minutes. Slides were re-hydrated by incubation in PBS 2 × for 5 minutes each.

Slides were then stained with Haematoxylin and Eosin as following protocol:

Sections were placed in haematoxylin for 5 minutes, washed and incubated in tap water for ~2minutes to 'Blue' sections. Then sections were placed in eosin for less than 45 seconds, dehydrated by incubation in 95% Ethanol for 2 × 1 minute, then in

xylene for 2 × 1 minute, mounted for preservation.

3. Results

3.1. TKTL1 protein is localized mainly in cytoplasm and has moderate stability

In order to figure out the localization and lifespan of TKTL1, a GFP-TKTL1 (GFP, green fluorescence protein) fusion protein under a Tet regulated CMV promoter in the pcDNA4/TO vector (Figure 5A) was genereated. As a control, a GFP expression cassette was also generated in this vector. The HCT116 derived cell line TR5 which constitutively expresses Tet repressor (pcDNA6/TR, Figure 5A) was used for transfection. TR5 cell clones expressing the Tet regulated GFP or GFP-TKTL1 fusion proteins were established and used to determine the localization and lifespan of the TKTL1 protein.

GFP or GFP-TKTL1 expression was triggered by the addition of final concentration of 1 μg/ml Doxycycline (Dox) for 12 hours, green fluorescence signals were detected by fluorescence microscopy and FACS. Cell images were taken 12 hours after Doxycycline treatment, as shown in Figure 5B. Only in the GFP expression cell clones, the green fluorescence was ubiquitously distributed in the cell. In contrast, green signals from the GFP-TKTL1 fusion protein only appeared in the cytoplasm, fully sparing the nucleus (Figure 5B).

To analyse the life-span of TKTL1, GFP and GFP-TKTL1 expression was induced by Dox treatment for 12 hours. Then the cells were cultured in Dox free medium for an additional 12, 36, 60 and 84 hours, and GFP signals were detected by FACS. In GFP expression cells, the green fluorescence positive cell population and fluorescence intensity were not changed over the whole observation period, while in GFP-TKTL1 expression cells, green fluorescence signals were reduced stepwise from 90% to almost zero (Figure 5D and E). This experiment showed that GFP-TKTL1 and thus also TKTL1 have a moderate stability, having a half-life of about 24 hours as extrapolated from the Figure 5E. The intermediate stability makes TKTL1 suppression by RNA interference technology an achievable strategy.

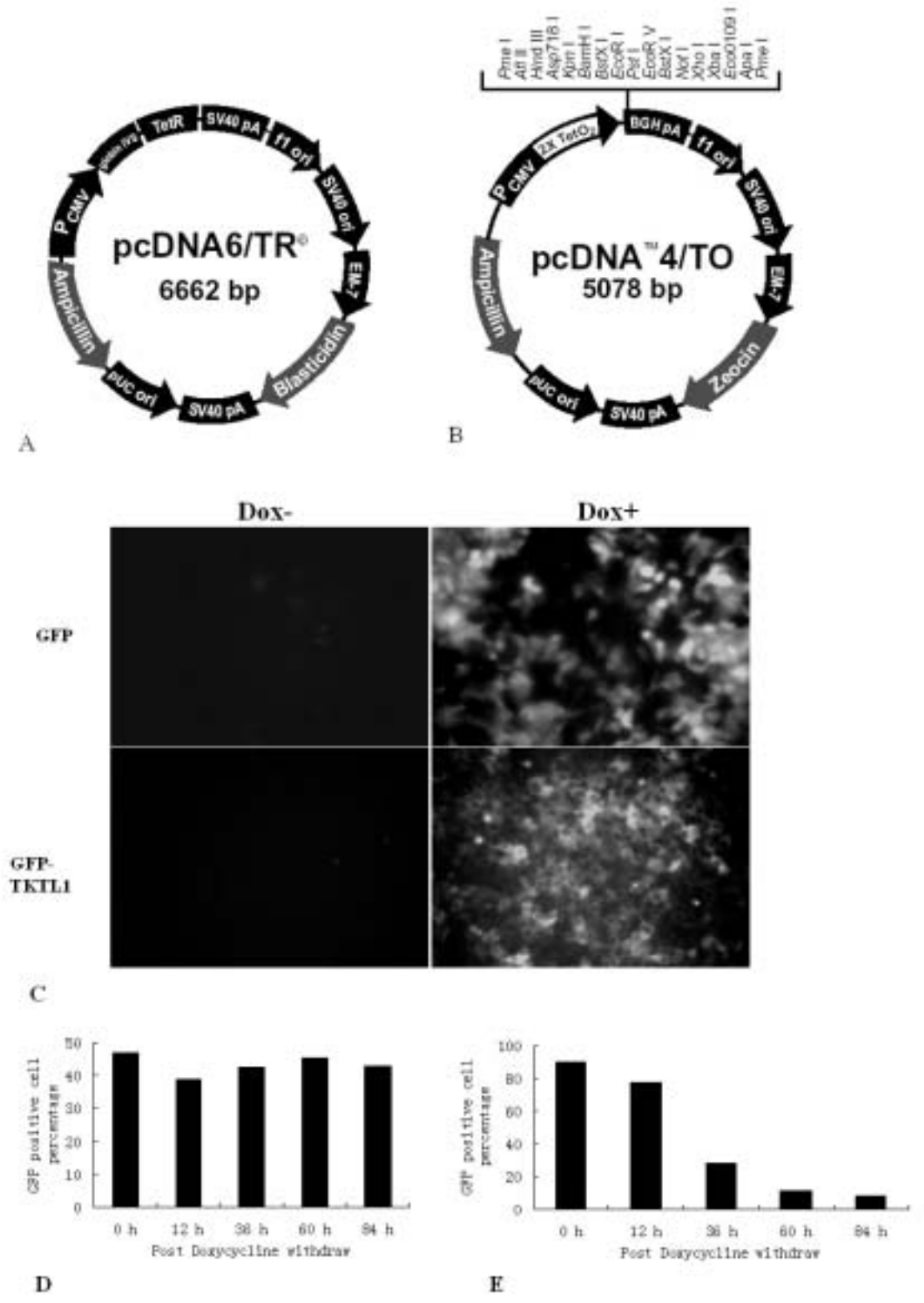

Figure 5. **Moderate stability and cytoplasmic localization of GFP-TKTL1 proteins.** TR5 cells are HCT116 cells stably transfected with pcDNA6/TR plasmids (A). Tet regulated GFP or GFP-TKTL1 expression cassettes were inserted into the HindIII-XbaI sites of plasmid pcDNA4/TO. (C) With and without Doxycycline induction for 24 hours, cells were observed under fluorescence microscope at 200-fold magnification. FACS analysis showed green cells

percentage in total cell population for GFP-only expressing cells (D) and GFP-TKTL1 fusion protein expressing cells (E).

3.2. siRNA-mediated suppression of TKTL1 expression

In order to suppress expression of the endogenous TKTL1 in human cells siRNA target sequences were identified by an online algorithm (Qiagen, Hilden, Germany). The three most promising TKTL1 siRNAs were selected and assayed in cell cultures for their effects on endogenous TKTL1 expression. One siRNA targeting TKT was used as control. The positions of the different siRNAs on the TKTL1 mRNA relative to the genetic structure of the gene as well as their exact sequence are given in Table 3 and Figure 7.

The siRNAs were transfected into human colon carcinoma cells HCT116 grown in a 6-well plate by Lipofectamine 2000. To each well, 1 ng of siRNA was delivered. Two days after transfection, cells were harvested and total RNAs were extracted with Trizol (2.2.9.1.) and subjected to semi-qRT-PCR to detect TKTL1 transcripts (2.2.9.2. and 2.2.9.3.). In parallel, the expression level of β-actin mRNA was analyzed and used to normalize the expression level. In repeated experiments, siRNAs #1 and #2 showed the strongest suppression of TKTL1 mRNA whereas siRNAs #3 was less efficient (semi-qRT-PCR, Figure 6). The siRNA specifically targeting the TKT housekeeping gene did not affect the highly related TKTL1 (Table 3 and Figure 6).

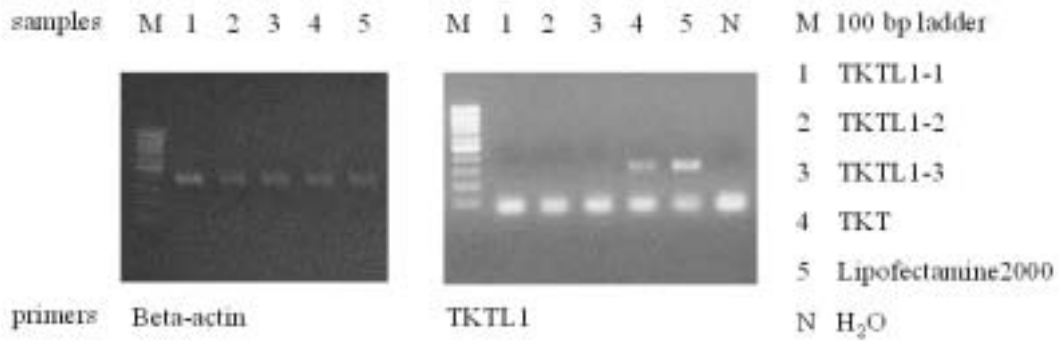

Figure 6 siRNA-mediated TKTL1 suppression in HCT116 cells. Cells were transiently transfected with the TKTL1 siRNA oligos 1, 2, and 3 as shown in Table 3, siRNA 4 targets the TKT mRNA whereas sample (5) represents mock-transfected cells. TKTL1 siRNA oligos 1, 2, and 3 lead to the suppression of TKTL1 mRNA as determined by semi qRT-PCR.

3.3. shRNA-mediated suppression of TKTL1 expression

Since siRNAs allow only a transient suppression of the targeted gene, we analyzed whether the highly active RNAi target sequences #1 and #2 identified above are also functional as shRNAs that allow long-term suppression of TKTL1 gene expression. The targeted TKTL1 sequences are shown in Figure 7.

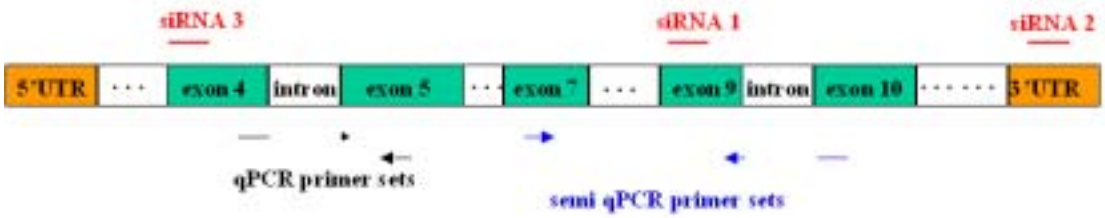

Figure 7 Localization of siRNA targets and RT-PCR primer sets. Part of the gene structure of TKTL1 is shown above, siRNA targeted sequences are located in exon 9, 4 and 3'-UTR (the 3'-untranslated region), respectively. The sense primer sets for semi qRT-PCR detecting TKTL1 are located in exon 7, the reverse primer spans an intron between exon 9 and 10. Quantitative RT-PCR primer sets are located in exon 4 and 5, the forward primer spans an intron. These primers could only detect TKTL1 transcripts and have poor affinity to genomic DNA.

We used pSUPER.neo+GFP or pSUPERior.puro plasmids as shRNA delivery system (Figure 4). In pSUPER.neo+GFP vectors, the shRNA expression cassette is driven by an H1-promoter, which is RNA polymerase III (Pol III)-dependent. Pol III has a simple structure, a well-defined transcription start-site, and it naturally drive the transcription of small RNAs (Myslinski et al., 2001). The vector also encodes an *egfp* gene allowing selection of transfected cells and a Neomycin resitant gene for selection of stably transfected cell clones. When it was neccessary to avoid eGFP interference, pSUPERior.puro was used, which contains a puromycin selection marker and a Tet-responsive H1 promoter containing two copies of the 19 bp *tet* operator region. When transfected into Tet repressor-expressing cell lines, the expression of shRNA could be tightly controlled by the addition of Tetracycline/Doxycyclin (van de Wetering et al., 2003). In cells without Tet repressor expression, the shRNA is constitutively expressed.

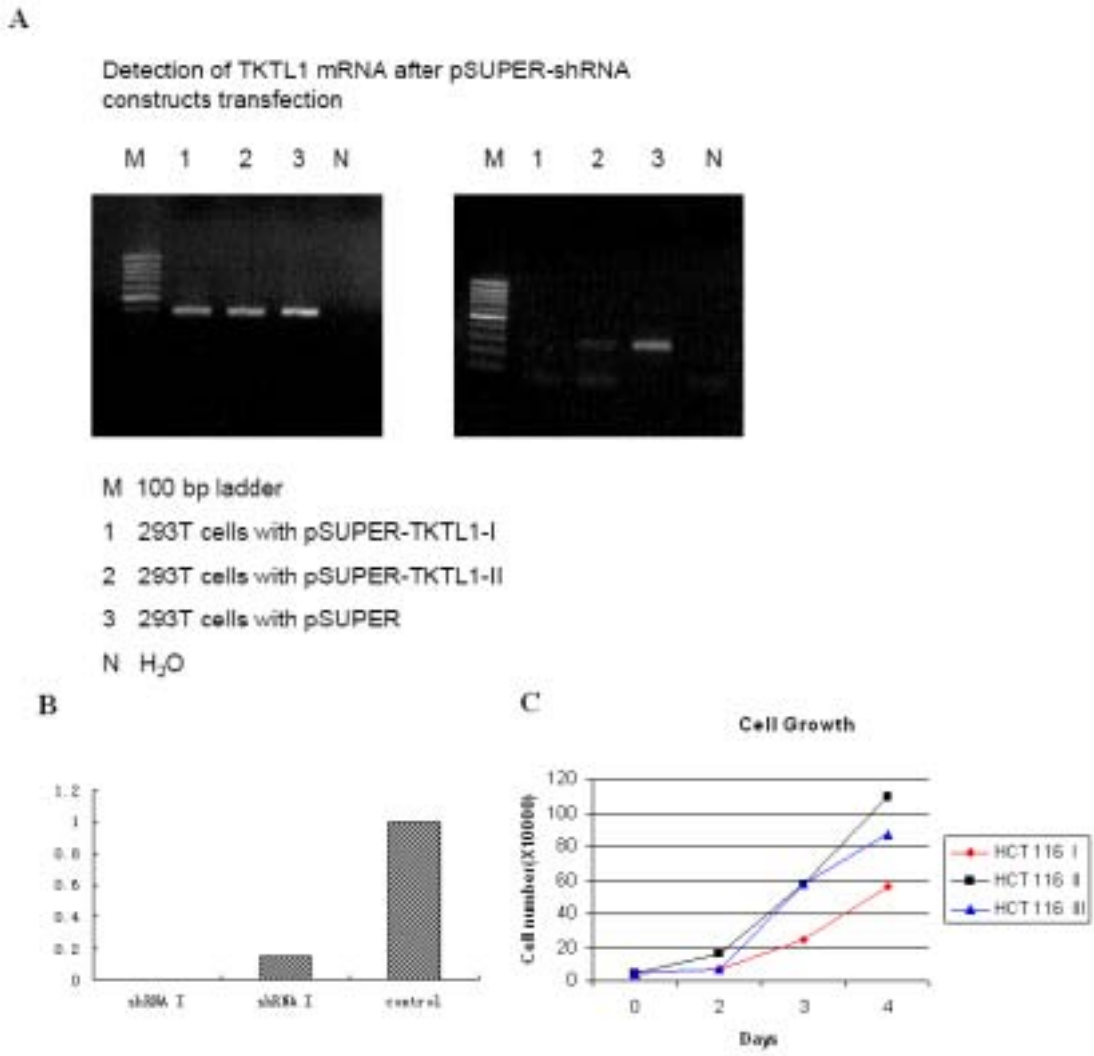

Figure 8 Suppression of TKTL1 by shRNA constructs. (A) shRNA efficacy was test on 293T cells using semi quantitative RT-PCR. The left gel figure shows β-actin amplificates, the right gel figure shows TKTL1 amplicates. (B) shRNA effect on stably transfected HCT116 cells using real-time RT-PCR. (C) Growth curve of stable shRNA transfected HCT116 cells.

For cloning of the TKTL1 shRNA clones, shRNA sense and anti-sense primers comprising the target sequences #1 and #2 were annealed and inserted into the H1-promoter driven shRNA expression plasmid pSUPER.neo+GFP or pSUPERior.puro using HindIII-BglII sites (2.2.7.). The vectors containing siRNA targeted sequence #1 and #2 were named pSUPER-TKTL1-I and pSUPER-TKTL1-II respectively. Besides directing shRNA expression, the vectors encode neomycin or puromycin resistance allowing selection of stable single-cell clones, a technique

absolutely required when long-term studies of growth-attenuated cells are planned.

To assess the efficacy of the constructs, both pSUPER.neo+GFP based TKTL1 shRNA vectors and the empty control vector were transfected into 293T cells. Two days after transfection, TKTL1 mRNA levels were analyzed by semi-qRT-PCR. As shown in Figure 8A, TKTL1 mRNA levels were reduced when transfected with both shRNA vectors. Constructs pSUPER-TKTL1-I had a much stronger suppressive effect, while pSUPER-TKTL1-II showed only a moderate effect, reducing TKTL1 transcripts to ~20% of control cells.

Based on these findings, stable HCT116 cell clones with both shRNA and control vectors were established by G418 selection. The TKTL1 RNA level was checked by real-time RT-PCR. Results similar to those of transiently transfected 293T cells were obtained (Figure 8A and B). We noticed that TKTL1 shRNA treated cells grew slower than controls, and the growth curve of these cells clearly confirmed the phenomenon (Figure 8C). The growth kinetics of TKTL1 shRNA treated cells seems to be correlated with TKTL1 expression level, since pSUPER-TKTL1-II vector induced slighter TKTL1 suppression and the HCT116 cells with this vector showed almost no difference in growth rate compared to control in the first three days, but revealed a slight reduction at day 4 (Figure 8C).

We further isolated individual single cell clones. Since pSUPER-TKTL1-I had stronger suppressive effect, we used only this vector to obtain single-cell clones (clone names begin with I), while clones from the empty vectors were also collected (clone names begin with III). Independent shRNA-I cell clones displayed clonal variation with respect to TKTL1 expression between a 10- to more than 100-fold TKTL1 mRNA suppression (Figure 9A).

By using the TKTL1-specific monoclonal antibody described previously (Coy et al., 2005), it was not possible to detect endogenous TKTL1 protein expression

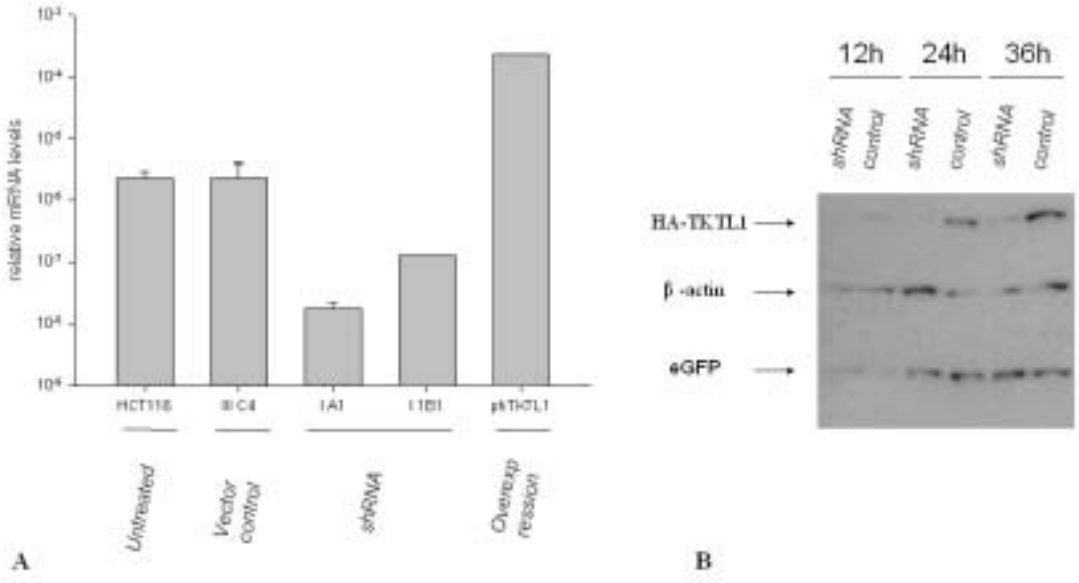

Figure 9 Characterization of stable HCT116 cell lines carring TKTL1-shRNA vectors. (A) TKTL1 expression was analysized by real-time RT-PCR. The relative TKTL1 mRNA expression normalized to the endogenous β-actin is shown. Vector control cell clones showed TKTL1 expression levels similar to untreated HCT116 cells. TKTL1-1 shRNA transfected cell clones (IA1 and I1B1) showed strong suppression of TKTL1, only less than 1/10 and 1/100 of the transcripts were still detectable. Error bars represent standard deviation. (B) TKTL1-shRNA treated (IA1) and vector control cell clones (IIIC4) were plated in 12-well plates and transfected with 0.1 µg of expression vector-coding HA-tagged TKTL1 together with eGFP overexpression plasmids. TKTL1 was detected with an anti-HA antibody, β-actin and eGPF were detected with corresponding antibodies as loading and transfection controls. About 24 and 36 hours after transfection, much less HA-TKTL1 proteins were detected in shRNA treated cell clones, confirming that the shRNA in fact suppressed TKTL1 expression.

in HCT116 cells and hence also not the shRNA-mediated TKTL1 protein suppression. To circumvent this limitation, we transfected the well-established and characterized TKTL1-shRNA cell clone IA1 and control clone IIIC4 with HA-tagged hTKTL1 over-expression plasmid. Subsequent immunoblotting using the high-affinity anti-HA monoclonal antibody to target the HA-TKTL1 fusion protein, a clear repression of HA-TKTL1 protein expression in TKTL1 shRNA-containing cells compared with the controls was reproducibly detectable (Figure 9B). These data confirm that TKTL1-suppressed cell clones have been successfully established.

3.4. Morphological changes of TKTL1 shRNA-treated HCT116 cell clones

HCT116 cells are epithelial-like human colon carcinoma cells, as shown in Figure 10A. HCT116 cells carrying the empty pSUPER.neo+eGFP vectors displayed a cell morphology almost identical to the original cells (Figure 10B). Under normal cell culture conditions, untreated and vector control treated HCT116 cells showed aggregated cell morphology with no clear boundary between cells and with cells piled up in layers even at low cell density. With TKTL1-suppressed by shRNA vectors (clone IA1 and I1B1), cells had different appearance. The cells became more flattened with fibroblast morphology and clear cell–cell margins (Figure 10C and D). The clear boundary implied that TKTL1 suppression induced morphological changes, which might be related to altered cell–cell adhesion.

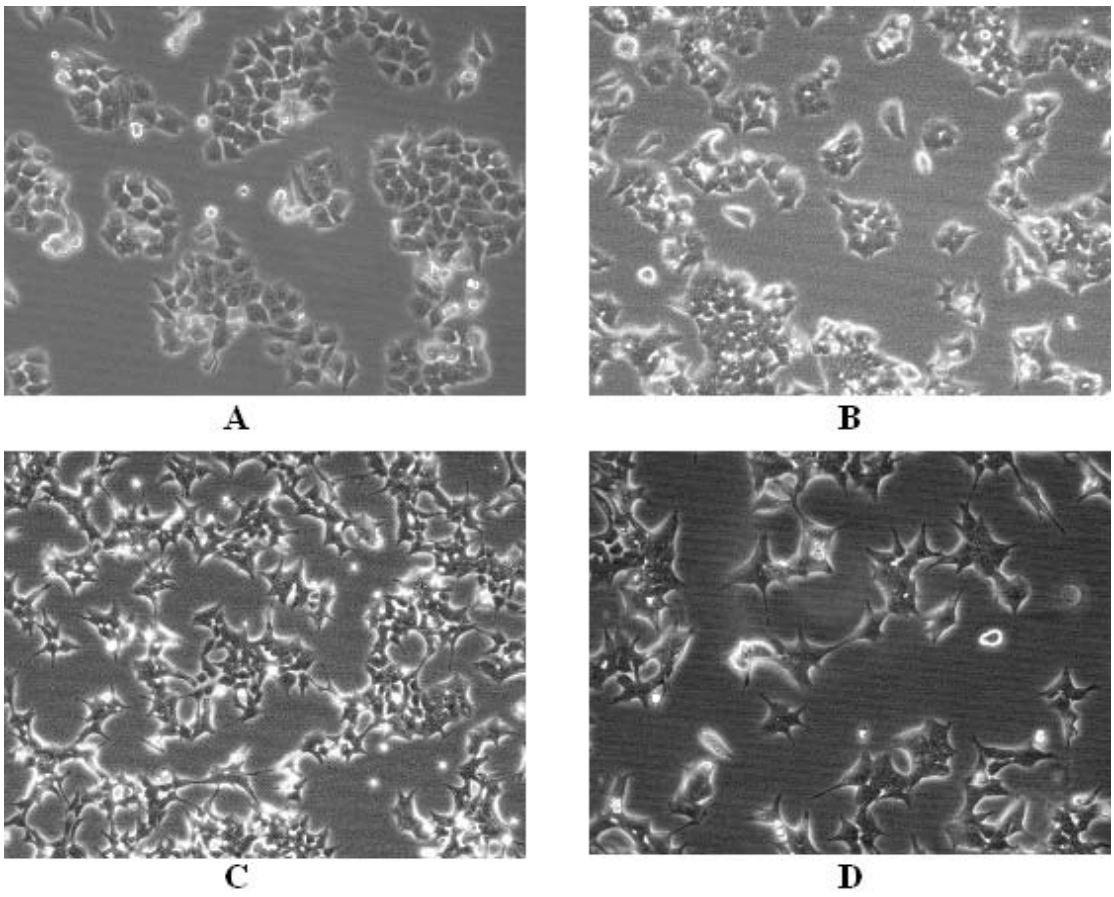

Figure 10 Cell morphology of shRNA treated HCT116 cells. (A) Untreated HCT116 cells; (B) HCT116 cells transfected with shRNA control vectors (clone IIIC4); C and D, HCT116 cells transfected with shRNA targeting TKTL1 (clone IA1 and I1B1 respectively). Compared to controls (A and B), the TKTL1-suppressed cells have clear cell-cell margin and more spikes.

Images were taken under Leica inverted contrast microscope at a magnification of 200 ×.

3.5. Altered glucose metabolism upon TKTL1 suppression

TKTL1 is considered to play a central role in glucose metabolism and aerobic glycolysis directly enhancing glucose consumption and lactic acid release. Thus, we first studied whether suppression of TKTL1 expression resulted in altered glucose metabolism or lactate production. First, siRNA technology was used to knock down TKTL1 gene. As shown in Figure 11, siRNA oligos 1 to 3 targeting TKTL1 showed a slowed D-Glucose concentration decline over 4 days of time (no medium replenished). Suppression of TKT had similar results, which served as a positive control for changes of the PPP pathway. The siRNA oligos TKTL1-2 and 3 induced less attenuation in D-glucose concentration compared the siRNA oligos tatgeting TKT and especially, TKTL1-1 oligo which had also the highest suppressive effect.

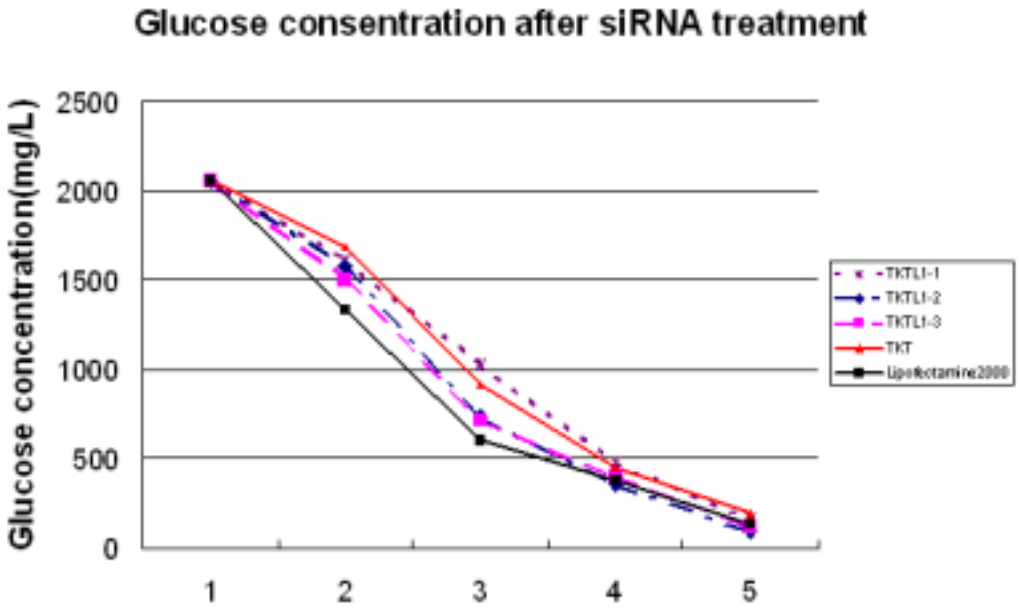

Figure 11 D-Glucose consumption of HCT116 cells after siRNA treatment. D-Glucose concentration was measured by UV methods (2.2.11.). The ransfection control (Lipofectamine 2000) group has the fastest decline of glucose concentration. Two siRNA oligos TKTL1-2 and 3 groups show a slightly attenuated decline effects on glucose concentration, while cells treated with siRNA TKT and TKTL1-1 have the slowest drop of D-Glucose concentration, meaning the slowest glucose consumption.

In addition, single-cell clones with repressed TKTL1 expression (IA1, I1B1) and control cell clone (IIIC4) were assayed for D-glucose consumption and L-lactic acid production. Identical amounts of cells were cultured as described in Materials and Methods and glucose consumptions and lactate production were determined for a 24 h interval (12 to 36 h after plating). To account for differences in cell growth, cell numbers were determined at the time of plating and harvest using a haemacytometer. Glucose metabolism and lactic acid production were normalized to the mean cell number (mean cell number: (cell number plated + cell number harvested)/2). We found that TKTL1-suppressed cell clones have reproducibly a reduced D-Glucose consumption rate. For instance, cell clone I1B1 only used up half of D-Glucose than control cell clones (IIIC4) within 24 hours, while shRNA-treated clone IA1 displayed about 30% lower glucose consumption (Figure 12A). The reduced glucose metabolism of cells with suppressed TKTL1 expression was paralleled by reduced L-lactic acid production. Within the 24 hours interval**,** the TKTL1-knock down clones produced around 30% less L-lactic acid than the control (Figure 12B). Overall, the data are in line with the concept that the suppressed TKTL1 expression in HCT116 cells blocks the D-Glucose flow into the PPP with the consequence that these cells consume less Glucose and thus also produce less lactic acid.

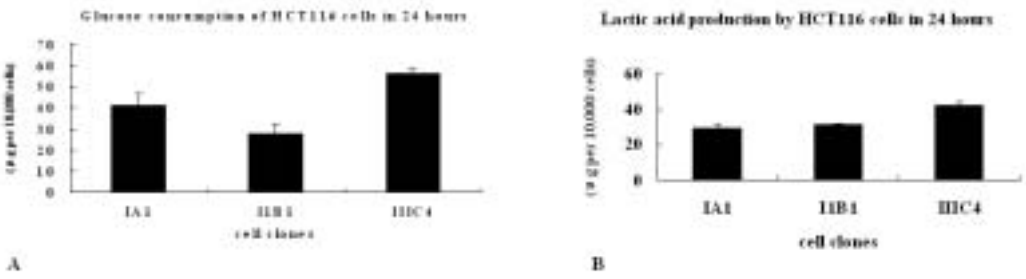

Figure 12 Metabolic features of TKTL1-suppressed HCT116 cells. About 4.0×10^4 cells were plated in 24 well-plates supplied with 0.5 L medium, 12 hours after plating, medium were changed and cells were incubated for additional 24 hours, then medium were collected for analysis. When harvested at 36 hours post plantation, cell numbers were counted using haemacytometer. (A) D-glucose consumption and (B) L-lactic acid production by cultured cells were calculated accordingly (2.2.11.) and then normalized to the mean cell numbers. Error bars represent standard deviation.

3.6. Reduced cell proliferation after shRNA-mediated TKTL1 suppression

Since TKTL1 is an important enzyme in the PPP, a pathway that is not only utilized for energy production but also in nucleic acid precursor synthesis and generation of redox equivalents, we studied whether suppression of TKTL1 expression has an effect on cell proliferation. Equal amounts of cells (2×10^5) were plated in 35 mm cell culture dishes with standard culture medium. Cells were harvested two days after plating and applied for cell cycle distribution analyse by FACS. These data revealed that the TKTL1-suppressed HCT116 cell clones had higher G0/G1 but lower S and G2/M phase peaks than corresponding empty vector-treated cells (Figure 13A, B). TKTL1-shRNA treated clones IA1 and I1B1 had about 80% of the cells in G0/G1 phase, ~10% cells in S phase and 10% in G2/M phase, while in control cells IIIC4, the S phase and G2/M phase cells increased to 18.4% and 20.9%, respectively. Thus upon TKTL1 suppression, the cell population entering cell cycle was reduced to half of the control cells. In line with this finding, cell growth kinetics showed that TKTL1-suppressed cells grew much slower than controls (Figure 13 C). For these experiments, 4×10^4 cells per well were seeded in 12-well plates and left to attach for 12 hours. Cells were harvested and counted using a hematocytometer every 24 hours. The experiment was done in triplicates, both TKTL1-shRNA treated cell clones showed similar growth kinetics. Within four days, the cell number raised from 4×10^4 to around 5×10^5, while control cell numbers reached, on average, 1.3×10^6, more than twice the number of TKTL1-shRNA treated cells. These data indicate that TKTL1 suppression leads to cell cycle arrest in the G0/G1 phase of the cell cycle, indicating that TKTL1 promotes cell cycle progression and proliferation.

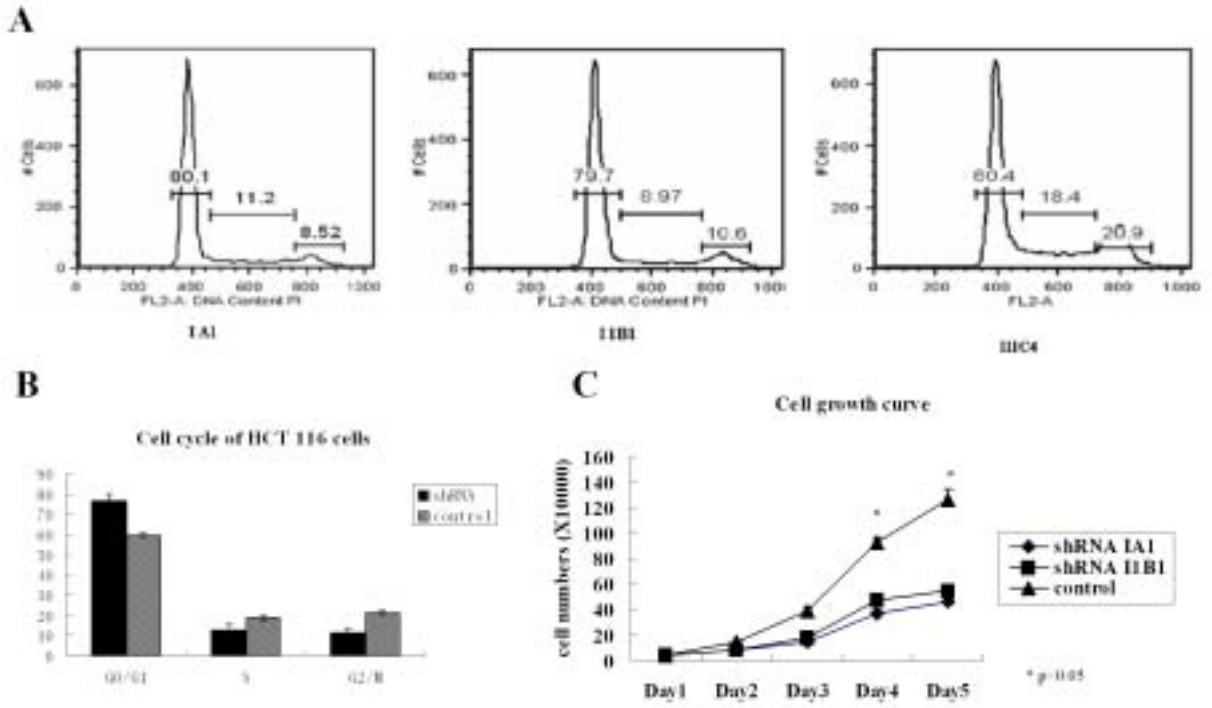

Figure 13 Growth patterns of TKTL1- and control shRNA treated HCT116 cells. (A) Cell cycle distribution by FACS showed that after TKTL1 was knocked down, cell clones (IA1 and I1B1) had only around half of percentage of cells in G2/M phase, lower S phase and comparatively higher G0/G1 phase peak. (B) Several measurement of cell cycle by FACS showed similar result. (C) Cell growth curve showed that compared to the control cell clone, TKTL1-suppressed cells grow slower, within 4 days time, they had only half of cell number of control clone. Error bars represent standard deviation of 3 experiments.

3.7. Changes of cell proliferation and survival related proteins upon suppression of TKTL1

Since it was already shown that cell cycle progression is arrested upon TKTL1 suppression, we analyzed the expression of important regulatory factors of the cell cycle. The expression of cell cycle checkpoint proteins, p21 and cyclin D1, was detected by western blot. The cyclin D1 proto-oncogene is an important regulator of G1 to S-phase transition in numerous cell types from diverse tissues. Binding of cyclin D1 to its kinase partners, the cyclin dependent kinases 4 and 6 (CDK4/6) results in the formation of active complexes that phosphorylate the Retinoblastoma tumor suppressor protein (RB). Hyperphosphorylation of RB results in the release of RB-sequesterd E2F transcription factors and the subsequent expression of genes

required for entry into S-phase. Cyclin-dependent kinase inhibitor 1A (p21, Cip1), encodes a potent cyclin-dependent kinase inhibitor. It binds to and inhibits the activity of cyclin-CDK2 or -CDK4 complexes, and thus functions as a negative regulator of cell cycle progression at G1. The cell cycle arrest upon TKTL1 suppression could be mediated by the increased p21 expression in TKTL1-suppressed HCT116 cells (Figure 14A).

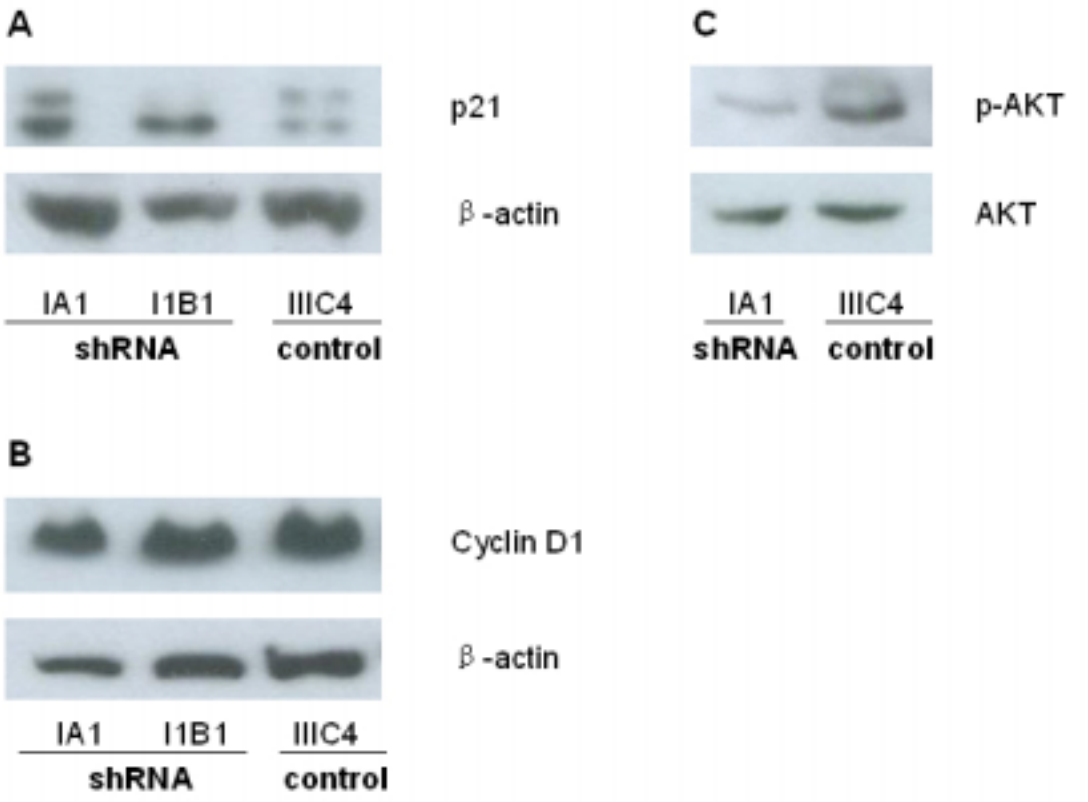

Figure 14 Expression of proliferation and survival related proteins by western blot. (A) In TKTL1-suppressed HCT116 cell clones (IA1 and I1B1), p21 is increased compared to control clone IIIC4. (B) Cyclin D1 is not significantly changed upon TKTL1 suppression. In these two expreriments, β-actin serves as a protein loading control. (C) The phosphorylated form of AKT (active form) is reduced in TLTL1-suppressed HCT116 cell clone IA1 compared to control clone IIIC4.

Akt (also known as protein kinase B, PKB) is a well-characterized protein for cancer cells to promote their survival capability. It also activates aerobic glycolysis in transformed cells (Elstrom et al., 2004). It is found that tumors that overexpress the TKTL1 protein also have activated Akt (phospho-Akt; p-Akt) (Langbein et al., 2006). So the Akt was also detected by western blot in TKTL1-suppressed and contol cells.

When equal amount of proteins were loaded, the amount of total Akt were similar, while the level of functionally active form p-Akt was reduced upon TKTL1 suppression (Figure 14C).

3.8. Pyruvate, not dNTP rescues the cell cycle arrest by TKTL1 suppression

Since pyruvate and ribose are two major end products of the PPP, we studied whether by adding either of them to TKTL1-suppressed cells, the G0/G0 arrest could be released. We added sodium pyruvate to a final concentration of 1 mM and dNTPs to 100 μM into the culture medium, incubated the cells for 48 hours, and analyzed the cell cycle distribution by FACS. As shown in Figure 15, addition of pyruvate or dNTP did not change S phase and G2/M phase percentage in control cell clone IIIC4, dNTP also did not change cell cycle distribution in TKTL1-shRNA treated cell clone IA1. However pyruvate almost completely diminished the arrest in G2/M phase in IA1 cells, indicating that the end product of the PPP, pyruvate, can in fact affect the cell cycle distribution of TKTL1-suppressed cells.

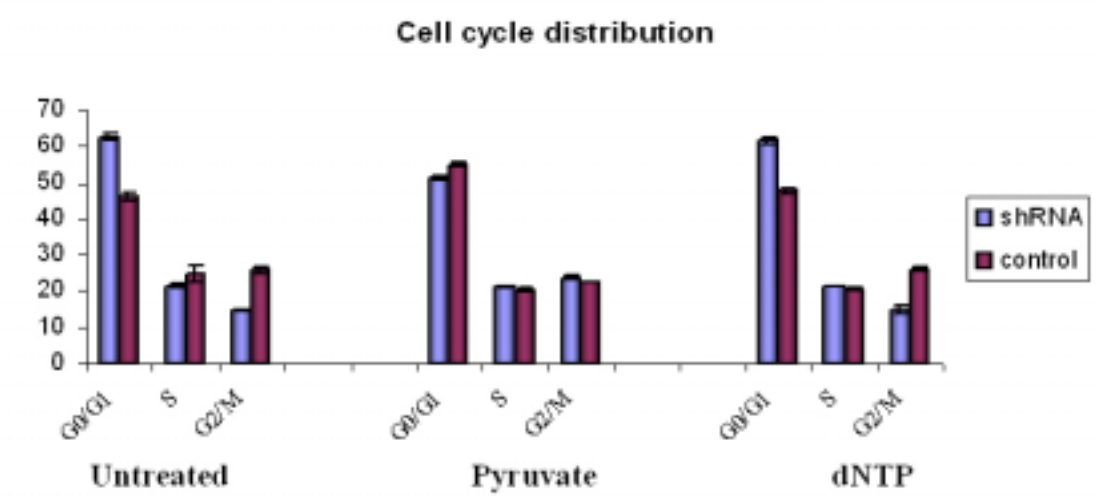

Figure 15 Effect of pyruvate and dNTP on cell cycle progression. TKTL1-shRNA treated and vector control treated cells were incubated with culture medium with either 1 mM sodium pyruvate or 100 μM dNTP. Cell cycle distribution was determined by FACS analysis. The addition of dNTP did not influent cell cycle distribution in both cell clones, while the addition of pyruvate clearly increased S and G2/M phase of TKTL1-shRNA treated cell clones, but had no such effect on vector control cell clones. Error bars represent standard deviation of 3 experiments

3.9. TKTL1-suppressed HCT116 cells have higher resistance to serum

starvation.

Fast growing tumor cells require more nutrients than normal cells due to their vast demand for nucleic acids, proteins and lipids synthesis. Necrosis in the midst of the tumor normally results from fast growing of the tumor and insufficient blood supply for the nutrients. Here we test whether withdraw of glucose or serum leads to cell death in cell culture conditions.

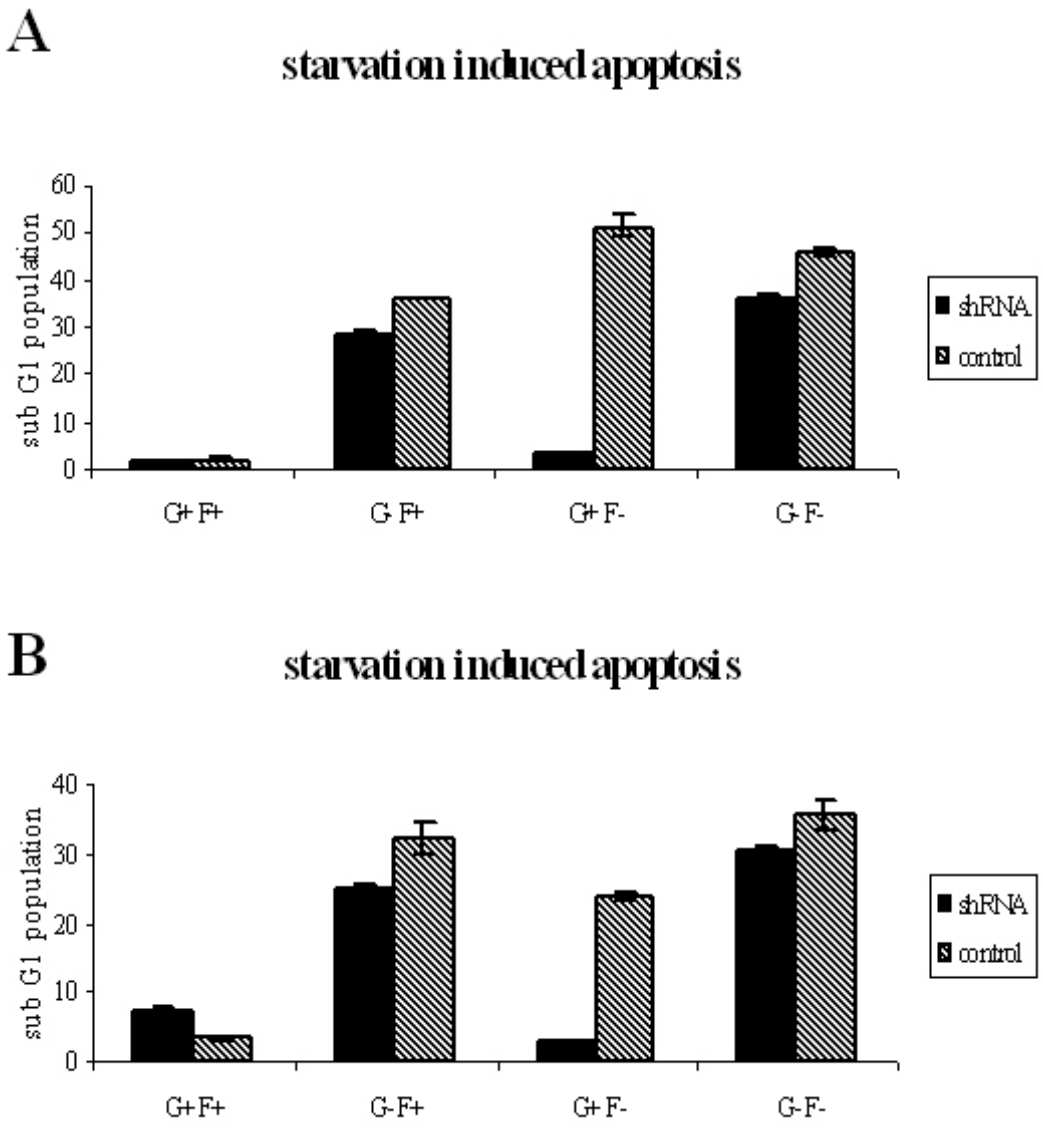

Figure 16 Glucose (G) and/or FBS (F) starvation induced cell death. SubG1 cells were analyzed by FACS to determine apoptosis in (A) G418 selection cell clones and (B) Puromycin selection cell clones. Bars show the subG1 apoptotic fraction of total cells. Error bars represent standard deviation.

HCT116 cells were first grown to confluency on 6-well plates, then either glucose

or/and FBS was withdrawn, cells were cultured for an additional 24 hours, whereafter cell death was detected by FACS anaysis. We used 2 different sets of HCT116 cells, one group contained G418 resistant cells (Figure 16A), the other contained puromycin resistant cells (Figure 16B). The results in both sets of cells were similar, indicating that the selection procedure *per se* had not affect starvation resistance.

All the cells were very sensitive to glucose depletion, the apoptotic cells (sub-G1) increased dramatically. In G418 resistant cells, TKTL1-suppressed cells had ~30% of sub G1 fraction when glucose was absent (G-F+), when both glucose and FBS were absent (G-F-), the apoptotic fraction increased to ~40%, the control cells under these conditions had around 1/5 more cells in apoptotic fraction. In puromycin resistant cells, situation was similar, only the apoptotic fraction was in general lower. Under the condition that only FBS was absent (G+F-), TKTL1-suppressed cells didn't show a significant increase in apoptotic cells, while those control cells were still sensitive to FBS starvation, the apoptotic fraction increased to ~50% in G418 resistant cells and ~25% in puromycin resistant cells. This experiment shows that after TKTL1 suppression, cells were less sensitive to FBS-starvation induced cell death than controls.

3.10. TKTL1-suppressed cells have enhanced mitochondrial respiration

Cancer cells normally use aerobic glycolysis to degrade glucose as energy supply (Warburg, 1956a). Since the PPP is an important pathway to degrade glucose and transketolases are controlling the non-oxidative step of this pathway, we asked whether blocking TKTL1 may cause energy shortage and would thus lead to increased utilization of the respiration chain. We thus measured oxygen consumption of cancer cells with suppressed TKTL1 by shRNA.

A Clark oxygen electrode was used to measure the actual oxygen concentration in solutions. First, about 3×10^6 shRNA-treated or control HCT116 cells were suspended in 1.5 ml pre-warmed MiR05 medium in the measuring chamber, which was placed in water bath to maintain the temperature at 37 ^{o}C. Oxygen concentration was recorded using the Oxyg32 software. As shown in Figure 17 A, B and C, shRNA treated

HCT116 cells displayed a much faster decline of the oxygen concentration, while the decline of the oxygen concentration in control cells was minor. The data are graphically presented in Figure 17D. When 20 µl of 2.0 M sodium pyruvate and 5 µl of 0.5 M maleic acid were added to stimulate aerobic respiration, a significantly faster decrease of the oxygen concetration was recorded for TKTL1-suppressed clone I5, compared to control cell clone IIIC4 (Figure 17 E and F). The decline rate was 16.6 nM/min when TKTL1 was suppressed, while the rate of control cells was only 7.15 nM/min.

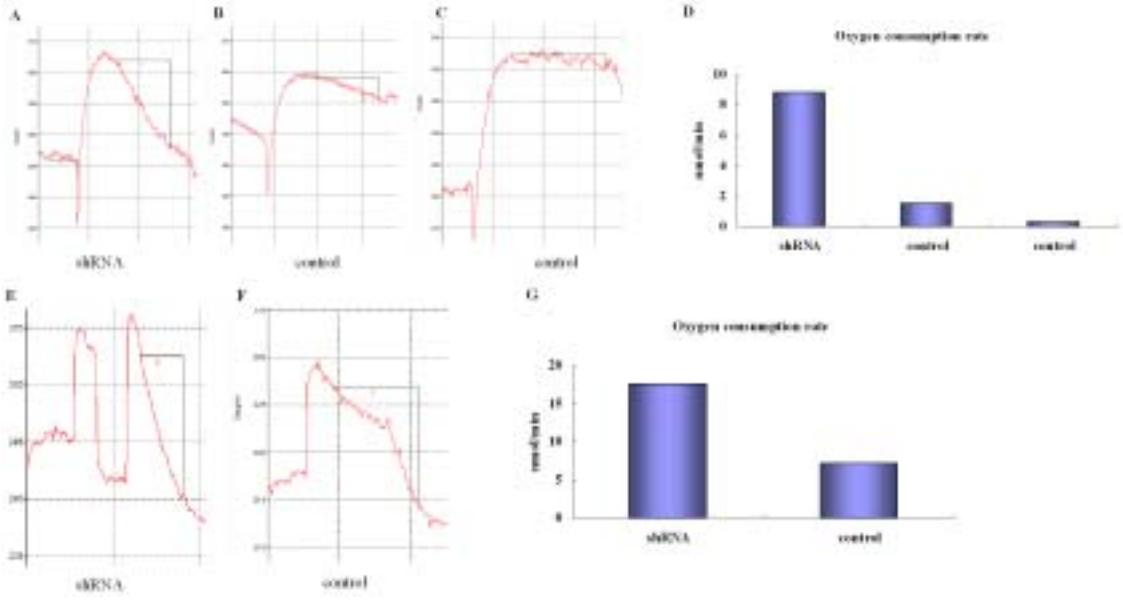

Figure 17 Oxygen consumption of TKTL1-suppressed HCT116 cells. (A) TKTL1-suppressed and (B, C) control HCT116 cells showed different oxygen concentration decline pattern at 37 ^{o}C. (D) Graphic presentation of the oxygen consumption rate of TKTL1-suppressed and control HCT116 cells. In addition, TKTL1-suppressed (E) and control cells (F) also showed different oxygen concentration decline patter when pyruvate and maleic acid were present at 30 ^{o}C. (G) Graphic presentation of oxygen consumption rate of TKTL1-suppressed and control HCT116 cells after pyruvate and malate addition.

In the previous experiments, we showed that oxygen consumption is increased after TKTL1 suppresion (Figure 17). Thus we checked whether the expression of enzymes controlling the flow of pyruvate into mitochondria and fatty acids β-oxidation is also changed. It is found that in TKTL1-suppressed cells, the transcripts

for PDK2 (pyruvate dehydrogenase kinase isoform 2), a negative regulator of mitochondrial respiration via TCA Cycle (Patel and Roche, 1990; Roche and Hiromasa, 2007), were reduced to around 40% of those of control cells. Reduced amounts of PDK activity lead to increased PDH (pyruvate dehydrogenase) activity and thus more pyruvate is hydrolyzed to enter mitochondria for energy production via TCA Cycle. In contrast, the transcripts for MCAD (medium-chain Acyl-CoA dehydrogenase), an enzyme reguired for the degradation of fatty acids as a cellular energy source (Liu, 2006), were reduced to around 60% of those of control (Figure 18A), pointing to reduced fatty acid catabolism.

The mitochondrial membrane potential (Δψm) is an important parameter of mitochondrial function used as an indicator of cell health. The activation of oxidative phosphorylation in cancer cells leads to the breakdown of the Δψm (Bonnet et al., 2007). Upon TKTL1 suppression, the mitochondria membrane potential was slightly decreased (Figure 18B), suggesting increased activity of oxidative phosphorylation.

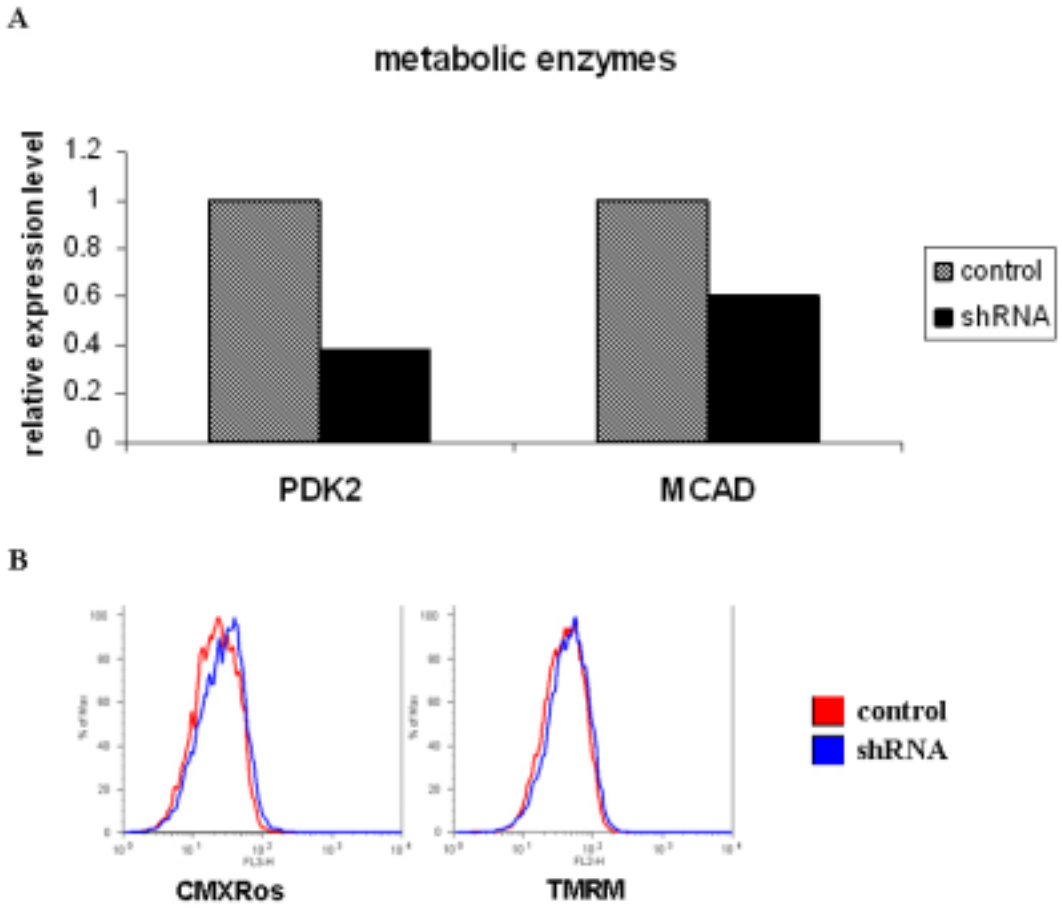

Figure 18 Increased mitochondrial respiration of TKTL1-suppressed HCT116 cells. (A) The expression levels of mitochondrial metabolic related genes PDK2 and MCAD in control or TKTL1-shRNA treated HCT116 cells were analyzed by qRT-PCR. Histogram shows the relative expression level of PDK2 and MCAD. (B) Mitochondrial membrane potential (Δψm) was measured by using fluorescence dye CMXRos or TMRM and analyzed by FACS. The histogram shows that Δψm of shRNA treated HCT116 cell clone (IA1) was slightly lower than control clone (IIIC4).

These data indicate that HCT116 carcinoma cells have lower mitochondrial respiration and higher fatty acids β-oxidation to generate energy. Upon TKTL1 suppression, mitochondrial respiration in HCT116 cells is reinitiated to generate energy. This is in line with the finding that TKTL1-suppressed cells have higher oxygen consumption rates, suggesting that the TKTL1-suppressed cells have more active mitochondrial functions.

3.11. TKTL1-suppressed cells have increased intracellular ROS concentration

The PPP that is controlled by transketolase activity provides essential redox equivalents for reductive biosynthesis and/or detoxification of highly reactive oxygen species (ROS). For this reason, we analyzed whether down-regulation of TKTL1 leads to higher intracellular ROS levels.

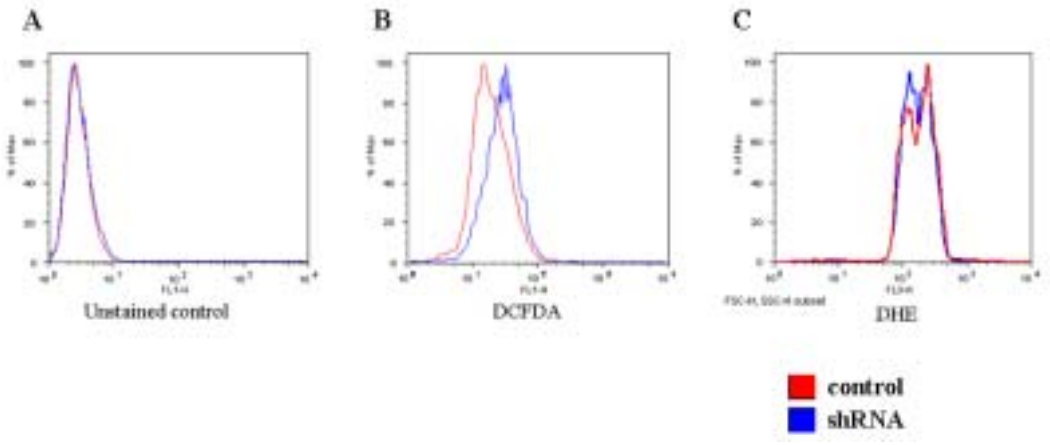

Figure 19 Increased intracullular ROS level of TKTL1-suppressed cells. Cells were stained with 5 μM DCFDA, DHE or DMSO (as unstained control) for 30 minutes at 37 ^{o}C, and then

analyzed by FACS. (A) A clear peak shift appears, indicating TKTL1-suppressed cell clone IA1 had enhanced intracellular H_2O_2 compare to control cell clone IIIC4. (B) The $O_2\bullet^-$ level determined by DHE staining was not changed.

In these experiments, intracellular ROS were stained with DCFDA or DHE and detected by FACS. Without any dye, TKTL1-suppressed and control cell clones showed almost identical fluorescence pattern (Figure 19A). Upon the addition of DCFDA or DHE, the intracellular H_2O_2 or $O_2\bullet^-$ was detected respectively (Figure 19B and C). The histogram of fluorescence intensity of these two cell clones (Figure 19B) revealed stronger H_2O_2 signals in TKTL1-suppressed cell clone (IA1) compared to vector treated control clone (IIIC4), while in DHE stained cells, the fluoresence signals were almost identical. These data suggest that after TKTL1 suppression, the intracellular H_2O_2 level is elevated while $O_2\bullet^-$ is not changed.

3.12. TKTL1-suppressed HCT116 cells have decreased anti-ROS defenses

The ROS detoxifying enzymes serve as defense system to protect cell from high concentration of ROS produced in mitochondria. Catalase and peroxiredoxins (Prx5 and Prx3) are very important genes which convert intracellular H_2O_2 to O_2 and H_2O (Deisseroth and Dounce, 1970; Fujii and Ikeda, 2002), while the PPARg coactivator 1a (PGC-1a) is required for the induction of many ROS-detoxifying enzymes (St-Pierre et al., 2006). Thus expression of PGC-1a and ROS detoxifying enzymes catalase, Prx5 and Prx 3 was analyzed by qRT-PCR. Compared to controls, shRNA treated, TKTL1-suppressed cells had significantly decreased expression level of these genes. PGC-1a and catalase expression in TKTL1-suppressed cells reduced to less than 10% of that of their control counterparts, while Prx3 and Prx5 expression in TKTL1-suppressed cells was reduced to about 20% (Figure 20). The reduction of ROS detoxifying enzymes and their regulators may explain why the intracellular ROS levels are higher in TKTL1-suppressed cells.

The NADPH/NAD+ ratio and the relative amount of reduced form of glutathione (GSH) represent the redox status of the cells, since NADPH and GSH are major redox equivalent to counteract oxidative stress inside the cells (Kirsch and De Groot, 2001;

Pastore et al., 2003). Since the PPP produces NADPH, it is conceivable that upon TKTL1 suppression, intracellular NADPH and GSH concentrations are reduced, represented by decreased NADPH/NADP$^+$ ratio and GSH content (Figure 20B and C). All these results show that the anti-ROS defence systems in TKTL1-suppressed cells are much weaker than controls.

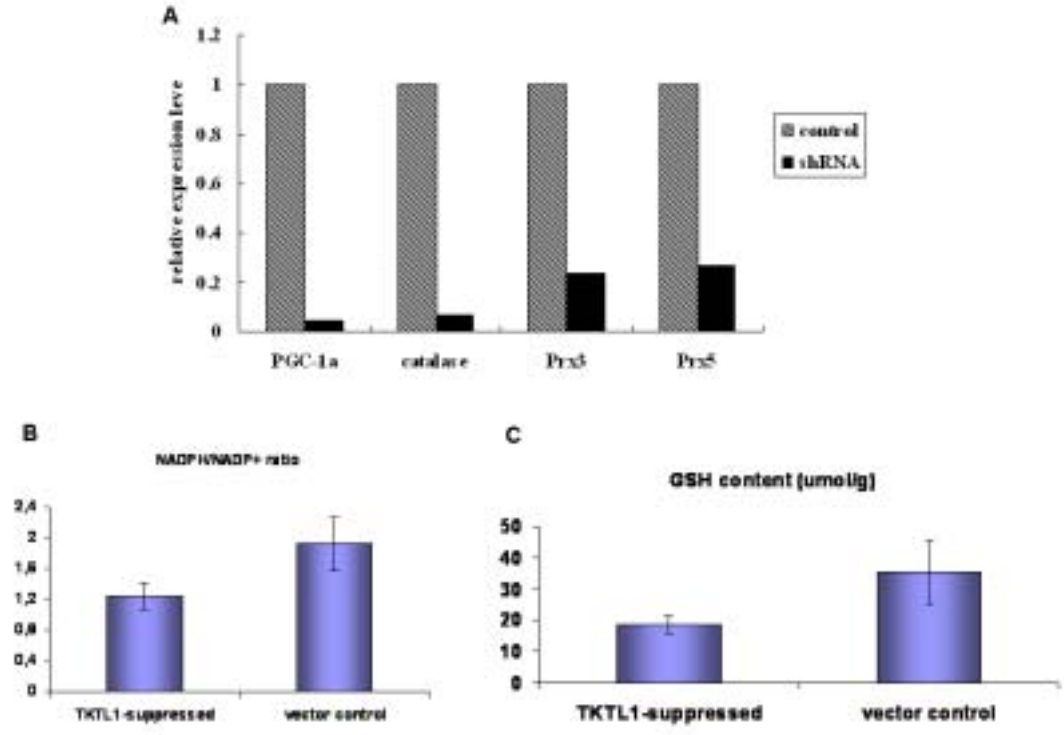

Figure 20 Decreased anti-ROS defences in TKTL1-suppressed cells. (A) ROS detoxifying enzymes and regulatory transcriptional factor PGC-1a were detected by qRT-PCR. The histogram shows the relative expression level of these genes. In TKTL1-suppressed HCT116 cells (shRNA group), all these genes are notably decreased. (B) The NADPH/NADP$^+$ ratio and (C) GSH content in TKTL1-suppressed HCT116 cells is significantly reduced.

3.13. TKTL1-suppressed HCT116 cells have increased sensitivity to oxidative stress inducing reagents

The ROS scavenging enzymes and redox equivalents in TKTL1-suppressed cells turned out to be less (Figure 20), raising the possibility that these cells are more susceptible to oxidative stress. TKTL1-suppressed and vector control HCT116 cells were thus challenged with oxidative stress-inducing reagents. Here, three different

reagents were used, H_2O_2, which serves as an extracellular ROS sourse, PEITC, which induces ROS in transformed cells and DEM, which depletes reduced GSH, a first-line anti-ROS agent. Cells were plated in 6-well plates, after attachment, cells were challenged with different concentration of these oxidative stress-inducing reagents for 24 hours. Total cells were harvested (including those floating in the medium) and analyzed by FACS (2.2.15.). In all assays, TKTL1-suppressed cells showed increased sensitivity towards ROS-induced apoptosis as indicated by the appearance of morphological alterations like cell shrinkage (Figure 22).

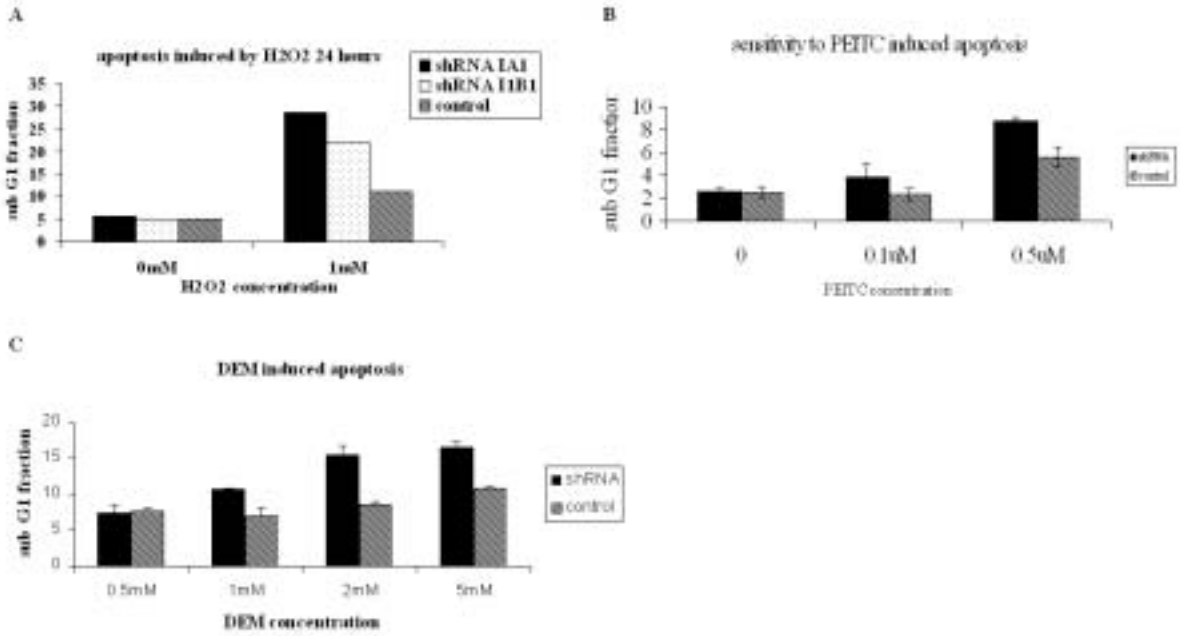

Figure 21 TKTL1 suppression leads to increased sensitivity towards oxidative stress. HCT116 cells were treated with H_2O_2, PEITC or DEM for 24 hours, apoptotic cells were represented as the sub-G1 fraction as masured by FACS. The histograms show sub-G1 fractions of HCT116 cells after different oxidative stress inducing reagents treatment. (A) TKTL1-shRNA treated cell clone IA1, I1B1 and control cell clone IIIC4 were treated with 1 mM H_2O_2 and dissolvent control (PBS) for 24 hours. (B) TKTL1-shRNA treated cell clone IA1 and control IIIC4 were treated with 0.1 and 0.5 µM PEITC or dissolvent control (absolute ethanol) for 24 hours. (C) TKTL1-shRNA treated cell clone I5 and vector control cell clone III43 were treated with 0.5, 1, 2 and 5 mM DEM or dissolvent control (DMSO) for 24 hours. Error bars represent standard deviation for 3 experiments.

In addition, cells subjected to oxidative stress-inducing reagents displayed increasing numbers of sub-G1 cells in a dose-dependent manner. Under all conditions

tested, TKTL1-suppressed cells had more sub-G1 fraction compared to vector control cells (Figure 21).

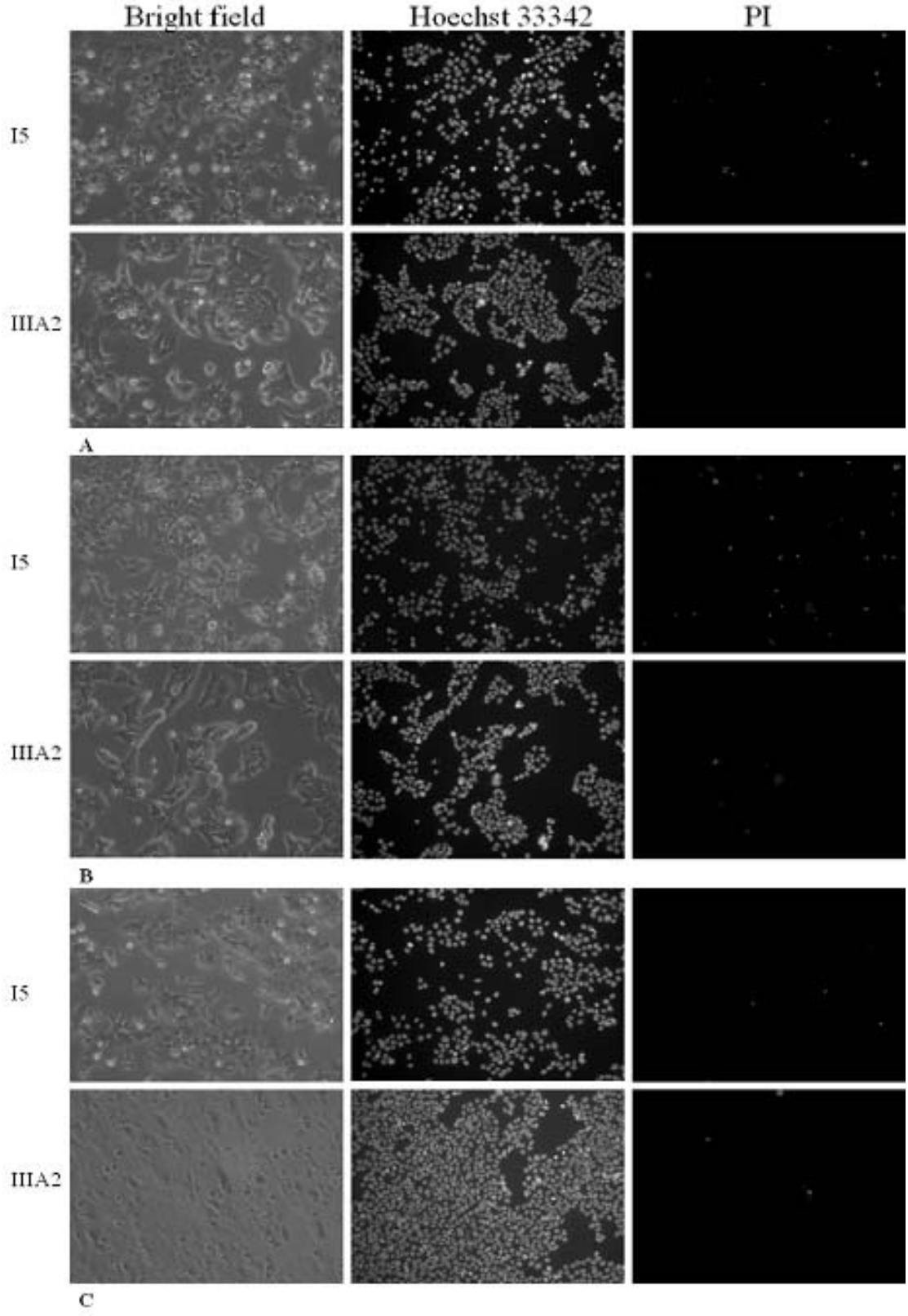

Figure 22 Increased apoptosis and necrosis in TKTL1-suppressed cells after treatment with

ROS-inducing drugs. When cells were treated with ROS inducing reagent, they showed different apoptotic phenotype such as cell shrinkage, chromosome condensation (Hoechst 33342) and necrosis phenotype (PI staining). Cells were treated with (A) 2 μM PEITC; (B) 0.5 mM H_2O_2 and (C) absolute ethanol as dissolvent control, images were taken to compare the percentage of apoptosis and necrosis.

Chromatin condensation paralleled by DNA fragmentation is one of the most important criteria which is used to identify apoptotic cells (Cohen and Duke, 1984). To confirm the sub-G1 analysis data, Hoechst 33342 was used to stain nuclei and determine the percentage of condensed nuclei, meanwhile propidiumiodide (PI) was used to stain necrotic cells (Shacter et al., 2000). Necrosis represents a passive consequence of gross injury to the cell, and compared to apoptosis, necrosis represents the more severe form of cell damage. The ratio of cells displaying features of both apoptosis and necrosis was counted as a consequence of the damage by ROS-inducing reagents. Cells were incubated with 1 μg/ml Hoechst 33342 and ROS inducing reagents or dissolvent (absolute ethanol) for 60 minutes, then incubated with 1 μg/ml PI for 5 minutes, then new culture medium was added. Live cell images in bright field, blue (for Hoechst 33342) and red channel (for PI) were taken using a Leica microscopy at 100 × magnification.

After 60 minutes of treatment with H_2O_2 (upper two panels) and PEITC (middle two panels), TKTL1-suppressed cells appeared contracted, with few filopodia, while the control cells (lower two panels) retained their round shape without obvious morphological changes. Since cell shrinkage as a hallmark was more obvious in TKTL1-suppressed cell clone (I5), gross morphology already pointed to an enhanced ROS sensitivity upon TKTL1 suppression. In TKTL1-suppressed clone I5, 2 μM PEITC or 0.1 mM H_2O_2 increased the number of cells with condensed DNA to ~20-22%, compared to ~10-12% for the correspondingly treated vector control cell clone (IIIA2). In parallel, PI-positive necrotic cells were increased in ROS-stressed, TKTL1-suppressed cells: treatment of 2 μM PEITC in creased nectotic cells from 0.2% to 3.2% and 0.5 mM H_2O_2 from 0.7% to 7.7% (Figure 22), respectively. These acummlative data on cell death confirmed that TKTL1 functions as an anti-ROS

scavenger.

The release of cytochrome c from mitochondria is considered a key initial step in the apoptotic process, although the precise mechanisms regulating this event remain elusive (Ott et al., 2002). To confirm that TKTL1-suppressed cells are more sensitive towards oxidative stress-induced apoptosis, cytochrome c localization was investigated after ROS-treatment. Cells were treated with either 0.1 mM H_2O_2 or 2 µM PEITC for 2 hours, afterwards, mitochondria were stained with 25 µM TMRM for 30 minutes, then the cells were fixed with 4% PFA/PBS and used for immunofluoresence staining. The samples were analyzed under confocol microscopy.

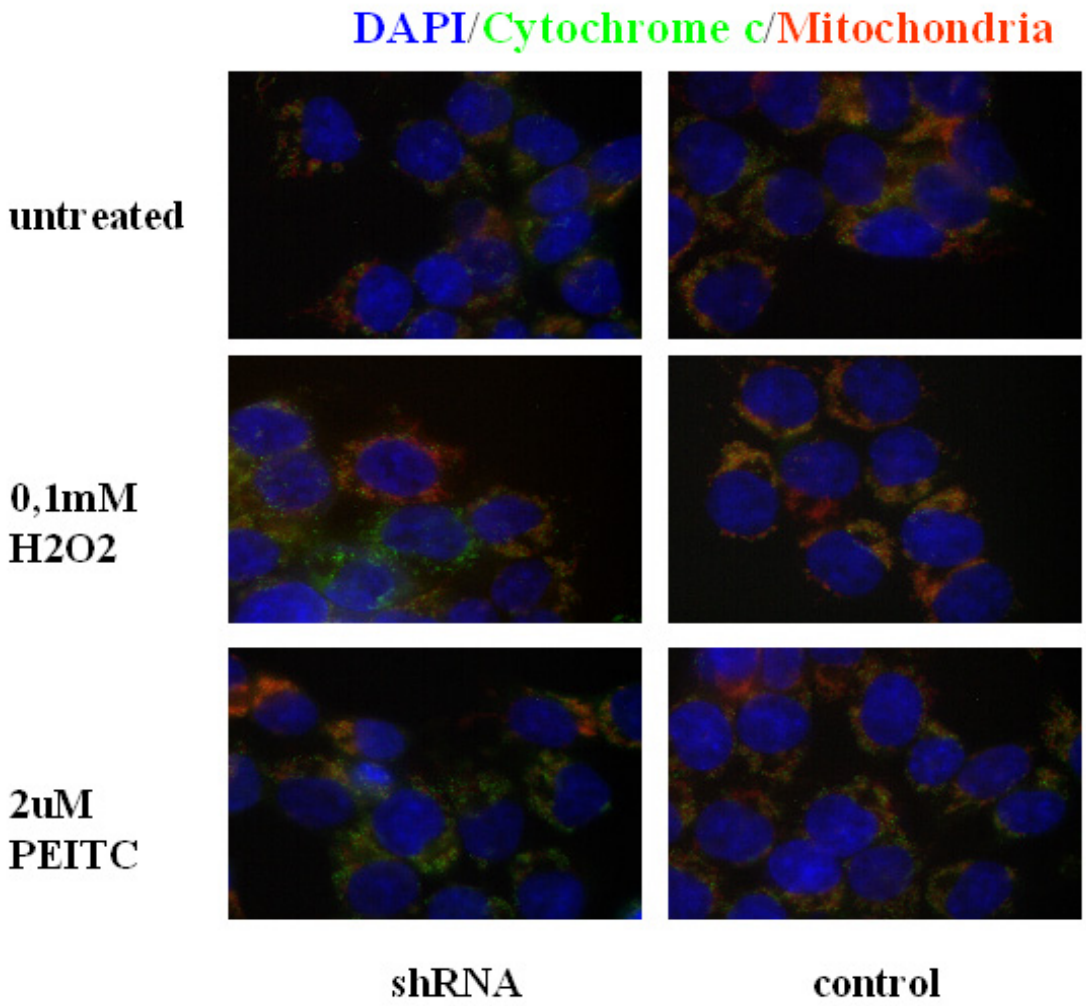

Figure 23 Cytochrome c release in TKTL1-suppressed cells after exposed to oxidative stress. TKTL1-suppressed (here named as shRNA group) and vector transfected control cells were used for detection of cytochorome c expression. Cells were treated either with 0.1 mM H_2O_2 or 2 µM

PEITC for 2 hours at cell culture conditions. Cells were stained with 25 μM TMRM for 20 minutes and then fixed and applied for immunofluorescence staining of cytochrome c. In merged images, green colour shows cytochrome c staining, red colour shows mitochondria and blue colour shows couterstaining of nuclei.

As shown in Figure 23, both TKTL1-suppressed and vector control cells did not show release of cytochrome c from mitochondria when not challenged by oxidative stress. After exposition to oxidative stress, in vector control cells, almost no cytochrome c was observed outside of the mitochondria, but an increased amount of TKTL1-suppressed cells already showed very clear green cytochrome c signals outside of the mitochondria. These data clearly indicate that TKTL1 contributes to the resistance to ROS-induced apoptosis in cancer cells, giving them growth and survival advantages under conditions of oxidative stress. Taken together, TKTL1 appears to have a protective effect against oxidative or radical stress.

3.14. TKTL1 suppression leads to cell senescence

Reactive oxygen species (ROS) serve many cellular functions; for example, second messengers, anti-bacterial agents, mutagens, aging-accelerants and growth stimulants. With regard to neoplasia, the general view is that ROS cause cancer through a number of mechanisms, including the induction of DNA damage and alteration of intracellular signaling (Finkel, 2003). In addition, high concentration of intracellular ROS can also induce cell senescence (Ramsey and Sharpless, 2006; Takahashi et al., 2006). Our previous findings showed increased ROS levels after TKTL1 was suppressed (Figure 19). We thus analyzed whether this change may affect the cell senescence phenotype. Cells with similar passage numbers were plated into a 24-well plate at the density of 2×10^4 cells per well. Cells were maintained at standard culture condition for 24 hours and then fixed and stained with the substrates for senescence associated β-Galactosidase (SA-β-gal) to identify senescent cells (Dimri et al., 1995). As shown in Figure 24A, shRNA-treated, TKTL1-suppressed cell clones strongly stained positive for β-gal (upper panels of Figure 24A), while in control cells, only few β-gal positive cells were present, a difference which is

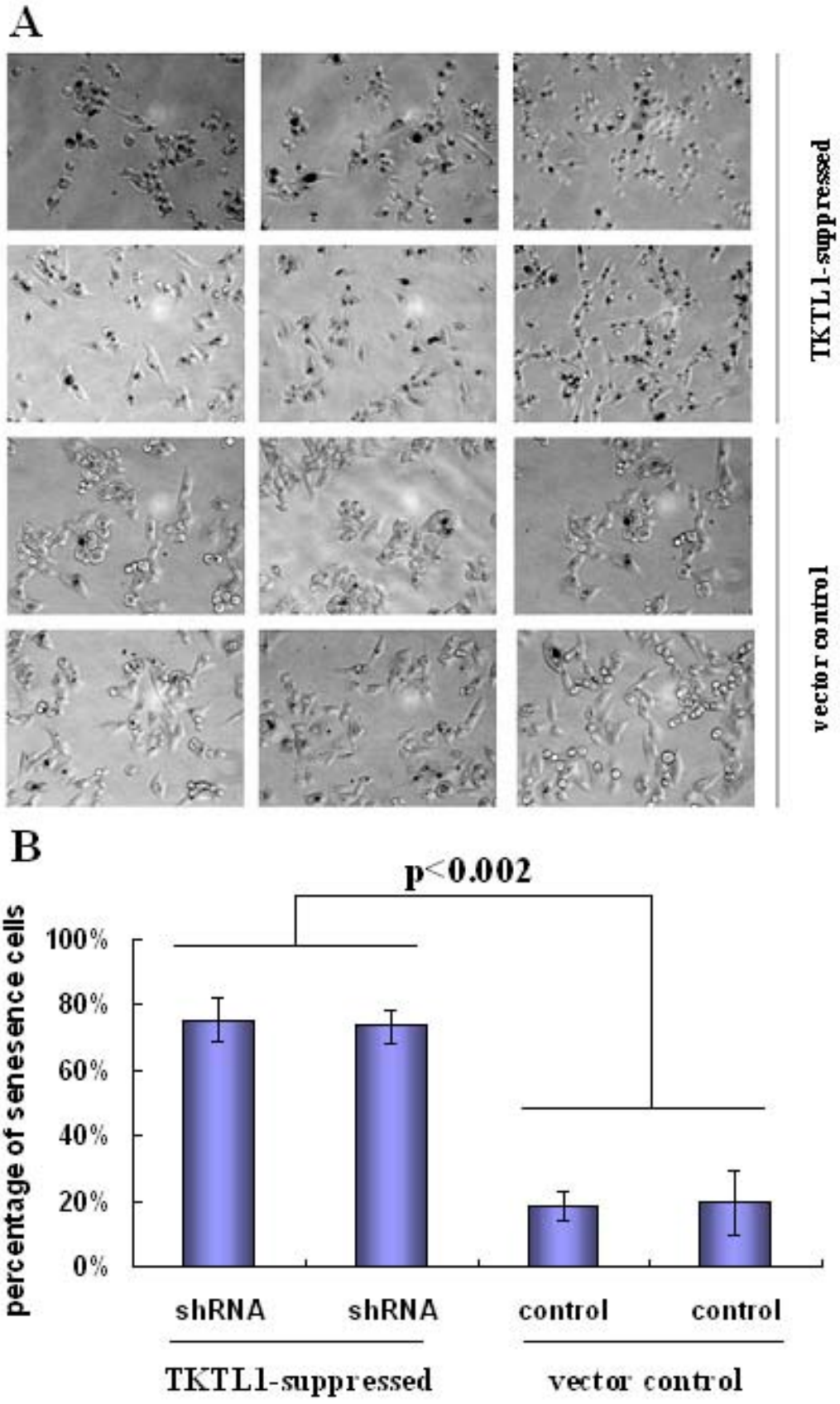

Figure 24 TKTL1 suppression leads to cell senescence. (A) Cells were fixed and stained for the detection of senescence associated β-gal. Every line of pictures represents three different staining

experiments of the TKTL1-suppressed clone IA1 and I5, and vector control clones IIIA2 and IIIC4. Pictures were taken at 400 × magnification. (B) SA-β-gal positive cells were counted, and the percentage of senescent cells is shown in the histogram. Error bars represent standard deviation of the three experiments.

statistically significant (Figure 24B). In all cell clones, the detaching cells which are mainly actually dividing were negative for SA-β-gal staining. Since senescence cells have a poor ability to divide, this observation confirms that the assay is very precise and specific.

3.15. Altered expression of HIF-1α upon shRNA-mediated TKTL1 suppression

Hypoxia is a common feature of many solid cancers and has been linked to malignant transformation, metastasis, and treatment resistance (Hockel and Vaupel, 2001). Cancer cell normally have high expression level of hypoxia-inducible factor 1α (HIF-1α), a key transcription factor which up-regulates angiogenic signaling, glucose transporters and glycolytic enzymes, to achieve adaptation to the hypoxic condition (Semenza, 2003). HIF-1α is also activated by aerobic glycolysis, more specifically, the end product of glycolysis: pyruvate and lactate (Lu et al., 2002).

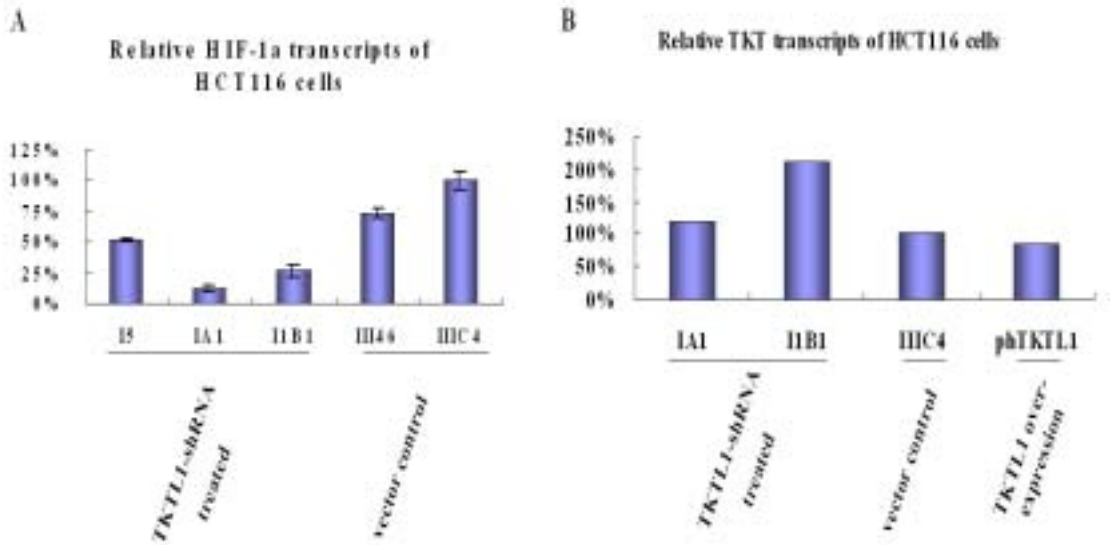

Figure 25 Expression pattern of hypoxia inducible factor HIF-1α. (A) Relative HIF-1α

expression pattern of different TKTL1-shRNA treated and vector control HCT116 clones (B) The expression of house-keeping gene transketolase (TKT), which serves as a transcription control, is only affected in a single case (clone I1B1) by changes in the TKTL1 expression level. Error bars represent standard deviation.

In TKTL1-suppressed HCT116 cells, HIF-1α expression is attenuated as determined by qRT-PCR (Figure 25A). Since suppression of TKTL1 reduces the activity of the PPP, in which riboses are generated for NTP and dNTP synthesis (precursors of RNA and DNA), the reduction of HIF-1α could be the result of an attenuated overall transcription level. Thus the expresseion of the house-keeping gene transketolase (TKT) was analyzed. The expression of TKT was in most clones unchanged except clone I1B1 (Figure 25B).

Since the oxygen concentration under normal cell culture conditions is unphysiologyically high (~21%), this leads to the ubiquitination of HIF-1α by the von Hippel–Lindau (VHL) protein and the subsequent proteasomeal degradation (Semenza, 2003). Two methods are used to mimic hypoxic conditions to block the degradation of HIF-1α. We used either 100 μM $CoCl_2$ for 24 hours (Chandel et al., 1998) or 5 μM MG132, a broad inhibitor of the proteasome, to block the proteasomal degradation of HIF-1α. Upon indirect immunofluoresence staining, TKTL1-suppressed cells showed very weak signals of HIF-1α, especially in the nucleus. Many of the vector control cells had strong HIF-1α signals and consistently accumulated in the nucleus (Figure 26A). When cells were treated with 5 μM MG132 for 24 hours, TKTL1-suppressed cell clones displayed HIF-1α signals mainly in the cytoplasm. In controls, one cell clone showed nuclear plus cytoplasmic accumulation and the other showed nuclear localization of HIF-1α. As a transcription factor, HIF-1α carries out its functions in the nucleus. These results suggest that HIF-1α activity is attenuated in TKTL1-suppressed cells.

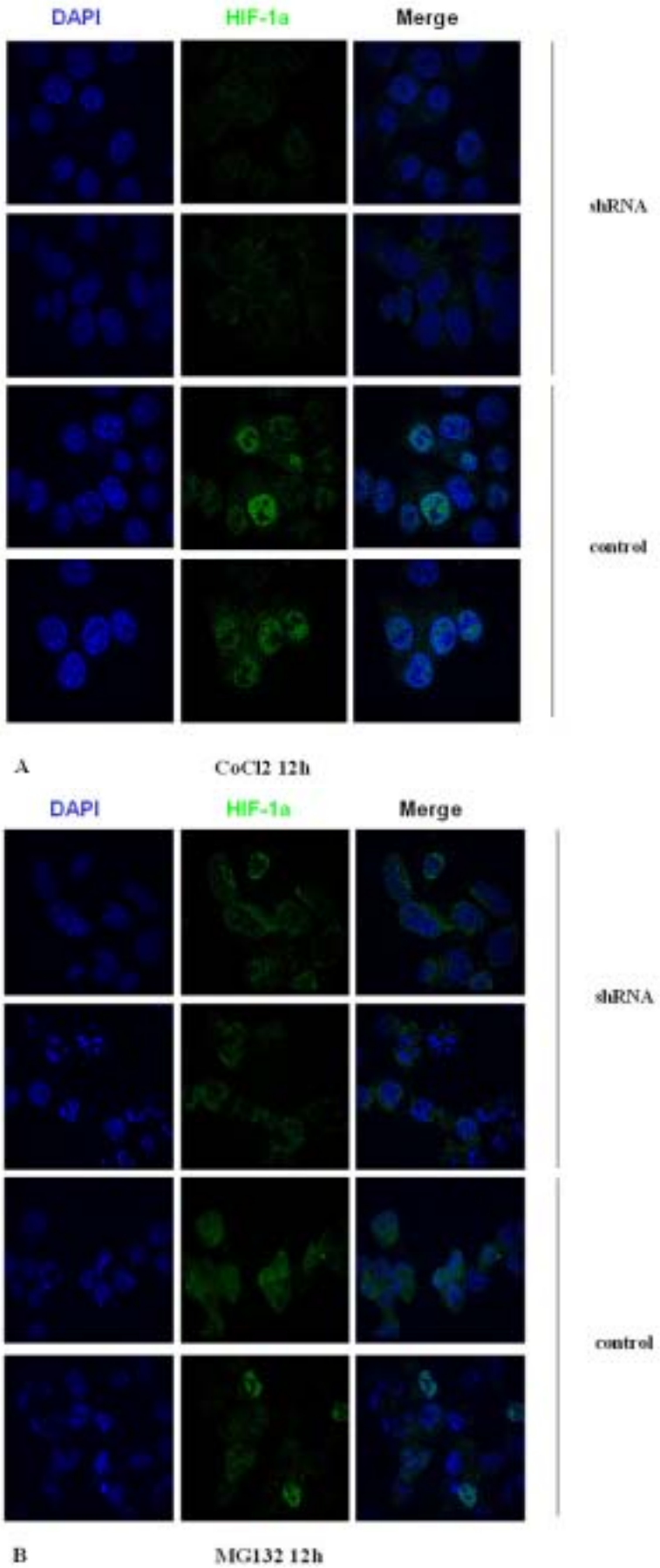

Figure 26 Induced accumulation of HIF-1α is retarded in TKTL1-suppressed HCT116 cells.

Control and TKTL1-suppressed HCT116 cells were treated with $CoCl_2$ (A) or MG132 (B) for 12 hours for HIF-1α accumulation. In the upper two panels, two shRNA-treated cell clones IA1 and I1B1 and in the lower panel control HCT116 cell clones IIIC4 and III46 were stained with an anti-HIF-1α antibody and detected by Alexa488-labeled secondary antibody.

3.16. Influence of TKTL1 on cell mobility and cell transformation

The Warburg effect of tumor cells results in the production of large amount of lactic acid compared to normal cells (Figure 12). Lactic acid clearly contributes to the acidic tumor-microenvironment, and the low-pH environment surrounding tumors is supposed to accelerate tumors infiltration into surrounding tissues, leading to an enhanced metastatic potential. The activity and expression of heparanases, acid cathepsins, matrix metalloproteinases, and plasminogen activators have been demonstrated both in tissue culture and in tumor biopsies (Chambers and Matrisian, 1997). Such enzymes facilitate degradation of extracellular matrix, allowing release and detachment of tumor cells, as well as removing critical tissue barriers (connective tissue) that can physically impede or retard the movement of cells. The presence of this enzyme-rich and acidic environment not only facilitates tumor cell movement, but is a key to sprouting and integration of new vasculature (Gatenby and Gawlinski, 1996; Gatenby et al., 2006).

To study effects of TKTL1 on cell mobility and invasiveness, the in vitro invasive assay and wound closure assay were performed using cell clones with different expression levels of TKTL1.

In the in vitro invasion assay, NIH3T3 cells were used since NIH3T3 is a non-invasive cell line. HA-tagged TKT, TKTL1 and TKTL2 proteins were transiently introduced into the cells by transfection of overexpression vectors. Two days after transfection, the invasiveness of these cells was measured (protocol described in chapter 2.2.17.). Interestingly, only NIH3T3 cells transfected with the HA-TKTL1 overexpression vector showed a significant increase in invasiveness (Figure 27), while empty vector pcDNA3.1 and other transketolases (TKTL2 and TKT) did not affect this phenotype (Figure 27).

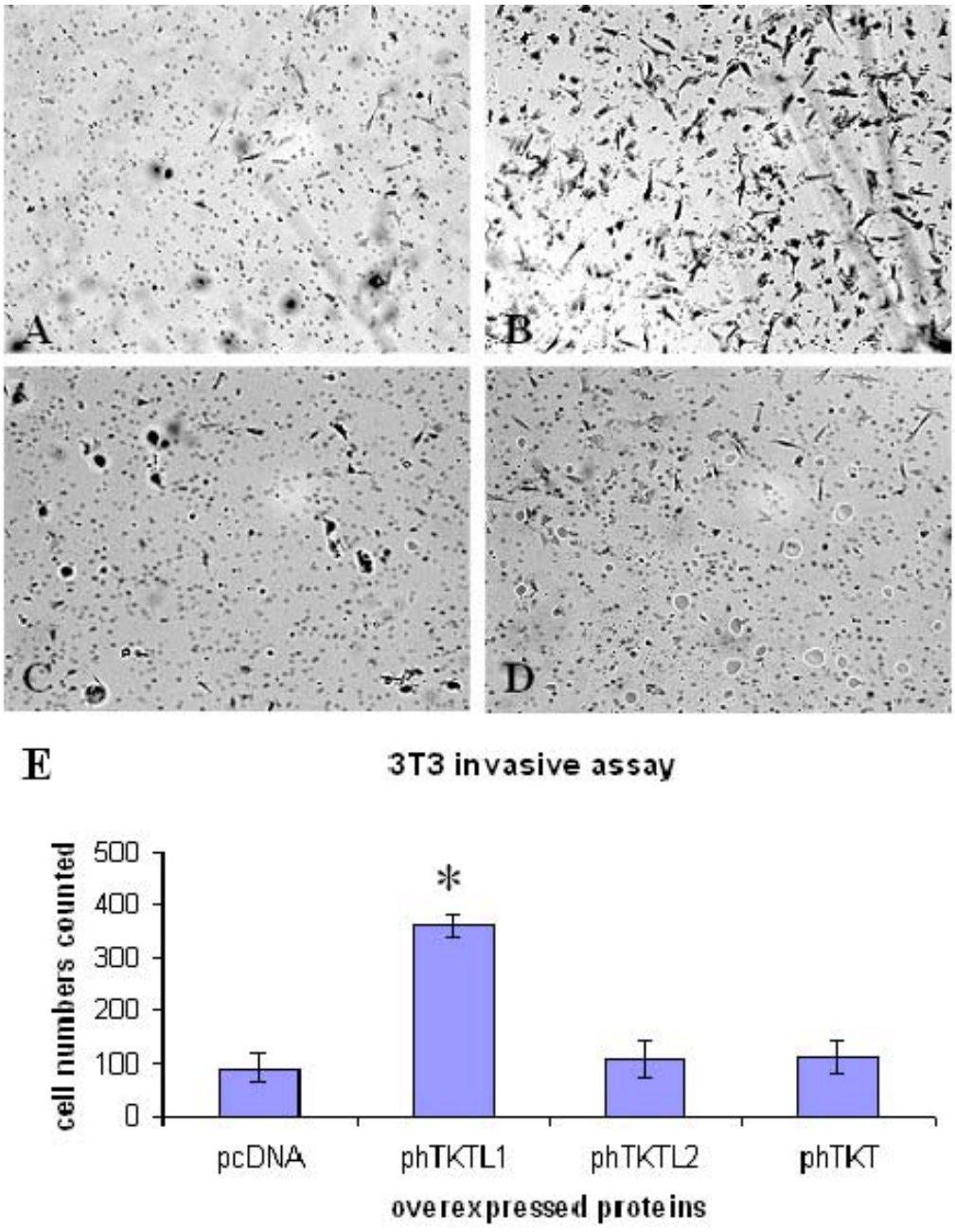

Figure 27 In vitro invasive assay of 3T3 cells transfected with transketolase overexpression plasmids. The assay was performed using Matrigel as reconstituted extracellular matrix in Falcon cell culture inserts in vitro. NIH3T3 cells were transfected with different transketolase-overexpression and empty (pcDNA3.1) plasmids by lipofectamine 2000. Two days after transfection, cells were transferred into matrigel-coated inserts (2.2.17.). Penetrated cells were fixed and stained, and images were taken under Leica inverted microscope at the magnification of 100 ×. A, 3T3 cells transfected with pcDNA3.1 empty vector as the negative control. B, 3T3 cells transfected with TKTL1 overexpression clone. C, 3T3 cells transfected with TKTL2 overexpression clone. D, 3T3 cells transfected with TKT overexpression clone. E, Number of penetrating cells per insert (y-axis) in each group. Data are reported as the mean ± SD for three independent experiments carried out in triplicate. * $p < 0.05$ compared to control (student t-test).

Error bars represent standard deviation.

Since the Matrigel invasiveness assay is not suitable for HCT116 cells due to their poor invasiveness and the fact that they easily detach the surface, we chose the wound closure assay (2.2.18.) to investigate the mobility of TKTL1-suppressed and vector control cells.

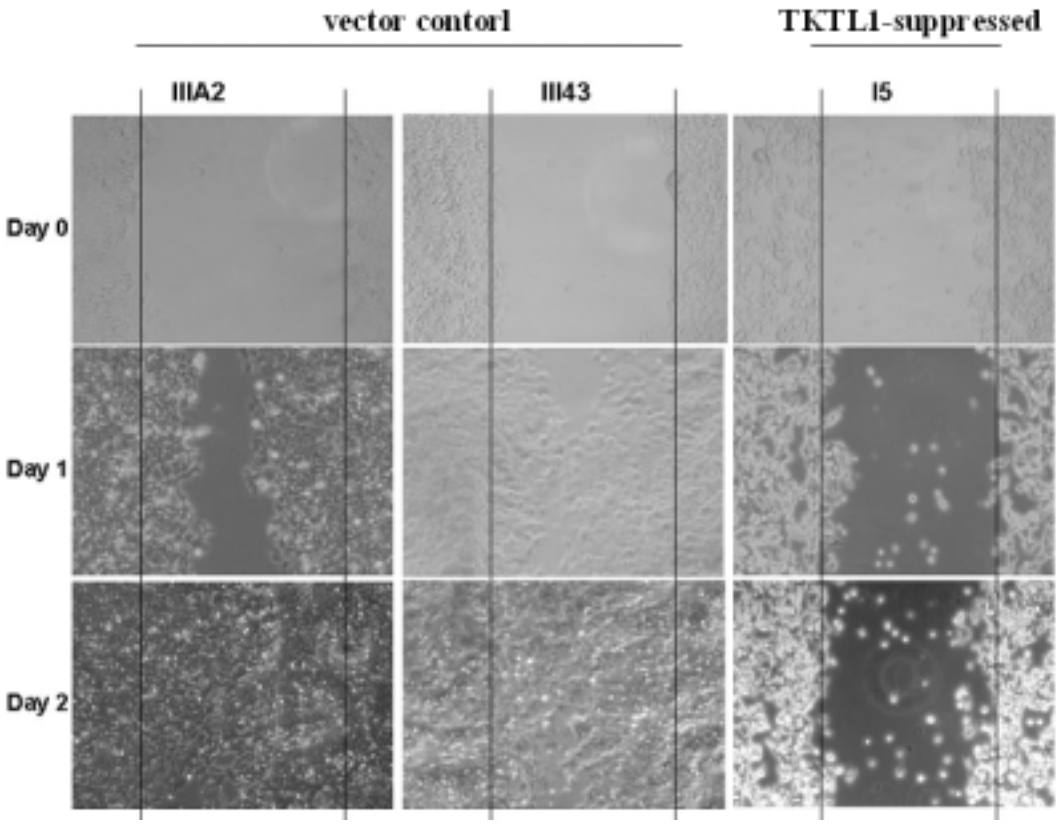

Figure 28 TKTL1 suppression leads to delayed wound closure. The wound closure assay was performed in 6-well dish. Scars were made using 200 µl pipette tips after cells reached confluency, cells were then observed for two days. Pictures show that TKTL1-suppressed cell clone (I5) had much slower wound healing speed compared to control cell clones (IIIA2 and III43).

After cells grew to confluency, scars were gently made using 200 µl pipette tips, cell debris was carefully removed by washing with PBS, new culture medium was changed every day. We marked specific spots to observe the wound healing process under light microscopy everyday after medium change. The scar areas in vector control cells (IIIA2 and IIIC4) were rapidly healed, covered by growing cells

emerging from the edge of the cut. Within two days, almost all of the scar area was covered. In contrast, the scar area of TKTL1-suppressed cells (I5) remained clear over an extended perioid of time (Figure 28). The images show that the proliferation and migration ability of HCT116 cells is significantly decreased after suppression of TKTL1, indicating that TKTL1 in carcinoma cells may contribute to the aggressiveness. Since the recovery speed of the wound closure depends on cell proliferation and mobility, TKTL1 expression may not only contribute to faster cell proliferation, but also to higher cell mobility, which might be directly related to an enhanced of production of lactic acid (Figure 12B).

3.17. TKTL1 suppression leads to decreased in vitro transformation of HCT116 cells

Transformed cells in culture are usually characterized by increased saturation density and anchorage-independent proliferation (Bignami et al., 1987). The ability of transformed cells to produce discrete focal areas (foci) in a dense monolayer and to form colonies in soft agar has been useful in identifying viral and cellular oncogenes (Land et al., 1983; Pozzatti et al., 1986). Since TKTL1 expression is closely related to cell proliferation (Figure 13), invasiveness (Figure 27) and migration (Figure 28), we were interested in investigating whether TKTL1 influences the transforming potential. The focus formation assay and saturation density assay were performed to test the in vitro transforming ability of HCT116 cell clones.

TKTL1-suppressed and control cell clones were plated in 10 cm dishes and cultured to 100% confluency. Cells were maintained for additional 2 weeks with medium changed every 2 to 3 days. Finally, cells were fixed by cold methanol and stained with 0.1% methylene blue (w/v) for 10 minutes and documented (Figure 29 A). Control cells had very strong blue staining, and a lot of foci were formed, while in TKTL1-suppressed cell clones, the blue staining was much weaker, and foci were barely seen. These data indicate that TKTL1 suppression leads to a reduction of focus formation in HCT116 cells.

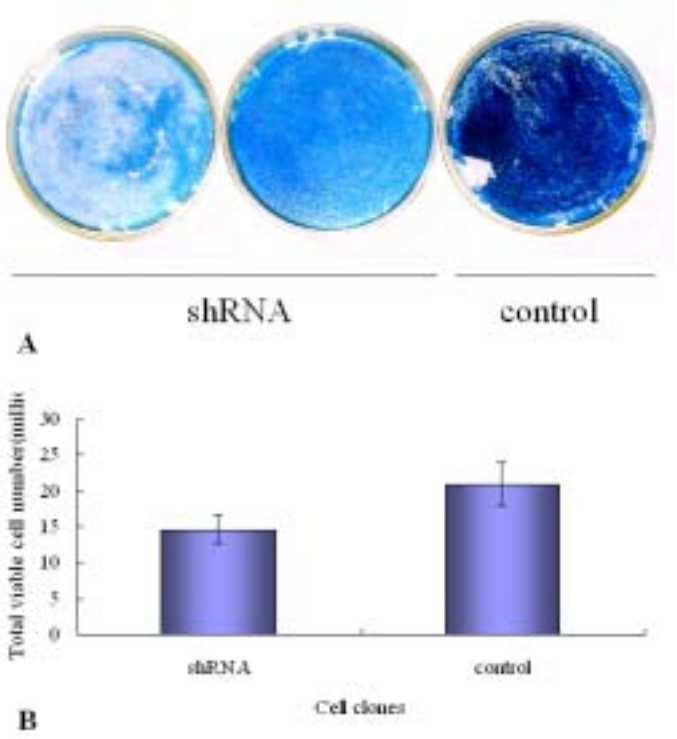

Figure 29 In vitro transformation of HCT116 cells with different TKTL1 expression patterns. (A) Focus formation in HCT116 cells clones after 3 weeks after reaching confluency, two shRNA treated cell clones (I5 and IA1) had much weaker staining compared to control (IIIC4). (B) Mean numbers of confluent HCT116 cell clones. Data are from three independent experiments. Error bars represent standard deviation. $p<0.05$

Since TKTL1 suppression via shRNA vectors in HCT116 cells leads to well-defined clearer cell-cell margins (Figure 10), TKTL1 may probably affect cell growth at high cell density. We thus checked the saturation density of TKTL1-suppressed and control cell clones. We plated 2×10^6 cells in each 10 cm dishes and cultured the cells to confluency with medium change every three days. After reaching confluency, cells were trypsinized and counted with a hematocytometer. Compared to control cells, TKTL1-suppressed cells reached around 25% less of the confluent density (Figure 29B). Taken these data together, we conclude that TKTL1 may play an important role in the process of transformation and maintenance of the tumor malignancy.

3.18. TKTL1 suppression affects cancer stem cells population marker

Cancer stem cells (CSC) or cancer-initiating cells (CIC) are cells within a cancer

cell population or tumor that have the exclusive ability to self-renew and to differentiate into the heterogeneous lineages of cancer cells that comprise the tumor. Recent studies indicated that $CD133^+$ colon carcinoma cells may be cancer stem cells (O'Brien et al., 2007; Ricci-Vitiani et al., 2007). We thus checked the CD133 expression in TKTL1-suppressed cells by qRT-PCR and found that the mRNA levels were reduced with clonal variation among different TKTL1-suppressed and control cell (Figure 30).

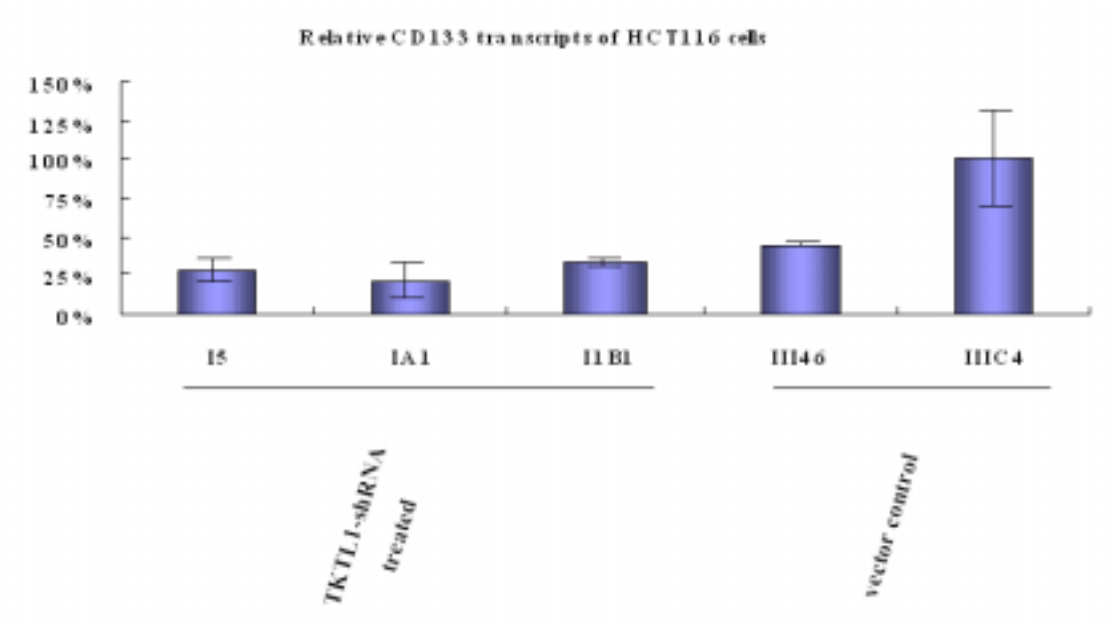

Figure 30 Expression pattern of the colon cancer stem cell marker CD133 in TKTL1-suppressed HCT116 cells. Relative CD133 expression of different TKTL1-suppressed and control HCT116 clones was determined by qRT-PCR. Error bars represent standard deviation.

3.19. TKTL1-suppressed cells formed smaller tumors in xenograft experiments

In order to assess the effect of TKTL1 on tumor growth, xenograft model in nude athymic mice was used. About 2×10^6 TKTL1-suppressed or vector control HCT116 cells were implanted subcutaneously into the right flanks of the mice hindlimbs (2.2.21.). The mice had free access to water and food. In the first set of experiments, 30 animals were divided into 2 groups: control cells xenograft (cell clone IIIC4, n =

15), and TKTL1-shRNA treated cells xenograft (cell clone IA1, n = 15). There were 3 mice in each group that did not develop tumors. During analysis, all 30 mice were divided into three groups: mice that did not carry visible tumors (tumor-free group, n=6), mice that carried tumors formed from TKTL1-suppressed HCT116 cells (TKTL1-supressed group, n=12) and mice that carried tumors formed from vector control HCT116 cells (vector control group, n=12). Control group mice rapidly developed tumors with a constant exponential tumor growth (Figure 31 and 32). TKTL1-suppressed groups had a significant decrease in tumor size upon weekly measurement of maximal diameter (a) and minimal diameter (b) using calipers, tumor volume was calculated with the formula $v=0.5 \times a \times b^2$ (Carlsson et al., 1983).

The tumor growth kinetics are shown in Figure 31A. Two weeks after cells injection, TKTL1-suppressed and control groups showed significant differences in tumor size ($p<0.01$). At 6 weeks after injection, the TKTL1-suppressed group tumors were normally ~6 mm in diameter, while control group tumors were from 10 mm and up to 20 mm in diameter. These clear differences are documented in Figure 31A and Figure 32A. After sacrifice, mice tumors were weighed on a balance (Sartorius). The result shows that TKTL1-suppressed IA1 tumors are much lighter than those derived from control cells (Figure 31B).

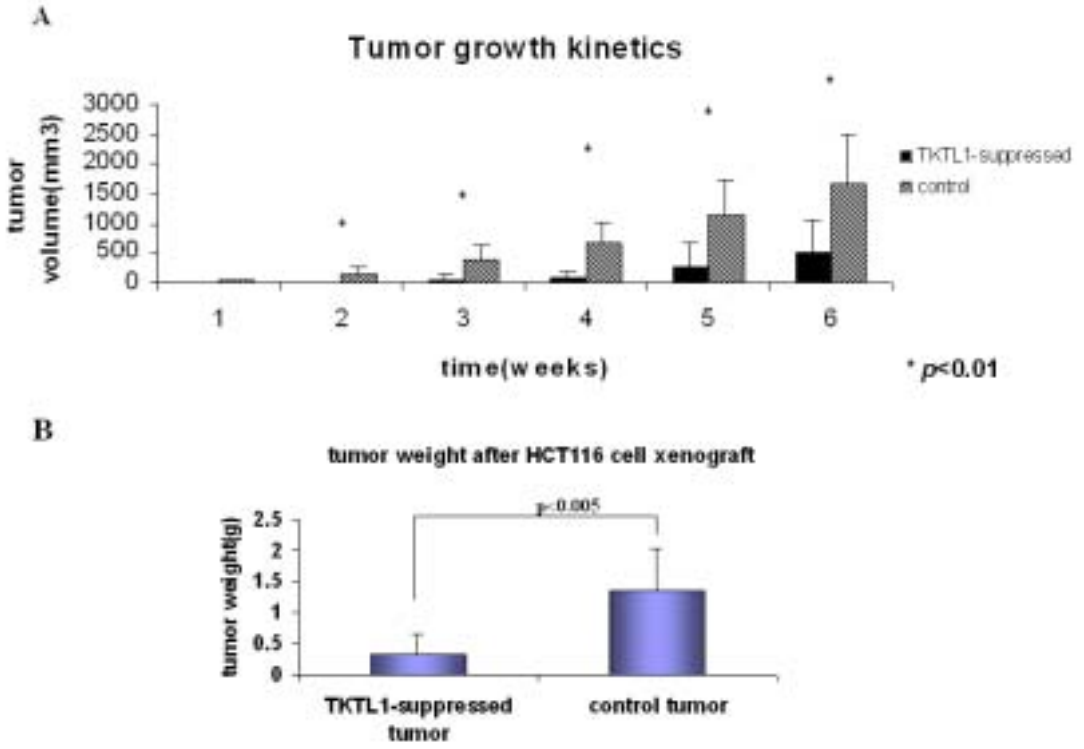

Figure 31 Smaller tumors formed by TKTL1-suppressed HCT116 cells. (A) Injection of TKTL1-suppressed and control HCT116 cells into the right flank of nude mice resulted in the development of measurable tumors within two weeks in 24 out of 30 animals. After injection, the size of tumors was measured weekly using calipers and the volume was calculated accordingly. * $p< 0.01$ versus controls (t-test). Error bars represent standard deviation. (B) Tumors were weighed at the time of euthanasia, the bars represent the mean values (each group n=12). TKTL1-suppressed tumors are much lighter than control tumors ($p<0.005$).

After sacrifice, tumors were carefully taken out and photographed (Figure 32B). The control tumors were not only much bigger, but also had more blood vessels on their surfaces even when the tumor sizes were similar.

The tumor samples were carefully fixed and will be applied for further studies to identify the properties of tumors, such as proliferation, apoptosis, vascularization and changes in important oncogenes and tumor suppressor genes. These will let us know how TKTL1 could affect tumor features in vivo.

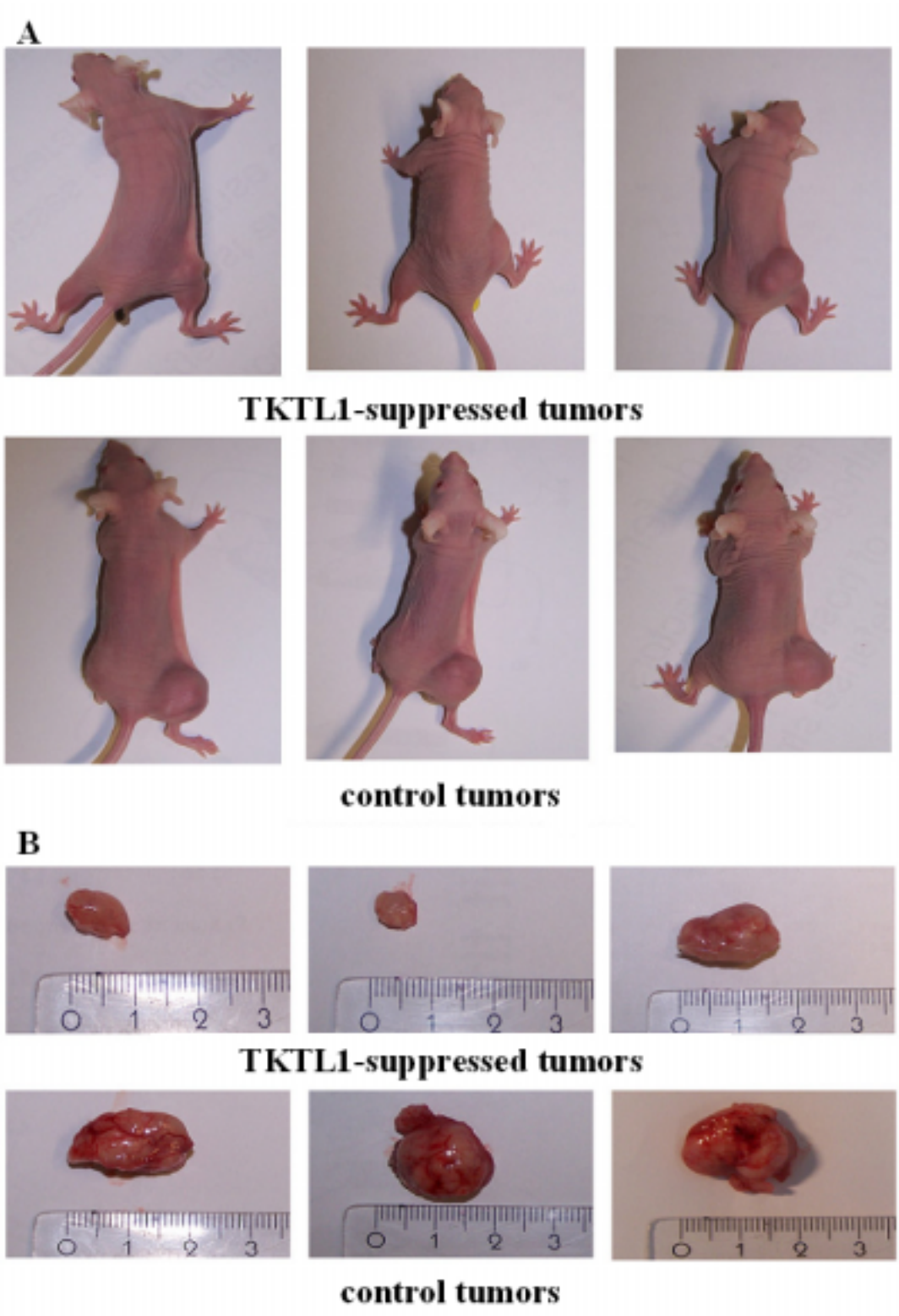

Figure 32 Images of TKTL1-suppressed and control tumors. (A) Before sacrifice, the images of mice carrying tumors were taken using digital camera, showing again that TKTL1-suppressed cell xenografts resulted in significantly smaller tumors. (B) The images of isolated tumors show that TKTL1-suppressed xenografts resulted in smaller tumors, which had less vascularization on their surfaces. * $p < 0.05$ versus controls (t-test). Error bars represent standard deviation.

3.20. TKTL1-suppressed tumors caused phenotypes indicative of cachexia

Cachexia is a syndrome characterized by enhanced catabolism of body fat and skeletal muscle and contributes to nearly one-third of all cancer deaths (Acharyya et al., 2004; Chamberlain, 2004). In the xenograft mice, cachexia phenotypes were determined to assess tumor malignancy. The following cachexia phenotypes were measured in these experiments: body weight (whole body weight subtracted by tumor weight), water and food uptake, para-renal fat tissue weight and left side of tibialis anterior (TA) muscle weight.

Food and water uptake were recorded two week after injection. Mice carrying TKTL1-supressed or vector control HCT116 cell xenografts were separated in different cages (5 mice per cage) and consumption of food and water was measured weekly for each cage. Upon tumor development, mice ate and drank less. A notable reduction of food uptake was only observed starting the 5th week for control animals and the 6th week for TKTL1-suppressed tumor group (Figure 33A). Water uptake in TKTL1-suppressed group mice increased slightly while in control group it remained to a constant level (Figure 33B).

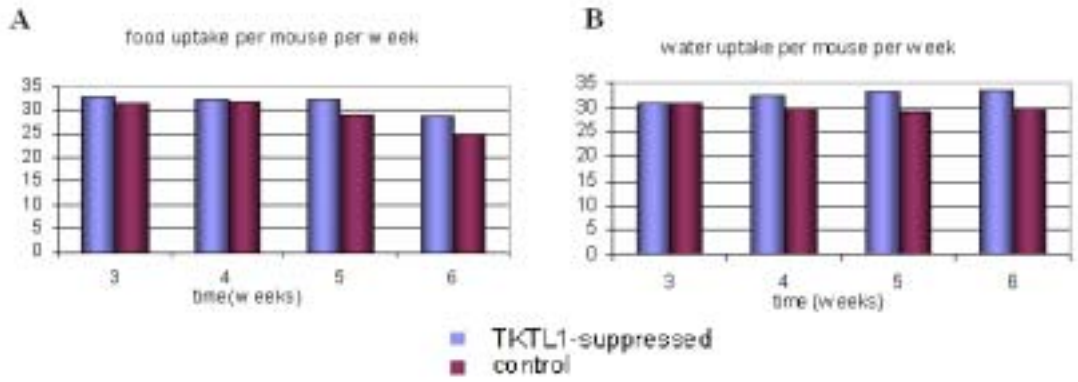

Figure 33 Food and water uptake of tumor xenograft mice. Two weeks after cell injection, food (A) and water (B) consumption was recorded weekly. The values are averages for each mouse per week.

Patients with cancer cachexia show a progressive loss of body weight, which is mainly due to loss of fat and skeletal muscle (Chamberlain, 2004). Mice body weight

was measured weekly, the upper panel of Figure 34A displays the body weight with tumors, while in the lower panel, the tumor mass was subtracted. The tumor-free mice group (n=6) gained body weight by time. TKTL1-suppressed group had a similar tendency of body weight increase, while the vector control group did not gain body weight. Thus, at the end of the experiment, the vector control group mice were significantly lighter. When tumor weight was subtracted from total body weight, TKTL1-suppressed group did not show any obvious difference to tumor-free group, both gained weight gradually. The control group mice showed decreased body weight from the third week, and the difference was significant for the last 3 weeks compared to TKTL1-suppressed group. These data showed that TKTL1-suppressed tumors caused less severe cachexia phenotypes.

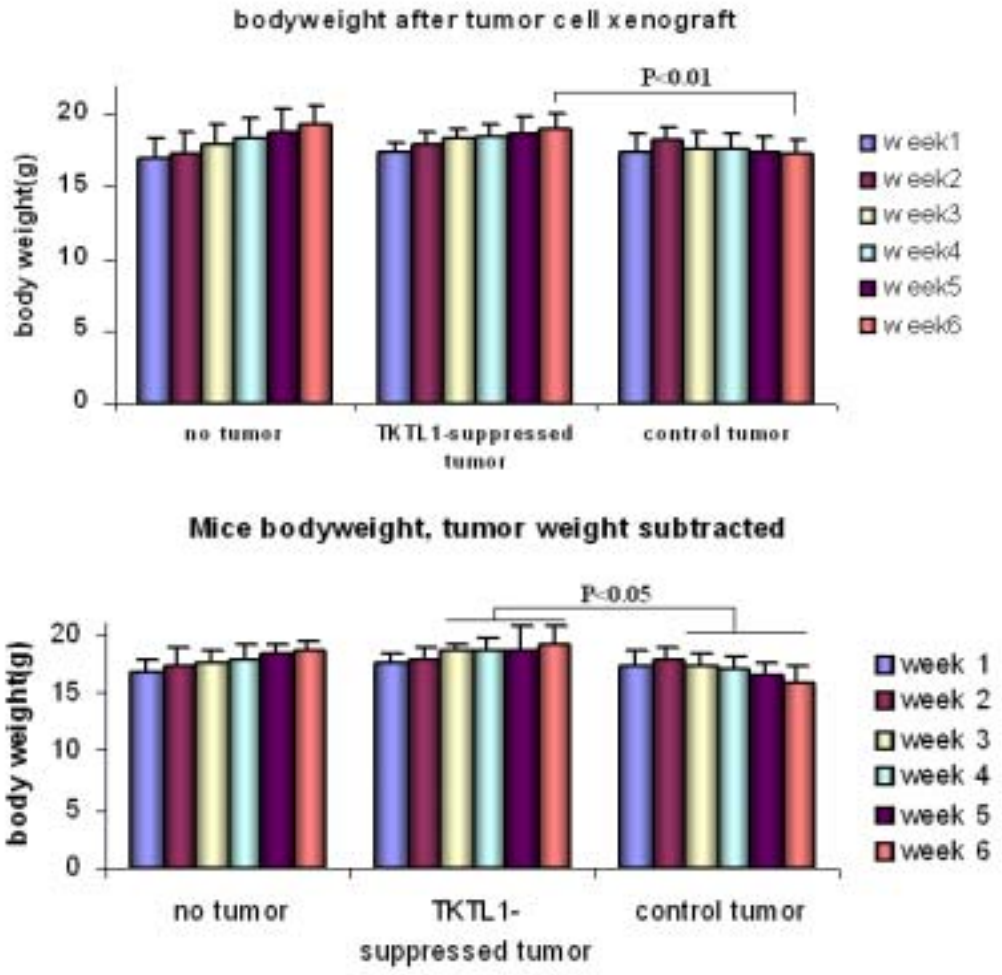

Figure 34 Body weight changes among tumor-free mice, TKTL1-suppressed tumor and control tumor bearing mice. The upper panel shows body weight including tumors, mice in both

tumor-free and TKTL1-suppressed groups gained body weight gradually, while body weight of control tumor group mice remained constant. Only in week 6, the difference between TKTL1-suppressed and control tumor group is significant ($p<0.01$). The lower panel shows bodyweight without tumors. Similar resultes were observed in both tumor-free and TKTL1-suppressed groups, while in control tumor group, mice body weight even showed a gradual decrease. In the last 4 weeks, the difference between TKTL1-suppressed and control tumor group is significant ($p<0.05$). Error bars represent standard deviation.

When comparing both sides of para-renal fat tissues, tumor-free group mice had 25~30 milligrams of fat on both sides. In TKTL1-suppressed tumor group mice, fat weight was slightly reduced (~20 mg), while the tumor-bearing control group mice consistently displayed a remarkable reduction to about 10 milligrams each. This observation correlates to the fact that animals with rapidly developing tumors lost weight under ad libitum feeding conditions (Figure 34). We also looked into the TA muscle weight on the opposite site of injection. In tumor-free group, the TA muscle weight was around 40 milligrams each, vector control group mice had a strong reduction of the TA muscle weight to ~25 milligrams, while in TKTL1-suppressed tumor mice, weight of the left TA muscles was only slightly reduced to ~35 milligrams (Figure 35B).

Despite the fat mobilisation described above, there was a decrease in blood glucose levels in contol group compared to TKTL1-suppressed group. Hypoglycemia occurs in mice bearing a cachexia-inducing tumor, although the mechanism by which this occurs is not known (McDevitt and Tisdale, 1992). Compared to tumor-free animals (~120 mg/dL Blood glucose), both TKTL1-suppressed and control tumor groups had lower blood glucose. Blood glucose of TKTL1-suppressed tumor group mice was slightly reduced to ~110 mg/dL, while control tumor group mice had ~20% lower blood glucose (~95 mg/dL), a difference that turned out to be statistically significant (Figure 35C).

Interestingly, an additional important cachexia phenotype, increased liver weight, was not consistently observed in this experiment. Compared to tumor-free mice, TKTL1-suppressed tumor bearing mice had a slight increase in liver weight, but control tumor bearing mice had significantly reduced liver weight (Figure 35D).

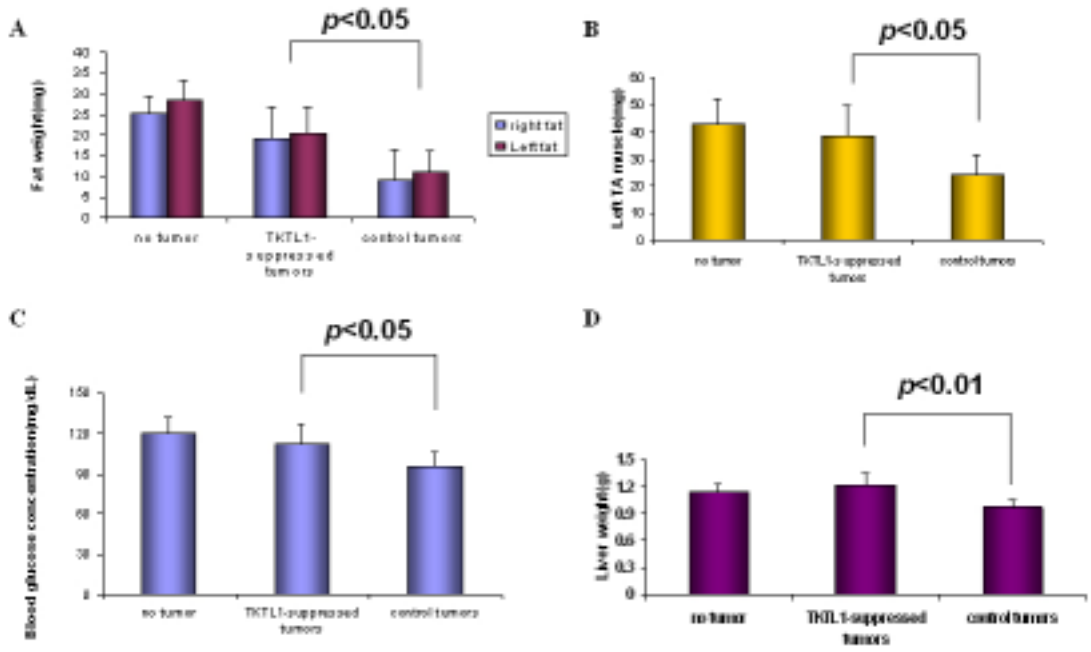

Figure 35 Cachexia related phenotypes of TKTL1-suppressed and control tumors bearing mice. (A) para-renal fat tissues; (B) left side of TA muscles; (C) blood glucose and (D) liver weight were compared among tumor-free animals (n=6), TKTL1-suppressed and control tumors bearing animals. Error bars represent standard deviation.

3.21. TKTL1 suppression tumors had less necrosis

Central necrosis is a common feature in invasive cancers and is associated with poor outcome and tumour aggressiveness. It is thought that tumor necrosis is caused by chronic ischaemia (i.e. hypoxia, low pH, low glucose, high lactate) within tumours, caused by vascular collapse, blood shunting to other sites and/or rapid tumour cell growth overtaking the rate of neovascularization in a given area (Leek et al., 1999). The necrosis inside a solid tumor is associated with increased risk of developing an invasive cancer in the future (Demirag et al., 2005; Edwards et al., 2003; Lee et al., 2006; Sengupta et al., 2005).

In xenograft experiments, we found that the tumors formed by TKTL1-suppressed HCT116 cells normally had less necrosis area (normally less than 30% of the tumor section with a single exception of 60%), while tumors in control group contained necrosis area of almost up to 80% (Table 5).

Case	Necrosis area (%)	Tumor size (~mm^3)
TKTL1-suppressed tumors	60	1170
	<30	350
	<20	120
	15	2430
	20	100
Control tumors	50	1520
	80	1960
	80	1110
	80	2120
	80	2400
	80	2410

Table 5 Necrosis area of xenograft tumors. Five TKTL1-suppressed and 6 control tumors were analyzed. H&E staining shows significant differences in necrosis area of these tumors. The necrosis area seems not to be related to tumor size.

4. Discussion

Tumors normally have abnormal metabolism properties owing to the abnormal growth. Aerobic glycolysis (or Warburg effect) is a very common metabolic feature of tumors, although the molecular basis has not been identified yet. However, the biological consequence of the aerobic glycolysis, the enhanced metabolism of glucose, is already successfully applied in the clinic by the PET technique to visualize tumors and metastases (Downey et al., 2004; Kumar et al., 2005).

Recent studies already show that transketolase-like protein 1 (TKTL1) is specifically over-expressed in tumors predicting poor cancer patient survival. In contrast, TKT and TKTL2 expression was not altered, suggesting that TKTL1 may play a major role in tumor-specific glucose metabolism (Langbein et al., 2006). The gene silencing of TKTL1 by siRNA led to inhibition of cell proliferation (Hu et al., 2007). Here we confirmed and extended these studies, we found evidence that TKTL1 in HCT116 cells functions as a metabolic switch to aerobic glycolysis, which not only provides cancer cells with significant advantages for survival of high oxidative stress, but also increases the malignant phenotypes of tumor cells by enhanced cell mobility and vilbility.

4.1. Metabolic changes after TKTL1 suppression

When TKTL1 was suppressed by shRNA constructs as done in this study, it is conceivable that the treated cells displayed a lower glucose consumption rate (Figure 12), since TKTL1 controls the non-oxidative phase of the PPP, which is also a very important glucose metabolic pathway. About 20% of the lactate is produced from degradation of glucose via the PPP. In the present study, TKTL1 suppression led to about 30% less lactate production rate (Figure 12), suggesting that TKTL1 plays a major role in lactate production via the PPP.

TKTL1 seems to be closely related to carcinoma cell growth/proliferation, and thus overexpression of TKTL1 in carcinoma cells may function as a supportive factor for energy and nutrients supply due to the advantages of glycolysis. The highly

expressed TKTL1 in carcinoma cells could help to fulfill the huge demands for energy and nutrients, meanwhile it may also make these cells more addicted to aerobic glycolysis.

The fast growing feature of cancer brings a tremendous demand for energy supply. However in cancer, mitochondrial glucose oxidation is generally attenuated or even inhibited and energy production relies mainly on the cytoplasmic glycolysis. Although glycolysis is en inefficient way to produce energy in the form of ATP compared to oxidative phosphorilation (OXPHOS), it has many advantages: the reaction occuors directly after glucose is transported into the cell; the ATP produced in the cytoplasma could be used directly for other biochemical reaction; the intermediate products are used as precursors for macromolecule synthesis like lipids, proteins and nucleic acids. The cytoplasmic localized TKTL1 (Figure 7) facilitates fast glucose degradation once glucose is transported into the cell. Since glycolysis is not inficient, cancer cells need other energy production form, such as fatty acids β-oxidization, to fill the energy gap (Figure 18). The overexpression of TKTL1 in cancer cells is associated with increased PDK (Figure 18), which inactivates PDH to transform pyruvate into acyl-CoA. Inactivation of PDH blockes the carbon flow entering mitochondria and TCA cycle. Since oxygen is mainly consumed at mitochondria via OXPHOS, cancer cells may thus have a lower oxygen consumption rate (Figure 17). Meanwhile, surplus pyruvate is transformed into lactate even in the presence of oxygen. Since released lactate is correlated with metastases and poor patient survival (Stern et al., 2002; Walenta et al., 2000), blocking TKTL1 activity may thus reduce tumor invasiveness and could achieve better patient's prognosis.

HIF-1α and metabolism are closely connected: on one hand, HIF-1α could upregulate glucose metabolic enzymes, which favors the degradation of glucose and production of energy (Semenza, 2003), it also controls the switch from TCA cycle to glycolysis (Kim et al., 2006). On the other hand, some of the metabolic intermediates of glycolysis or TCA cycle could lead to HIF-1α stabilization (Lu et al., 2002; Tomlinson et al., 2002). When TKTL1 is over-expressed, the production of lactate could stabilize HIF-1α (Figure 26), the activated HIF-1α then increase the expression

of metabolic enzymes and glucose transporters. This positive feedback makes TKTL1 over-expressing cancer cells consume high amounts of glucose, suppress mitochondria respiration, and thus making malignant cells more addicted to glycolysis for energy supply. The data presented here suggest that TKTL1, as well as HIF-1α could be a link between metabolism and cancer.

4.2. TKTL1 and cell growth

Studies utilizing radioactively labeled glucose revealed that glucose is the main source of tumor cell RNA and DNA pentoses (Boros et al., 1997; Horecker et al., 1958) and *de novo* lipid synthesis (Lee et al., 1995) besides its central role in energy production. The strong proliferation of tumor cells is governed by the replication of DNA in the S phase where the conversion of glucose to ribose is controlled by non-oxidative pentose phosphate pathway. It is thus not surprising that TKTL1-suppressed cells showed slower growth and enhanced numbers of cells arrested in the G0/G1 phase of the cell cycle as observed by flow cytometry (Figure 13).

The immortalization and malignant transformation of cells is mainly determined by genetically altered genes or their aberrant expression (Weng et al., 1999). Genetic alterations acquired by tumors cells also modify their biochemical pathways to support tumor growth, viability, and spread. The effect of TKTL1 on cell growth occurs not only in vitro, but also in vivo. In the tumor xenograft animal model, control tumors grew much faster than TKTL1-suppressed tumors (Figure 31). These data indicate that TKTL1 plays a very important role in cancer growth.

4.3. ROS production and protection upon TKTL1 suppression

Growing evidence suggests that cancer cells exhibit increased intrinsic ROS stress, due in part to oncogenic stimulation, hypoxic environment, and mitochondrial dysfunction (Pelicano et al., 2004). High-level ROS in cancer cells serve as the constant source of endogenous DNA-damage agents, leading to genomic instability,

and developing drug resistance, which gives cancer cells advantages in growth and survival from anti-cancer therapy. However, high-level ROS may also cause damage, depending on the levels and duration of ROS stress, to various cellular components including DNA, proteins, and lipid membranes (Hensley et al., 2000). A classical function of the PPP in mammalian cells is to provide NADPH redox equivalents through carbon flow from C_6 sugars (hexoses) to C_5 sugars (pentoses), while, the thioredoxin antioxidant system is amplified in malignant cells (Schumacker, 2006). These factors may contribute to the anti-ROS defense in cancer cells. The increased anti-ROS enzymes and redox equivalents in cancer cells seem to be regulated by expression of TKTL1. Upon TKTL1 suppression, both the ROS detoxifying enzymes and redox agents (GSH and NADPH) are impaired (Figure 20). Thus, blocking the PPP by TKTL1 suppression may disturb this redox balance and increase the susceptibility of the affected cells towards oxidative stress. For instance, extracellular oxidative stress upon addition of H_2O_2, intracellular stress through PEITC (generating ROS inside cells) or reagents which deplete anti-ROS agent GSH (DEM) resulted in a proportionally increased amount of ROS-induced apoptosis in TKTL1-suppressed cell clones (Figure 21). The TKTL1-suppressed clone I1B1 which has an increased TKT expression showed only minor effects upon TKTL1 suppression (Figure 9 and 25), which may explain the higher tolerence to H_2O_2 treatment (Figure 21A), since TKT also function in the PPP which produces anti-ROS agent (NADPH). These data indicate that tumor cells may benefit from high-level expression of TKTL1 when facing oxidative stress.

Four recent reports dispel doubts that cellular senescence is an important anticancer defense in vivo (Braig et al., 2005; Chen et al., 2005; Collado et al., 2005; Michaloglou et al., 2005). Furthermore, they even show that activated oncogenes (mutant genes that have the potential to transform normal cells into a cancerous state) induce cellular senescence in vivo, a phenomenon previously seen only in cell culture. The findings support the idea that the senescence response is a failsafe mechanism that prevents the proliferation of cells at risk for neoplastic transformation. ROS have an unexpected role in inducing and maintaining senescence-induced tumor

suppression (Lee et al., 1999). Since carcinoma cells are normally rapidly dividing, with low numbers of senescent cells even in the presence of enhanced oxidative stress, there must be some mechanisms to counteract ROS-induced cellular senescence. In our experiments, we showed that TKTL1-suppressed HCT116 cells showed a very strong senescence phenotype (Figure 24), while in the corresponding controls, senescent cells were barely seen. This raises the possibility that TKTL1 plays a role in anti cellular senescence process by providing sufficient quantities of redox equivalents. Upon mutations in oncogenes, many of which would lead to increased ROS, as well as cellular senescence, some of the transformed cells could activate anti-ROS defense systems to regain growth and survial advantages.

In addition, low energy metabolism favors stress-induced premature senescence (SIPS) (Toussaint et al., 2000b). This may also contribute cell cycle arrest after TKTL1 was suppressed. Pyruvate protect cells against SIPS induced by different types of stress while specific defence mechanisms, e.g. antioxidants, protect only against specific stress, as, for instance, oxidative stress (Toussaint et al., 2000a). The senescence-protection activity of pyruvate may explain the release of cell cycle arrest of TKTL1-suppressed cells upon presence of pyruvate (Figure 15). These data indicate TKTL1 may protect cancer cell from senescence by two mechanisms: reduction of ROS and increased pyruvate supply (via glycolysis).

4.4. TKTL1 and malignancies

It is now well accepted that several phenotypic traits of cancer such as invasion and metastasis may arise from the unique physiological environments created by tumors. Such environments encompass features such as low pH, hypoxia and nutrient depletion. These micro-environmental changes adversely affect the normal cells in the vicinity of the tumor, leading to disruption of metabolism, degradation of protein synthesis and even damage to their DNA. Such micro-environmental stresses therefore either lead to the destruction of normal cells, which would be subsequently replaced by dividing tumor cells, or favor the evolution of subpopulations of more

aggressive phenotypes, which are better adapted to survive in adverse conditions. Both factors contribute to the malignancy (tendency for invasion and metastasis) of the tumor (Rockwell et al., 2001). Here we showed that only overexpression of TKTL1, but not other transketolases, leads to increased invasiveness of NIH3T3 cells (Figure 27), suggesting that only TKTL1 contributes to the transforming potential and is related to malignancy.

Decreased CD133 expression after TKTL1 suppression is a very interesting phenomenon (Figure 30), although these effects may be only indirect consequences of TKTL1 suppression. It may indicate that TKTL1 not only functions as a metabolic enzyme, but also as a regulator of apparently unrelated cellular pathways like growth control, etc. Whether the protein level as well as the “stemness” of these cells also changed as we show here at the transcriptional level still needs to be elucidated.

Hypoxic regions exist in almost all solid tumours, and tumour oxygenation greatly affects tumour growth, malignant progressions, tumour prognosis and therapy efficacy (Hockel and Vaupel, 2001). The direct induction of angiogenesis by HIF-1α in cancers makes it a very important target for anti cancer therapy. It is shown that HIF-1α transcripts were reduced upon TKTL1 suppression under normoxic culture conditions (Figure 25), and under mimic hypoxic conditions, the expression of HIF-1α in TKTL1-suppressed cells was not only reduced but the ability of HIF-1α to enter the nucleus was also attenuated or even inhibited (Figure 26). Since HIF-1α is a transcription factor needed for the expression of hypoxic related survival factors, it only functions when present in nucleus. In addition, HIF-1 is a transcriptional complex that plays a pivotal role in angiogenesis related gene (VEGF, SDF-1, etc) expression (Semenza, 2003, 2007). So the suppression of TKTL1 may support any anti-angiogenesis cancer therapy.

Upregulation of catabolism, rather than defects in anabolism, appear to be most important for the loss of lipid from human adipose tissue in the contest of cancer cachexia. Loss of fat occurs when the metabolic demands on an organism are high, since fat constitutes 90% of the adult fuel reserves. Mobilisation of fat in cancer cachexia provides an energy source for the host when the metabolic demand is high.

Increased glucose utilisation by the tumour (Mulligan and Tisdale, 1991) results in an increased lactate production, the secreted lactate is uptaken in the liver to enter the Cori cycle (Holroyde et al., 1975) to form glucose, which consumes 6 moles of ATP per mole of glucose formed. However in tumors, aerobic glycolysis only generates 2 moles of ATP by degrading 1 mole of glucose. Thus for each cycle of degradation of glucose to lactate (in tumors) and reformation of glucose from lactate (in livers), there are 4 ATP consumed. Since TKTK1 is responsible for more lactic acid production in tumors (Figure 12), the faster the tumor grows, the more critical the energy shortage occurs for the cancer patients. These traits thus may account for the more severe cachexia phenotypes in control tumor mice, for example, the reduced body and fat tissue weight (Figure 34 and 35).

In the ongoing experiments, the tumor samples formed from TKTL1-suppressed or vector control HCT116 cells will be further studied. By comparison tumor features between TKTL1-suppressed and control samples, we could know how TKTL1 affects tumor malignancies in vivo.

4.5. TKTL1 suppression as a strategy of anti-cancer treatment?

Aerobic glycolysis, as “cancer’s sweet teeth”, has been considered as anti-cancer therapy targets from long ago. To block the tumor-specific glycolysis is the key issue. Since only in cancers TKTL1 is highly expressed, the therapeutic potential of TKTL1 suppression could be very specific and effective for cancer treatment. As TKTL1 is an enzyme which needs thiamin as its co-substrate, it is possible to manipulate TKTL1 activities by simply adjusting food diet in patients. For instance, thiamine analogues are already used for clinical trial for cancer treatment since they target thiamine transport to block transketolase activity. The disadvantage is it could block all transketolases activity, which may bring certain side effects since TKT is needed for maintain normal cell functions.

Recently, it was also shown that small molecule dichloroacetate (DCA) has the capacity of killing most of cancers (Bonnet et al., 2007). The addition of DCA to

cancer cells turns the mitochondria on again, providing cancer cells with energy supply again from OXPHOS, thus cancer cells become less dependent on aerobic glycolysis. The re-initiation of mitochondrial function kills the cancer cells by apoptosis. In our study, we found that suppression of TKTL1 could have similar effect as DCA, e.g. decreasing PDK activity by reducing its transcription, breakdown of mitochondria membrane potential (Figure 18), reduced tumor growth (Figure 31). This implicates that TKTL1 suppression would have similar clinical applications as DCA for cancer treatment.

All our data show the strong involvement of TKTL1 in cancer cell growth, malignancy, and viability. Due to its specific over-expression in tumor and malignant cells (Coy et al., 2005), TKTL1 may be considered as a strong candidate for anti-cancer therapy.

Since not all the tumors are TKTL1 positive, the test for TKTL1 thus enables physicians to use a form of treatment for the tumor that is specifically tailored to the individual situation of the patient. For the TKTL1-positive tumors, it might be very useful to use treatments to block TKTL1 activities either by drugs specifically block TKTL1 activity or by RNA interference technology using viral vectors.

5. References

Acharyya, S., Ladner, K.J., Nelsen, L.L., Damrauer, J., Reiser, P.J., Swoap, S., and Guttridge, D.C. (2004). Cancer cachexia is regulated by selective targeting of skeletal muscle gene products. The Journal of clinical investigation *114*, 370-378.

Alberts, B. (2002). Molecular biology of the cell, 4th edn (New York, Garland Science).

Anderson, S., Bankier, A.T., Barrell, B.G., de Bruijn, M.H., Coulson, A.R., Drouin, J., Eperon, I.C., Nierlich, D.P., Roe, B.A., Sanger, F., *et al.* (1981). Sequence and organization of the human mitochondrial genome. Nature *290*, 457-465.

Andreyev, A.Y., Kushnareva, Y.E., and Starkov, A.A. (2005). Mitochondrial metabolism of reactive oxygen species. Biochemistry (Mosc) *70*, 200-214.

Banmeyer, I., Marchand, C., Verhaeghe, C., Vucic, B., Rees, J.F., and Knoops, B. (2004). Overexpression of human peroxiredoxin 5 in subcellular compartments of Chinese hamster ovary cells: effects on cytotoxicity and DNA damage caused by peroxides. Free radical biology & medicine *36*, 65-77.

Beckman, K.B., and Ames, B.N. (1998). The free radical theory of aging matures. Physiological reviews *78*, 547-581.

Behrend, L., Henderson, G., and Zwacka, R.M. (2003). Reactive oxygen species in oncogenic transformation. Biochemical Society transactions *31*, 1441-1444.

Bignami, M., Rosa, S., La Rocca, S.A., Falcone, G., and Tato, F. (1987). Tumor promoters enhance v-myc-induced focus formation in mammalian cell lines. Annals of the New York Academy of Sciences *511*, 343-349.

Bohr, V.A. (2002). Repair of oxidative DNA damage in nuclear and mitochondrial DNA, and some changes with aging in mammalian cells. Free radical biology & medicine *32*, 804-812.

Bonnet, S., Archer, S.L., Allalunis-Turner, J., Haromy, A., Beaulieu, C., Thompson, R., Lee, C.T., Lopaschuk, G.D., Puttagunta, L., Bonnet, S., *et al.* (2007). A mitochondria-K+ channel axis is suppressed in cancer and its normalization promotes apoptosis and inhibits cancer growth. Cancer cell *11*, 37-51.

Boros, L.G., Puigjaner, J., Cascante, M., Lee, W.N., Brandes, J.L., Bassilian, S., Yusuf, F.I., Williams, R.D., Muscarella, P., Melvin, W.S., *et al.* (1997). Oxythiamine and dehydroepiandrosterone inhibit the nonoxidative synthesis of ribose and tumor cell proliferation. Cancer research *57*, 4242-4248.

Braig, M., Lee, S., Loddenkemper, C., Rudolph, C., Peters, A.H., Schlegelberger, B., Stein, H., Dorken, B., Jenuwein, T., and Schmitt, C.A. (2005). Oncogene-induced senescence as an initial barrier in lymphoma development. Nature *436*, 660-665.

Brandon, M., Baldi, P., and Wallace, D.C. (2006). Mitochondrial mutations in cancer. Oncogene *25*, 4647-4662.

Bykova, I.A., Solovjeva, O.N., Meshalkina, L.E., Kovina, M.V., and Kochetov, G.A. (2001). One-substrate transketolase-catalyzed reaction. Biochemical and biophysical research communications *280*, 845-847.

Carew, J.S., and Huang, P. (2002). Mitochondrial defects in cancer. Molecular cancer *1*, 9.

Carlsson, G., Gullberg, B., and Hafstrom, L. (1983). Estimation of liver tumor volume using different formulas - an experimental study in rats. Journal of cancer research and clinical oncology *105*, 20-23.

Chamberlain, J.S. (2004). Cachexia in cancer--zeroing in on myosin. The New England journal of medicine *351*, 2124-2125.

Chambers, A.F., and Matrisian, L.M. (1997). Changing views of the role of matrix metalloproteinases in metastasis. Journal of the National Cancer Institute *89*, 1260-1270.

Chandel, N.S., Maltepe, E., Goldwasser, E., Mathieu, C.E., Simon, M.C., and Schumacker, P.T. (1998). Mitochondrial reactive oxygen species trigger hypoxia-induced transcription. Proceedings of the National Academy of Sciences of the United States of America *95*, 11715-11720.

Chen, Z., Trotman, L.C., Shaffer, D., Lin, H.K., Dotan, Z.A., Niki, M., Koutcher, J.A., Scher, H.I., Ludwig, T., Gerald, W.*, et al.* (2005). Crucial role of p53-dependent cellular senescence in suppression of Pten-deficient tumorigenesis. Nature *436*, 725-730.

Chipuk, J.E., Bouchier-Hayes, L., and Green, D.R. (2006). Mitochondrial outer membrane permeabilization during apoptosis: the innocent bystander scenario. Cell death and differentiation *13*, 1396-1402.

Cohen, J.J., and Duke, R.C. (1984). Glucocorticoid activation of a calcium-dependent endonuclease in thymocyte nuclei leads to cell death. J Immunol *132*, 38-42.

Collado, M., Gil, J., Efeyan, A., Guerra, C., Schuhmacher, A.J., Barradas, M., Benguria, A., Zaballos, A., Flores, J.M., Barbacid, M.*, et al.* (2005). Tumour biology: senescence in premalignant tumours. Nature *436*, 642.

Copeland, W.C., Wachsman, J.T., Johnson, F.M., and Penta, J.S. (2002). Mitochondrial DNA alterations in cancer. Cancer investigation *20*, 557-569.

Coy, J.F., Dressler, D., Wilde, J., and Schubert, P. (2005). Mutations in the transketolase-like gene TKTL1: clinical implications for neurodegenerative diseases, diabetes and cancer. Clinical laboratory *51*, 257-273.

Croteau, D.L., and Bohr, V.A. (1997). Repair of oxidative damage to nuclear and mitochondrial DNA in mammalian cells. The Journal of biological chemistry *272*, 25409-25412.

Dang, C.V., and Semenza, G.L. (1999). Oncogenic alterations of metabolism. Trends in biochemical sciences *24*, 68-72.

Davies, K.J. (1999). The broad spectrum of responses to oxidants in proliferating cells: a new paradigm for oxidative stress. IUBMB life *48*, 41-47.

Deisseroth, A., and Dounce, A.L. (1970). Catalase: Physical and chemical properties, mechanism of catalysis, and physiological role. Physiological reviews *50*, 319-375.

Demirag, F., Unsal, E., Yilmaz, A., and Caglar, A. (2005). Prognostic significance of vascular endothelial growth factor, tumor necrosis, and mitotic activity index in malignant pleural mesothelioma. Chest *128*, 3382-3387.

Dimri, G.P., Lee, X., Basile, G., Acosta, M., Scott, G., Roskelley, C., Medrano, E.E., Linskens, M., Rubelj, I., Pereira-Smith, O.*, et al.* (1995). A biomarker that identifies senescent human cells in culture and in aging skin in vivo. Proceedings of the National Academy of Sciences of the United States of America *92*, 9363-9367.

Downey, R.J., Akhurst, T., Gonen, M., Vincent, A., Bains, M.S., Larson, S., and Rusch, V. (2004). Preoperative F-18 fluorodeoxyglucose-positron emission tomography maximal standardized uptake value predicts survival after lung cancer resection. J Clin Oncol *22*, 3255-3260.

Dringen, R. (2000). Metabolism and functions of glutathione in brain. Progress in neurobiology *62*, 649-671.

Edwards, J.G., Swinson, D.E., Jones, J.L., Muller, S., Waller, D.A., and O'Byrne, K.J. (2003). Tumor necrosis correlates with angiogenesis and is a predictor of poor prognosis in malignant mesothelioma. Chest *124*, 1916-1923.

Elstrom, R.L., Bauer, D.E., Buzzai, M., Karnauskas, R., Harris, M.H., Plas, D.R., Zhuang, H., Cinalli, R.M., Alavi, A., Rudin, C.M., *et al.* (2004). Akt stimulates aerobic glycolysis in cancer cells. Cancer research *64*, 3892-3899.

Esteban, M.A., and Maxwell, P.H. (2005). HIF, a missing link between metabolism and cancer. Nature medicine *11*, 1047-1048.

Esterbauer, H., Schaur, R.J., and Zollner, H. (1991). Chemistry and biochemistry of 4-hydroxynonenal, malonaldehyde and related aldehydes. Free radical biology & medicine *11*, 81-128.

Finkel, T. (2003). Oxidant signals and oxidative stress. Current opinion in cell biology *15*, 247-254.

Fujii, J., and Ikeda, Y. (2002). Advances in our understanding of peroxiredoxin, a multifunctional, mammalian redox protein. Redox Rep *7*, 123-130.

Garber, K. (2004). Energy boost: the Warburg effect returns in a new theory of cancer. Journal of the National Cancer Institute *96*, 1805-1806.

Gatenby, R.A., and Gawlinski, E.T. (1996). A reaction-diffusion model of cancer invasion. Cancer research *56*, 5745-5753.

Gatenby, R.A., Gawlinski, E.T., Gmitro, A.F., Kaylor, B., and Gillies, R.J. (2006). Acid-mediated tumor invasion: a multidisciplinary study. Cancer research *66*, 5216-5223.

Gatenby, R.A., and Gillies, R.J. (2004). Why do cancers have high aerobic glycolysis? Nature reviews *4*, 891-899.

Gibbs, M., and Horecker, B.L. (1954). The mechanism of pentose phosphate conversion to hexose monophosphate. II. With pea leaf and pea root preparations. The Journal of biological chemistry *208*, 813-820.

Glinsky, G.V., Ivanova, Y.A., and Glinskii, A.B. (2003a). Common malignancy-associated regions of transcriptional activation (MARTA) in human prostate, breast, ovarian, and colon cancers are targets for DNA amplification. Cancer letters *201*, 67-77.

Glinsky, G.V., Krones-Herzig, A., and Glinskii, A.B. (2003b). Malignancy-associated regions of transcriptional activation: gene expression profiling identifies common chromosomal regions of a recurrent transcriptional activation in human prostate, breast, ovarian, and colon cancers. Neoplasia (New York, NY *5*, 218-228.

Green, D.R., and Reed, J.C. (1998). Mitochondria and apoptosis. Science (New York, NY *281*, 1309-1312.

Griffith, O.W., and Meister, A. (1985). Origin and turnover of mitochondrial glutathione. Proceedings of the National Academy of Sciences of the United States of America *82*, 4668-4672.

Harris, A.L. (2002). Hypoxia--a key regulatory factor in tumour growth. Nature reviews *2*, 38-47.

Hatefi, Y. (1985). The mitochondrial electron transport and oxidative phosphorylation system. Annual review of biochemistry *54*, 1015-1069.

Hensley, K., Robinson, K.A., Gabbita, S.P., Salsman, S., and Floyd, R.A. (2000). Reactive oxygen species, cell signaling, and cell injury. Free radical biology & medicine *28*, 1456-1462.

Hockel, M., and Vaupel, P. (2001). Tumor hypoxia: definitions and current clinical, biologic, and molecular aspects. Journal of the National Cancer Institute *93*, 266-276.

Holroyde, C.P., Gabuzda, T.G., Putnam, R.C., Paul, P., and Reichard, G.A. (1975). Altered glucose metabolism in metastatic carcinoma. Cancer research *35*, 3710-3714.

Horecker, B.L., Domagk, G., and Hiatt, H.H. (1958). A comparison of C14-labeling patterns in deoxyribose and ribose in mammalian cells. Archives of biochemistry and biophysics *78*, 510-517.

Horecker, B.L., Gibbs, M., Klenow, H., and Smyrniotis, P.Z. (1954). The mechanism of pentose

phosphate conversion to hexose monophosphate. I. With a liver enzyme preparation. The Journal of biological chemistry *207*, 393-403.

Hu, L.H., Yang, J.H., Zhang, D.T., Zhang, S., Wang, L., Cai, P.C., Zheng, J.F., and Huang, J.S. (2007). The TKTL1 gene influences total transketolase activity and cell proliferation in human colon cancer LoVo cells. Anti-cancer drugs *18*, 427-433.

Huang, L.E., Gu, J., Schau, M., and Bunn, H.F. (1998). Regulation of hypoxia-inducible factor 1alpha is mediated by an O2-dependent degradation domain via the ubiquitin-proteasome pathway. Proceedings of the National Academy of Sciences of the United States of America *95*, 7987-7992.

Hyltander, A., Drott, C., Korner, U., Sandstrom, R., and Lundholm, K. (1991). Elevated energy expenditure in cancer patients with solid tumours. Eur J Cancer *27*, 9-15.

Jaakkola, P., Mole, D.R., Tian, Y.M., Wilson, M.I., Gielbert, J., Gaskell, S.J., Kriegsheim, A., Hebestreit, H.F., Mukherji, M., Schofield, C.J., *et al.* (2001). Targeting of HIF-alpha to the von Hippel-Lindau ubiquitylation complex by O2-regulated prolyl hydroxylation. Science (New York, NY *292*, 468-472.

Kanbagli, O., Ozdemirler, G., Bulut, T., Yamaner, S., Aykac-Toker, G., and Uysal, M. (2000). Mitochondrial lipid peroxides and antioxidant enzymes in colorectal adenocarcinoma tissues. Jpn J Cancer Res *91*, 1258-1263.

Kim, J.W., Tchernyshyov, I., Semenza, G.L., and Dang, C.V. (2006). HIF-1-mediated expression of pyruvate dehydrogenase kinase: a metabolic switch required for cellular adaptation to hypoxia. Cell metabolism *3*, 177-185.

King, A., Selak, M.A., and Gottlieb, E. (2006). Succinate dehydrogenase and fumarate hydratase: linking mitochondrial dysfunction and cancer. Oncogene *25*, 4675-4682.

Kirsch, M., and De Groot, H. (2001). NAD(P)H, a directly operating antioxidant? Faseb J *15*, 1569-1574.

Konstantinov, A.A., Peskin, A.V., Popova, E., Khomutov, G.B., and Ruuge, E.K. (1987). Superoxide generation by the respiratory chain of tumor mitochondria. Biochimica et biophysica acta *894*, 1-10.

Kovina, M.V., and Kochetov, G.A. (1998). Cooperativity and flexibility of active sites in homodimeric transketolase. FEBS letters *440*, 81-84.

Kumar, R., Xiu, Y., Mavi, A., El-Haddad, G., Zhuang, H., and Alavi, A. (2005). FDG-PET imaging in primary bilateral adrenal lymphoma: a case report and review of the literature. Clinical nuclear medicine *30*, 222-230.

Kung, A.L., Wang, S., Klco, J.M., Kaelin, W.G., and Livingston, D.M. (2000). Suppression of tumor growth through disruption of hypoxia-inducible transcription. Nature medicine *6*, 1335-1340.

Land, H., Parada, L.F., and Weinberg, R.A. (1983). Tumorigenic conversion of primary embryo fibroblasts requires at least two cooperating oncogenes. Nature *304*, 596-602.

Langbein, S., Zerilli, M., Zur Hausen, A., Staiger, W., Rensch-Boschert, K., Lukan, N., Popa, J., Ternullo, M.P., Steidler, A., Weiss, C., *et al.* (2006). Expression of transketolase TKTL1 predicts colon and urothelial cancer patient survival: Warburg effect reinterpreted. British journal of cancer *94*, 578-585.

Lass, A., Forster, M.J., and Sohal, R.S. (1999). Effects of coenzyme Q10 and alpha-tocopherol administration on their tissue levels in the mouse: elevation of mitochondrial alpha-tocopherol by coenzyme Q10. Free radical biology & medicine *26*, 1375-1382.

Lee, A.C., Fenster, B.E., Ito, H., Takeda, K., Bae, N.S., Hirai, T., Yu, Z.X., Ferrans, V.J., Howard, B.H., and Finkel, T. (1999). Ras proteins induce senescence by altering the intracellular levels of reactive

oxygen species. The Journal of biological chemistry *274*, 7936-7940.

Lee, S.E., Byun, S.S., Oh, J.K., Lee, S.C., Chang, I.H., Choe, G., and Hong, S.K. (2006). Significance of macroscopic tumor necrosis as a prognostic indicator for renal cell carcinoma. The Journal of urology *176*, 1332-1337; discussion 1337-1338.

Lee, W.N., Byerley, L.O., Bassilian, S., Ajie, H.O., Clark, I., Edmond, J., and Bergner, E.A. (1995). Isotopomer study of lipogenesis in human hepatoma cells in culture: contribution of carbon and hydrogen atoms from glucose. Analytical biochemistry *226*, 100-112.

Leek, R.D., Landers, R.J., Harris, A.L., and Lewis, C.E. (1999). Necrosis correlates with high vascular density and focal macrophage infiltration in invasive carcinoma of the breast. British journal of cancer *79*, 991-995.

Lenzen, S., Drinkgern, J., and Tiedge, M. (1996). Low antioxidant enzyme gene expression in pancreatic islets compared with various other mouse tissues. Free radical biology & medicine *20*, 463-466.

Liu, Y. (2006). Fatty acid oxidation is a dominant bioenergetic pathway in prostate cancer. Prostate cancer and prostatic diseases *9*, 230-234.

Lu, H., Forbes, R.A., and Verma, A. (2002). Hypoxia-inducible factor 1 activation by aerobic glycolysis implicates the Warburg effect in carcinogenesis. The Journal of biological chemistry *277*, 23111-23115.

Mamchaoui, K., and Saumon, G. (2000). A method for measuring the oxygen consumption of intact cell monolayers. American journal of physiology *278*, L858-863.

Mannella, C.A. (2006). Structure and dynamics of the mitochondrial inner membrane cristae. Biochimica et biophysica acta *1763*, 542-548.

Martensson, J., Lai, J.C., and Meister, A. (1990). High-affinity transport of glutathione is part of a multicomponent system essential for mitochondrial function. Proceedings of the National Academy of Sciences of the United States of America *87*, 7185-7189.

McCord, J.M., Keele, B.B., Jr., and Fridovich, I. (1971). An enzyme-based theory of obligate anaerobiosis: the physiological function of superoxide dismutase. Proceedings of the National Academy of Sciences of the United States of America *68*, 1024-1027.

McDevitt, T.M., and Tisdale, M.J. (1992). Tumour-associated hypoglycaemia in a murine cachexia model. British journal of cancer *66*, 815-820.

Michaloglou, C., Vredeveld, L.C., Soengas, M.S., Denoyelle, C., Kuilman, T., van der Horst, C.M., Majoor, D.M., Shay, J.W., Mooi, W.J., and Peeper, D.S. (2005). BRAFE600-associated senescence-like cell cycle arrest of human naevi. Nature *436*, 720-724.

Mulligan, H.D., and Tisdale, M.J. (1991). Lipogenesis in tumour and host tissues in mice bearing colonic adenocarcinomas. British journal of cancer *63*, 719-722.

Munoz-Pinedo, C., Ruiz-Ruiz, C., Ruiz de Almodovar, C., Palacios, C., and Lopez-Rivas, A. (2003). Inhibition of glucose metabolism sensitizes tumor cells to death receptor-triggered apoptosis through enhancement of death-inducing signaling complex formation and apical procaspase-8 processing. The Journal of biological chemistry *278*, 12759-12768.

Myslinski, E., Ame, J.C., Krol, A., and Carbon, P. (2001). An unusually compact external promoter for RNA polymerase III transcription of the human H1RNA gene. Nucleic acids research *29*, 2502-2509.

O'Brien, C.A., Pollett, A., Gallinger, S., and Dick, J.E. (2007). A human colon cancer cell capable of initiating tumour growth in immunodeficient mice. Nature *445*, 106-110.

Olafsdottir, K., and Reed, D.J. (1988). Retention of oxidized glutathione by isolated rat liver

mitochondria during hydroperoxide treatment. Biochimica et biophysica acta *964*, 377-382.

Orrenius, S., Gogvadze, V., and Zhivotovsky, B. (2007). Mitochondrial oxidative stress: implications for cell death. Annual review of pharmacology and toxicology *47*, 143-183.

Ott, M., Robertson, J.D., Gogvadze, V., Zhivotovsky, B., and Orrenius, S. (2002). Cytochrome c release from mitochondria proceeds by a two-step process. Proceedings of the National Academy of Sciences of the United States of America *99*, 1259-1263.

Packer, L., Weber, S.U., and Rimbach, G. (2001). Molecular aspects of alpha-tocotrienol antioxidant action and cell signalling. The Journal of nutrition *131*, 369S-373S.

Panfili, E., Sandri, G., and Ernster, L. (1991). Distribution of glutathione peroxidases and glutathione reductase in rat brain mitochondria. FEBS letters *290*, 35-37.

Papandreou, I., Cairns, R.A., Fontana, L., Lim, A.L., and Denko, N.C. (2006). HIF-1 mediates adaptation to hypoxia by actively downregulating mitochondrial oxygen consumption. Cell metabolism *3*, 187-197.

Pastore, A., Federici, G., Bertini, E., and Piemonte, F. (2003). Analysis of glutathione: implication in redox and detoxification. Clinica chimica acta; international journal of clinical chemistry *333*, 19-39.

Patel, M.S., and Roche, T.E. (1990). Molecular biology and biochemistry of pyruvate dehydrogenase complexes. Faseb J *4*, 3224-3233.

Pedersen, P.L. (1978). Tumor mitochondria and the bioenergetics of cancer cells. Progress in experimental tumor research Fortschritte der experimentellen Tumorforschung *22*, 190-274.

Pelicano, H., Carney, D., and Huang, P. (2004). ROS stress in cancer cells and therapeutic implications. Drug Resist Updat *7*, 97-110.

Pelicano, H., Xu, R.H., Du, M., Feng, L., Sasaki, R., Carew, J.S., Hu, Y., Ramdas, L., Hu, L., Keating, M.J., *et al.* (2006). Mitochondrial respiration defects in cancer cells cause activation of Akt survival pathway through a redox-mediated mechanism. The Journal of cell biology *175*, 913-923.

Peluso, G., Nicolai, R., Reda, E., Benatti, P., Barbarisi, A., and Calvani, M. (2000). Cancer and anticancer therapy-induced modifications on metabolism mediated by carnitine system. Journal of cellular physiology *182*, 339-350.

Pollard, P.J., Briere, J.J., Alam, N.A., Barwell, J., Barclay, E., Wortham, N.C., Hunt, T., Mitchell, M., Olpin, S., Moat, S.J., *et al.* (2005). Accumulation of Krebs cycle intermediates and over-expression of HIF1alpha in tumours which result from germline FH and SDH mutations. Human molecular genetics *14*, 2231-2239.

Pozzatti, R., Muschel, R., Williams, J., Padmanabhan, R., Howard, B., Liotta, L., and Khoury, G. (1986). Primary rat embryo cells transformed by one or two oncogenes show different metastatic potentials. Science (New York, NY *232*, 223-227.

Punnonen, K., Ahotupa, M., Asaishi, K., Hyoty, M., Kudo, R., and Punnonen, R. (1994). Antioxidant enzyme activities and oxidative stress in human breast cancer. Journal of cancer research and clinical oncology *120*, 374-377.

Rais, B., Comin, B., Puigjaner, J., Brandes, J.L., Creppy, E., Saboureau, D., Ennamany, R., Lee, W.N., Boros, L.G., and Cascante, M. (1999). Oxythiamine and dehydroepiandrosterone induce a G1 phase cycle arrest in Ehrlich's tumor cells through inhibition of the pentose cycle. FEBS letters *456*, 113-118.

Ramanathan, A., Wang, C., and Schreiber, S.L. (2005). Perturbational profiling of a cell-line model of tumorigenesis by using metabolic measurements. Proceedings of the National Academy of Sciences of the United States of America *102*, 5992-5997.

Ramsey, M.R., and Sharpless, N.E. (2006). ROS as a tumour suppressor? Nature cell biology *8*,

1213-1215.

Ricci-Vitiani, L., Lombardi, D.G., Pilozzi, E., Biffoni, M., Todaro, M., Peschle, C., and De Maria, R. (2007). Identification and expansion of human colon-cancer-initiating cells. Nature *445*, 111-115.

Roche, T.E., and Hiromasa, Y. (2007). Pyruvate dehydrogenase kinase regulatory mechanisms and inhibition in treating diabetes, heart ischemia, and cancer. Cell Mol Life Sci *64*, 830-849.

Rockwell, S., Yuan, J., Peretz, S., and Glazer, P.M. (2001). Genomic instability in cancer. Novartis Foundation symposium *240*, 133-142; discussion 142-151.

Russell, S.T., and Tisdale, M.J. (2002). Effect of a tumour-derived lipid-mobilising factor on glucose and lipid metabolism in vivo. British journal of cancer *87*, 580-584.

Saraste, M. (1999). Oxidative phosphorylation at the fin de siecle. Science (New York, NY *283*, 1488-1493.

Schofield, C.J., and Ratcliffe, P.J. (2004). Oxygen sensing by HIF hydroxylases. Nature reviews *5*, 343-354.

Schumacker, P.T. (2006). Reactive oxygen species in cancer cells: live by the sword, die by the sword. Cancer cell *10*, 175-176.

Selak, M.A., Armour, S.M., MacKenzie, E.D., Boulahbel, H., Watson, D.G., Mansfield, K.D., Pan, Y., Simon, M.C., Thompson, C.B., and Gottlieb, E. (2005). Succinate links TCA cycle dysfunction to oncogenesis by inhibiting HIF-alpha prolyl hydroxylase. Cancer cell *7*, 77-85.

Semenza, G.L. (2003). Targeting HIF-1 for cancer therapy. Nature reviews *3*, 721-732.

Semenza, G.L. (2007). Vasculogenesis, angiogenesis, and arteriogenesis: mechanisms of blood vessel formation and remodeling. Journal of cellular biochemistry *102*, 840-847.

Semenza, G.L., Roth, P.H., Fang, H.M., and Wang, G.L. (1994). Transcriptional regulation of genes encoding glycolytic enzymes by hypoxia-inducible factor 1. The Journal of biological chemistry *269*, 23757-23763.

Sengupta, S., Lohse, C.M., Leibovich, B.C., Frank, I., Thompson, R.H., Webster, W.S., Zincke, H., Blute, M.L., Cheville, J.C., and Kwon, E.D. (2005). Histologic coagulative tumor necrosis as a prognostic indicator of renal cell carcinoma aggressiveness. Cancer *104*, 511-520.

Shacter, E., Williams, J.A., Hinson, R.M., Senturker, S., and Lee, Y.J. (2000). Oxidative stress interferes with cancer chemotherapy: inhibition of lymphoma cell apoptosis and phagocytosis. Blood *96*, 307-313.

Sohal, R.S. (2002). Role of oxidative stress and protein oxidation in the aging process. Free radical biology & medicine *33*, 37-44.

St-Pierre, J., Drori, S., Uldry, M., Silvaggi, J.M., Rhee, J., Jager, S., Handschin, C., Zheng, K., Lin, J., Yang, W.*, et al.* (2006). Suppression of reactive oxygen species and neurodegeneration by the PGC-1 transcriptional coactivators. Cell *127*, 397-408.

Stadtman, E.R., and Oliver, C.N. (1991). Metal-catalyzed oxidation of proteins. Physiological consequences. The Journal of biological chemistry *266*, 2005-2008.

Starke-Reed, P.E., and Oliver, C.N. (1989). Protein oxidation and proteolysis during aging and oxidative stress. Archives of biochemistry and biophysics *275*, 559-567.

Stern, R., Shuster, S., Neudecker, B.A., and Formby, B. (2002). Lactate stimulates fibroblast expression of hyaluronan and CD44: the Warburg effect revisited. Experimental cell research *276*, 24-31.

Storey, K.B. (1996). Oxidative stress: animal adaptations in nature. Brazilian journal of medical and biological research = Revista brasileira de pesquisas medicas e biologicas / Sociedade Brasileira de Biofisica [et al *29*, 1715-1733.

Takahashi, A., Ohtani, N., Yamakoshi, K., Iida, S., Tahara, H., Nakayama, K., Nakayama, K.I., Ide, T., Saya, H., and Hara, E. (2006). Mitogenic signalling and the p16INK4a-Rb pathway cooperate to enforce irreversible cellular senescence. Nature cell biology *8*, 1291-1297.

Tischler, M.E., Hecht, P., and Williamson, J.R. (1977). Effect of ammonia on mitochondrial and cytosolic NADH and NADPH systems in isolated rat liver cells. FEBS letters *76*, 99-104.

Tomlinson, I.P., Alam, N.A., Rowan, A.J., Barclay, E., Jaeger, E.E., Kelsell, D., Leigh, I., Gorman, P., Lamlum, H., Rahman, S., *et al.* (2002). Germline mutations in FH predispose to dominantly inherited uterine fibroids, skin leiomyomata and papillary renal cell cancer. Nature genetics *30*, 406-410.

Toussaint, O., Dumont, P., Dierick, J.F., Pascal, T., Frippiat, C., Chainiaux, F., Sluse, F., Eliaers, F., and Remacle, J. (2000a). Stress-induced premature senescence. Essence of life, evolution, stress, and aging. Annals of the New York Academy of Sciences *908*, 85-98.

Toussaint, O., Medrano, E.E., and von Zglinicki, T. (2000b). Cellular and molecular mechanisms of stress-induced premature senescence (SIPS) of human diploid fibroblasts and melanocytes. Experimental gerontology *35*, 927-945.

Turrens, J.F. (2003). Mitochondrial formation of reactive oxygen species. The Journal of physiology *552*, 335-344.

Turrens, J.F., Alexandre, A., and Lehninger, A.L. (1985). Ubisemiquinone is the electron donor for superoxide formation by complex III of heart mitochondria. Archives of biochemistry and biophysics *237*, 408-414.

Utsunomiya, H., Komatsu, N., Yoshimura, S., Tsutsumi, Y., and Watanabe, K. (1991). Exact ultrastructural localization of glutathione peroxidase in normal rat hepatocytes: advantages of microwave fixation. J Histochem Cytochem *39*, 1167-1174.

Vafa, O., Wade, M., Kern, S., Beeche, M., Pandita, T.K., Hampton, G.M., and Wahl, G.M. (2002). c-Myc can induce DNA damage, increase reactive oxygen species, and mitigate p53 function: a mechanism for oncogene-induced genetic instability. Molecular cell *9*, 1031-1044.

van de Wetering, M., Oving, I., Muncan, V., Pon Fong, M.T., Brantjes, H., van Leenen, D., Holstege, F.C., Brummelkamp, T.R., Agami, R., and Clevers, H. (2003). Specific inhibition of gene expression using a stably integrated, inducible small-interfering-RNA vector. EMBO reports *4*, 609-615.

Wahllander, A., Soboll, S., Sies, H., Linke, I., and Muller, M. (1979). Hepatic mitochondrial and cytosolic glutathione content and the subcellular distribution of GSH-S-transferases. FEBS letters *97*, 138-140.

Walenta, S., Wetterling, M., Lehrke, M., Schwickert, G., Sundfor, K., Rofstad, E.K., and Mueller-Klieser, W. (2000). High lactate levels predict likelihood of metastases, tumor recurrence, and restricted patient survival in human cervical cancers. Cancer research *60*, 916-921.

Wang, G.L., Jiang, B.H., Rue, E.A., and Semenza, G.L. (1995). Hypoxia-inducible factor 1 is a basic-helix-loop-helix-PAS heterodimer regulated by cellular O2 tension. Proceedings of the National Academy of Sciences of the United States of America *92*, 5510-5514.

Warburg, O. (1956a). On respiratory impairment in cancer cells. Science (New York, NY *124*, 269-270.

Warburg, O. (1956b). On the origin of cancer cells. Science (New York, NY *123*, 309-314.

Weinhouse, S. (1955). Oxidative metabolism of neoplastic tissues. Advances in cancer research *3*, 269-325.

Weng, G., Bhalla, U.S., and Iyengar, R. (1999). Complexity in biological signaling systems. Science (New York, NY *284*, 92-96.

Wikner, C., Meshalkina, L., Nilsson, U., Backstrom, S., Lindqvist, Y., and Schneider, G. (1995). His103

in yeast transketolase is required for substrate recognition and catalysis. European journal of biochemistry / FEBS *233*, 750-755.

Xu, R.H., Pelicano, H., Zhou, Y., Carew, J.S., Feng, L., Bhalla, K.N., Keating, M.J., and Huang, P. (2005). Inhibition of glycolysis in cancer cells: a novel strategy to overcome drug resistance associated with mitochondrial respiratory defect and hypoxia. Cancer research *65*, 613-621.

6. Acknowledgement

I wish to express my gratitude to all those who have made this thesis possible, expecially:

Prof. Dr. Martin Loechelt, my supervisor, for always supporting and helping me to do my best. For making me laugh about my mistakes and about other people, for teaching me about how research is done and how to present it to others. For your endless patience and help with technical questions.

Prof. Dr. Lutz Gissmann, my co-supervisor, for always supporting my project. For critical judgements and every advice I got from you to take important decisions. I could not have done this without you!

Dr. Johannes Coy and Prof. Axel zur Hausen, our cooperation partners, for providing us antibodies and carrying on all the tumor histology work. Respectively.

Madeleine Sporleder, our secretary, for helping me ordering reagents and all the other documentations.

Dr. Guillermo Barreto, for being my first teacher in molecular biology, providing me with unlimited help.

Dr. Haikun Liu, and Dr. Junwei Li, for discussions about science and support with thesis work and manuscripts, for a good friendship and lots of fun at work and after work hours.

Dr. Fabian Romen, Dr. Sarah Chareza, Dr. Weibin Liu, Perdita Backes, Daniel Maeda, Evi Schyr, our group members for fruitful and pleasant

collaborations, and all the other lab members of F020, for providing a friendly atmosphere.

Ying Ni, Yi Ni, Chao Yang, Xiaojia Deng, Lu Dai, Lei Gao, Dr. Wei Yao, Yingzi Ge, my Chinese friends in Heidelberg, for encouragement and support and being willing to listen to my work and non-work related problems as well as all the fun we had the whole time.

Finally I would like to thank my **mother** and my **father,** to whom I dedicate my thesis, for your eternal and unconditional support.